Impurity Band Broadening as the Origin of the Positive Magnetoresistance in the Dilute Magnetic Semiconductor Zinc Manganese Selenide

by

Steve Petznick

Supervised by
Prof. Dr. Peter J. Klar

A dissertation in partial fulfillment of the requirements for the degree of
Doctor rerum naturalium (Dr. rer. nat.) in Physics

Justus Liebig University Giessen

Faculty 07 - Mathematics and Computer Science, Physics, Geography

December 2015

For my wife

Contents

Abstract

This work is dedicated to give a novel explanation for the large positive magnetoresistance effect in the n-type dilute magnetic semiconductor zinc manganese selenide. This effect has been observed in experiment in the hopping transport regime. The appearance of hopping transport is a necessary requirement for this effect to occur, as is the presence and the amount of magnetic atoms in the material. In literature, no conclusive explanation for this large positive magnetoresistance effect is known. The nature of the hopping transport requires a precise knowledge of the energetic position of each donor level, as an thermally activated electron has to overcome the energy difference from one donor level to another. Another aspect of the transport mechanism is that each donor-bound electron interacts only with the manganese atoms in its vicinity. Therefore, our explanation is based on the statistical distribution of magnetic atoms in the crystal. The random distribution of manganese leads to fluctuations of the donor levels according to their local manganese contents. Due to the bowing of the conduction band edge a donor level with a high local manganese content has a low energy. The fluctuating donor levels are represented by their density of states. This donor energy distribution is called impurity band and can be described by its width and its shape. An external magnetic field leads to a downshift of the preferred spin state of each donor, which is proportional to the Brillouin function and to its local manganese content. The energetic position inside the impurity band at zero magnetic field and the magnetic field induced energetic downshift, both depending on the local manganese content, are relevant. For example, a donor level with a high local manganese content is low in energy and experiences a large downshift in energy. The combination of these two aspects leads to an increasing of the width of the impurity band, while its shape remains unaffected in a first approximation. Using only basic hopping rates, this increasing impurity band-width results in an increasing resistivity, i.e. a positive magnetoresistance. To quantify this process two theoretical approaches are presented, i.e. a scaling approach and simulations of the effect.

Zusammenfassung

Diese Arbeit ist dazu bestimmt, eine neue Erklärung für den großen positiven Magnetowiderstandseffekt im verdünnt magnetischen n-Typ Halbleiter Zinkmanganselenid zu liefern. Dieser Effekt wurde im Experiment beobachtet, genauer im Regime des Hopping-Transports. Dabei ist das Auftreten des Hopping-Transports eine notwendige Voraussetzung für diesen Effekt wie auch die Anwesenheit und die Menge magnetischer Atome in dem Material. In der Literatur ist keine schlüssige Erklärung für diesen großen positiven Magnetowiderstandseffekt bekannt. Die Natur des Hopping- Transports verlangt eine präzise Kenntnis der energetischen Position eines jeden Donatorniveaus, da ein thermisch aktiviertes Elektron die Energiedifferenz von einem Donator zum nächsten überwinden muss. Ein weiterer Aspekt des Transportmechanismus ist, dass jedes donatorgebundene Elektron nur mit den Manganatomen in seiner Umgebung interagiert. Daher basiert unsere Erklärung auf der statistischen Verteilung der Manganatome in dem Kristall. Die zufällige Verteilung von Mangan führt zu Fluktuationen der Donatorniveaus entsprechend ihrer lokalen Mangankonzentrationen. Aufgrund des Durchbiegens der Leitungsbandkante hat ein Donatorniveau mit hohem lokalem Mangangehalt eine niedrige Energie. Die fluktuierenden Donatorniveaus sind durch ihre Zustandsdichte dargestellt. Diese Verteilung der Donatorniveaus wird Störstellenband genannt und kann mittels ihrer Breite und Form beschrieben werden. Ein externes magnetisches Feld führt zu einer Verschiebung des bevorzugten Spinzustandes eines jeden Donators hin zu niedrigeren Energien, die proportional zu der Brillouinfunktion und zu seinem lokalen Mangangehalt ist. Die energetische Position innerhalb des Störstellenbandes ohne Magnetfeld und die magnetfeldinduzierte Verschiebung, beide abhängig von dem lokalen Mangangehalt, sind relevant. Zum Beispiel besitzt ein Donatorniveau mit einem hohen lokalen Mangangehalt eine niedrige Energie und erfährt eine große Verschiebung. Die Kombination dieser beiden Aspekte führt zu einer Verbreiterung des Störstellenbandes, während dessen Gestalt in erster Näherung unverändert bleibt. Nutzt man nun ausschließlich grundsätzliche Hopping-Raten, so resultiert aus dieser Verbreiterung des Störstellenbandes eine Zunahme des spezifischen elektrischen Widerstandes und damit ein positiver Magnetowiderstand. Um diesen Prozess zu quantifizieren werden zwei theoretische Ansätze vorgestellt, ein Skalierungsansatz und Simulationen des Effekts.

Chapter 1

Introduction

The material studied in this work is n-type zinc manganese selenide. This material is a dilute magnetic semiconductor due to the amount of manganese incorporated in the host material. The host material is the classical II-VI semiconductor zinc selenide. Due to the choice of this material two different fields are of importance, namely the physics of semiconductors and that of magnetism. One example for this dualism is the following parameter pair, the carrier concentration and the manganese content. An advantage of the material zinc manganese selenide is the independence of these two parameter. Furthermore high quality crystalline material can be grown by molecular beam epitaxy as thin films. These circumstances make it an ideal model system and testing ground to study the interplay of magnetic and semiconducting properties.

The electrical characterization offers only an indirect access on a number of basic physical properties. In other words one only measures the result not the origin. Therefore models are needed to connect the measurements to the underlying processes and mechanisms. As the main topic of this work is the explanation of the magnetoresistance effect in zinc manganese selenide, this nature of the indirect connection is our main concern. Even the determination of the transport mechanism belongs to this group of deduced information.

Zinc manganese selenide is used in model devices for spintronics such as spin-aligners, spin-LEDs, spin-filters and spin-transistors. These components can be integrated in devices such as spin computers or can be used for quantum cryptography. Also the design of spin superlattices is possible. For details refer to section 2.1.3. All these devices use the magnetically enhanced splitting mainly of the conduction band states which is of course relevant for our study as well. As all of these functions are only accessible at liquid helium temperature and thus are very costly not only in terms of money but also in terms of required laboratory equipment and techniques, no commercial applications are currently envisioned.

For comparison another well-established system is given which uses a magnetoresistance effect for magnetic field measurements. The most prominent application of this kind is the hard disc drive. To read information from a hard disc a magnetic field sensor is needed. This sensor works by the giant positive magnetoresistance effect, which converts the magnetic field direction into an electrical signal. But this effect occurs only at specially designed interfaces and is

many times larger than the one we discus in a bulk material without interfaces. Obviously this effect is apparent at room temperature in contrast to our effect. This difference of room and very low temperature arises from the ferromagnetic and paramagnetic behavior, respectively.

1.1 Motivation

The aim of this work is to motivate, to introduce and to quantify a novel explanation for the large positive magnetoresistance effect in bulk n-type zinc manganese selenide. This has to be done while taking into account the special role of the material being a dilute magnetic semiconductor and thus its enhanced magnetic properties. We share the observation of this effect with many other authors, cf. section 5.2. Until now no sufficient explanation for this behavior has been given. Obviously the giant positive magnetoresistance effect occurring at interfaces is ruled out as the origin. Another effect, namely the wave function shrinkage, is in no known way able to reproduce the characteristic magnetic field dependence of the measured curves. In the case of hopping transport via double occupation the shape could be explained but the temperature dependence, i.e. the transport mechanism, rules out the importance of this effect. Further information can be found in section 5.1.

We follow a different approach, namely a phenomenon correlated with the density of impurity states. Until now this has only once been used to interpret the negative magnetoresistance in general compound materials. We expand this concept to also explain positive magnetoresistance effects. Starting point for our model is the random nature of the spatial distributions of both manganese and donor atoms. In this point we follow the argumentation of Mycielski *et al.* but we introduce a novel feature. We will show that the conduction band bowing, which is enhanced in dilute magnetic semiconductor, is the main key to expand the argumentation of Mycielski *et al.* to positive magnetoresistance effects. The external magnetic field leads not only to a splitting of the density of impurity states following a Brillouin function behavior but also to its broadening with a similar dependence. This increasing impurity band-width leads to the observable large positive magnetoresistance effects.

Thus it is possible to consistently explain the uncommon behavior without needing collective processes like hopping of bound magnetic polaron or a minority transport mechanism at very low temperature like double occupation. A detailed discussion is given in section 5.1 and especially in section 5.1.6.

With this work we provide additional arguments for Mycielski's magnetoresistance explanation based on disorder. That gives his concept a further confirmation against another possible mechanism, namely the hopping of bound magnetic polarons.

This works is structured as follows. First the main underlying concepts and nomenclatures will be given, with further background to the samples and measurement techniques used. The transport mechanisms dominant at certain temperature intervals will be determined. The discussion in the other chapters will be based on this knowledge. Main magnetoresistance mechanisms known from literature will be presented and discussed. The characteristics of the measurements will be presented and a fit function is applied on them. The novel model will be presented in detail splitting at some point into two main theoretical approaches. After these

considerations, experimental effects near the limits of the applicability of the model are shown. Additionally measurements under hydrostatic pressure are presented and our argumentations are applied to these magnetoresistance measurements.

Chapter 2

Material System

2.1 Zinc manganese selenide

The ternary II-VI magnetic semiconductor alloy zinc manganese selenide ($Zn_{1-x}Mn_xSe$) is a direct band gap material with the conduction band minimum and valence band maximum at the Γ-point of the Brillouin zone for manganese concentrations up to about $x = 50\,\%$. So the band structure of zinc selenide on the right hand side of figure 2.1 is qualitatively the same for zinc manganese selenide. The quantity x thereby always denotes the manganese content on the cation sublattice, i.e. the fraction of zinc being isovalently substituted by manganese.

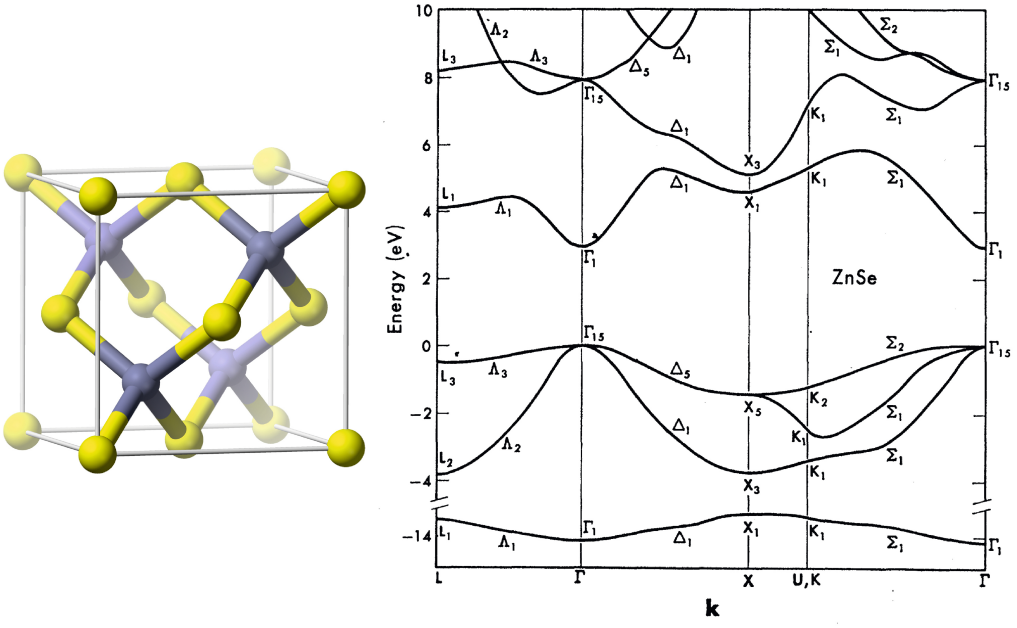

Figure 2.1: All zinc manganese selenide samples are crystallized in the zincblende structure. Zinc and manganese are situated at cationic sites while selenium and chlorine are on anionic sites (left). The main characteristics of the electronic bandstructure of zinc selenide still holds for zinc manganese selenide, they differ only slightly in terms of absolute values (right).

Zinc manganese selenide crystallizes like zinc selenide in the zincblende structure, cf. left hand side of figure 2.1. This was verified by Agarwal *et al.* [3] as well as by Hetterich *et al.* [24] in agreement with the previous work of Yoder-Short *et al.* [68]. Zinc manganese selenide belongs to the class of so called dilute magnetic semiconductors (DMSs), which will be discussed in detail in section 2.1.1.

In the literature there are various nomenclatures for zinc manganese selenide in use: mostly the constitutional formula $Zn_{1-x}Mn_xSe$, but also ZnMnSe, (Zn, Mn)Se and Zn(Mn)Se. General n-type doping for example would be indicated as n-ZnMnSe. To indicate a special dopand, for example chlorine, one may write ZnMnSe:Cl, beside just adding the prefix Cl-doped.

Agarwal *et al.* performed optical measurement on a sample with $x = 13\,\%$ manganese content and on a reference ZnSe-sample.[2] The authors showed that the effective mass in both materials increases with increasing carrier concentration. Extrapolating this data to $n = 0$ they obtain a conduction band effective mass $m^* = (0.093 \pm 0.08)\, m_e$ in zinc manganese selenide, which is lower than the known values of the pure host material zinc selenide, where $m^* = (0.135 \pm 0.005)\, m_e$[2] and references therein. Similar results are obtained by Hofmann *et al.* [25], with a value of $m^* = (0.086 \pm 0.004)\, m_e$ also for manganese content of $x = 13\,\%$. According to $\vec{k}\cdot\vec{p}$ theory a reduced effective mass may correlate with a reduced bandgap, which supports the strong bowing, cf. figure 6.1, and thus the starting point of our explanation.

The influence on the relative permittivity of zinc manganese selenide is less pronounced: $\varepsilon_{r,\infty} = 6.2 \pm 0.1$ [25] and $\varepsilon_{r,\infty} = 5.99$ [2], respectively, in comparison with $\epsilon_\infty = 6.11$ [2] for zinc selenide.

Both quantities, i.e. m^* and $\varepsilon_{r,\infty}$, have an influence on the donor in terms of binding energy and effective Bohr radius, as will be discussed in section 3.1 in more detail.

The incorporation of manganese into n-type zinc selenide has some known effects on the doping behavior. The main effect is the decreasing carrier concentration as the manganese

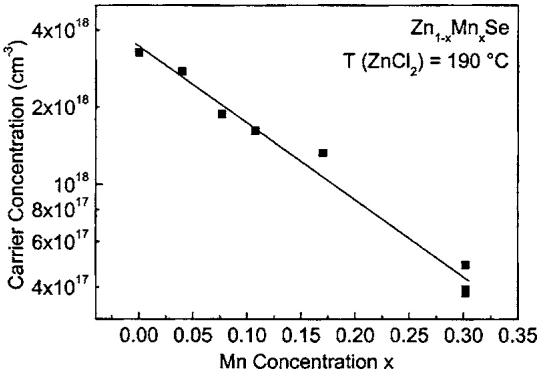

Figure 2.2: The carrier concentration n as a function of manganese content x from the work of Daniel *et al.* [9]. The carrier concentration in zinc manganese selenide shows roughly an exponential decrease as a function of the manganese content. The constant source temperature providing always the same nominal concentration of chlorine, i.e. donor atoms, should result in a rather constant carrier concentration. The origin of this discrepancy is unknown, but it could be related to the chlorine incorporation as well as to carrier traps.

content increases, while providing the same amount of donor atoms during growth and thus keeping its nominal concentration constant. This has been shown by Daniel *et al.* and its results are presented in figure 2.2.[9] There are two possible explanations. First, manganese and chlorine in this quaternary compound are no longer on the same lattice sites as in the ternary compounds, e.g. due to clustering of manganese and chlorine atoms or occupation of interstitial sites. Second, due to the presence of higher order manganese states like pairs, triplet and higher clusters electrons, contributing to the transport, could be trapped. In contrast to the isolated manganese states, which are located above the conduction band edge, these states extend below the conduction band edge. Daniel *et al.* suggest a related mechanism, in detail that these defect complexes act as carrier traps for conduction electrons.[9] Related to this a reduction of the maximal solubility of active donor atoms is observed, e.g. for $x = 13\,\%$ the dopability limit of the carrier concentration is just 1/5 of that in zinc selenide. Additionally the growth rate is increasing in the presence of manganese atoms, which was already considered in the discussion above.

The dependence of the direct energy band gap at the Γ-point, in the following referred to as band gap, on manganese content x in zinc manganese selenide exhibits a special feature. At low manganese contents it decreases with increasing x and before it starts to increase at higher manganese contents. In other words as a function of x the band gap, which is expected to increase linearly, shows a large bowing before it starts to tend towards a linearity. However in contrast common band gap bowing due to alloy disorder with the strongest effect at about $x = 50\,\%$, the bowing in zinc manganese selenide occurs only below $20\,\%$ of manganese. This topic is again relevant in section 6.1. All the details, including a figure depicting this effect, will be discussed there.

2.1.1 Dilute magnetic semiconductor (DMS)

Many properties of dilute magnetic semiconductors, also referred to as semimagnetic semiconductors, exhibit a strong dependence on magnetic fields due to the incorporation of magnetic ions into the host lattice. Such magnetic ions have a large number of unpaired localized electron spins in their core shells, examples are Cr, Mn, Fe, Co, Ni, etc. The physics of dilute magnetic semiconductors is somewhat a cross-discipline of the general field of semiconductors and the field of magnetism. In semiconductor physics the one-electron approximation in a periodic crystal is mainly used. While in magnetism many-particle phenomenona are important due to a variety of interactions. High quality growth of dilute magnetic semiconductor structures including low dimensional systems like quantum wells (QWs) and quantum dots (QDs) have in conjunction with the strong spin dependence of the electronic properties resulted in a new wave of activity in this field and made these materials applicable in modern devices.

A major advantage of the II-VI semiconductor zinc manganese selenide is based on its property that the content of the Mn^{2+}-cations $x_{Mn} \equiv x$ and donor density N_d can be tuned independently. Thus it is possible to adjust only the magnetic or only the electrical property by varying the corresponding quantity. In practice there is an interdependence of n and x that needs to be taken into account in order to compensate the effect depicted in figure 2.2. In the dilute magnetic semiconductor gallium manganese arsenide (GaMnAs), for example,

this it not possible as manganese in this case is simultaneously responsible for the magnetism and the electric doping.

2.1.2 Magnetic impurities

Manganese is an isovalent impurity on zinc site and below $x = 30\,\%$ zinc manganese selenide crystallizes in the zincblende structure, sometimes at even higher manganese contents by means of non-equilibrium epitaxial growth techniques such as molecular beam epitaxy (MBE).[37] Due to its five unpaired electrons in the 3d-shell each atom has a total angular momentum quantum number J of 5/2. This arises from the total spin ($S = 5/2$) and the total orbital momentum ($L = 0$) for the ground state of the 3d-shell and therefore in the following J will be referred to as manganese spin, which is short and commonly used but not quite correct. Zinc manganese selenide can be described well as a paramagnetic semiconductor as long as the manganese content is low. But due to the fact that manganese atoms couple antiferromagnetically to one another by superexchange interaction, in the limit of manganese selenide the crystal is antiferromagnetic. Fatah *et al.* could show that only the spins of nearest neighbor (NN) manganese atoms are compensating each other by antiferromagnetic pairing.[16] This behavior explains why in zinc manganese selenide the paramagnetic phase is dominant at low manganese contents and why the antiferromagnetic interaction becomes more and more dominant at high manganese contents. As the effect of this antiferromagnetic coupling scales with the amount of manganese this effect is small in our samples. In general it reduces the actual number of paramagnetic centers, so we are dealing with an effective manganese content $x_{\mathrm{eff}} = \bar{x} < x$ instead of the atomic amount x itself. Figure 2.3 shows the theoretical dependece of x_{eff} versus x done by Fatah *et al.* [16]. Experimental results by Heimbrodt and Klar [23] as well as by Twardowski *et al.* [65] support this statement.

The following considerations are for an ideal system in mean-field approximation, i.e. with

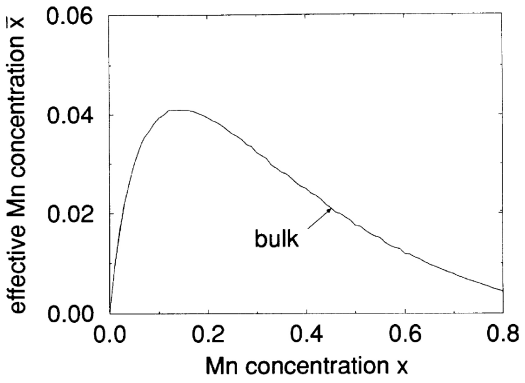

Figure 2.3: The effective manganese content $x_{\mathrm{eff}} = \bar{x}$ as a function of the atomic manganese content x modified from the work of Fatah *et al.* [16]. The dependence starts lineary at low x before it grows less and reaches its maximal value at around 15 %. Beyond that point it starts to decrease. This dependence results from the antiferromagnetic coupling of neighboring manganese atoms. Thus they no longer act as free spins and do not contribute to the paramagnetism as their total spin $S_{\mathrm{tot}} = 0$.

a homogeneous manganese distribution in space even on a microscopic level, in consequence a regular arrangement. So one can easily average over all the manganese ions in the crystal and look at only the mean value with no fluctuations. In chapter 6 we will come to the limits of this concept.

The mean magnetization M of such a system can be well described by the Brillouin function $\mathrm{B}_J(\xi)$,[23, 50]

$$M = N_0\, x_{\mathrm{eff}}\, g\, \mu_{\mathrm{B}}\, J\, \mathrm{B}_J(\xi)\ . \tag{2.1}$$

Here, x_{eff} is the effective manganese content, N_0 is the number of cations per unit volume and $J = 5/2$ is the manganese spin. The Landé factor of the 3d electrons in zinc manganese selenide is $g = 2$, and $\mu_{\mathrm{B}} = 5,788 \times 10^{-5}\,\mathrm{eV/T}$ is the Bohr magneton. The Brillouin function gives the measure of the spin polarization, i.e. the degree of manganese spins aligned to the external magnetic field and is defined as

$$\mathrm{B}_J(\xi) = \frac{2\,J+1}{2\,J}\coth\left(\frac{2\,J+1}{2\,J}\,\xi\right) - \frac{1}{2\,J}\coth\left(\frac{1}{2\,J}\,\xi\right)\ , \tag{2.2}$$

where ξ is the ratio of the Zeeman energy of the magnetic moment in the external field to the opposing energies. The energy of the thermal disorder $k_{\mathrm{B}}\,T$ and that of the antiferromagnetic interaction $k_{\mathrm{B}}\,\Theta$ oppose the paramagnetic ordering of the spins in a magnetic field. It is given by

$$\xi = \frac{g\,\mu_{\mathrm{B}}\,J\,B}{k_{\mathrm{B}}\,(T+\Theta)}\ , \tag{2.3}$$

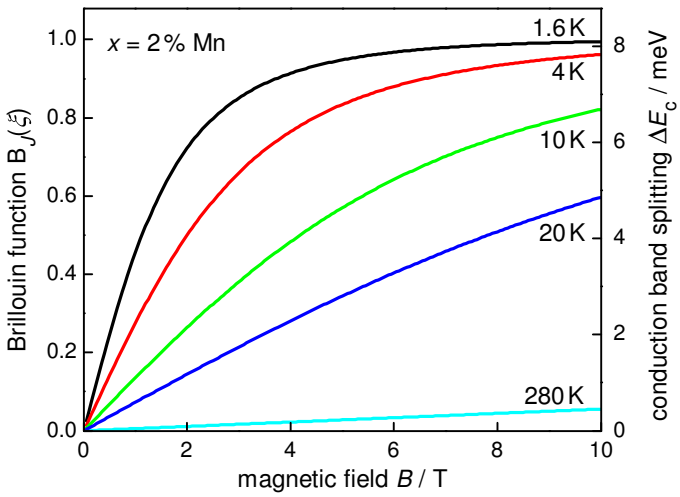

Figure 2.4: The Brillouin function $B_J(\xi)$ and the conduction band splitting ΔE_{c} as a function of magnetic field at some exemplary temperatures for the paramagnetic system zinc manganese selenide. The x-independent spin polarization, i.e. the degree of spin alignment, $B_J(\xi)$ shows its characteristic saturation, which occurs at lower magnetic fields for lower temperatures. The conduction band splitting ΔE_{c} is the energetic distance between the two spin states for a given manganese content (2 %). As in this case it is proportional to the Brillouin function, just like the magnetization, all three of them exhibit the same characteristics.

where k_B is the Boltzmann constant, T is the absolute temperature. The Curie-Weiss-like temperature Θ is introduced just like x_{eff} to account for residual antiferromagnetic coupling between manganese neighbours.

A plot of the Brillouin function versus the external magnetic field according to equation (2.2), is shown in figure 2.4 for various temperatures. The magnetization like the Brillouin function initially grows with increasing magnetic field, as the magnetic field tends to align the manganese spins of the atoms. The magnetization saturates when the spins are aligned along the field direction. On the other hand, increasing the temperature at a fixed magnetic field decreases the magnetization, because thermal fluctuations reduce the manganese spin alignment.

The Brillouin function also directly determines the conduction and the valence band splitting of spin-up and spin-down states as a function of magnetic field and temperature. In a dilute magnetic semiconductor this effect is called giant Zeeman splitting (GZS). In comparison the Landau level splitting and normal Zeeman level splitting are negligible at low temperatures, both effects are more than an order of magnitude smaller.

The giant Zeeman splitting occurs due to s,p-d exchange interaction between the extended band states of the host material and the localized magnetic moments of the 3d-shells of the magnetic impurities. The splitting occurs in the conduction band (s-d interaction) as well as in the valence band (p-d interaction). However, as we are dealing with transport in a n-type material, only the conduction band splitting ΔE_c, i.e. the energy difference between spin-up and spin-down states presented in figure 2.6, due to s-d exchange interaction is of relevance

$$\Delta E_c = N_0\,\alpha\,x_{\text{eff}}\,\langle J_z\rangle = N_0\,\alpha\,x_{\text{eff}}\,J\,\mathrm{B}_J(\xi), \tag{2.4}$$

where α and $N_0\,\alpha$ are the s-d exchange interaction parameter and energy, respectively, N_0 is again the density of cationic sites, and $\langle J_z\rangle = J\,\mathrm{B}_J$ is the average spin of a manganese atom in z-direction, i.e. the direction of the external magnetic field. In figure 2.5 one sees that the conduction band splitting as well as the magnetization increases for increasing manganese content x, e.g. for different samples.

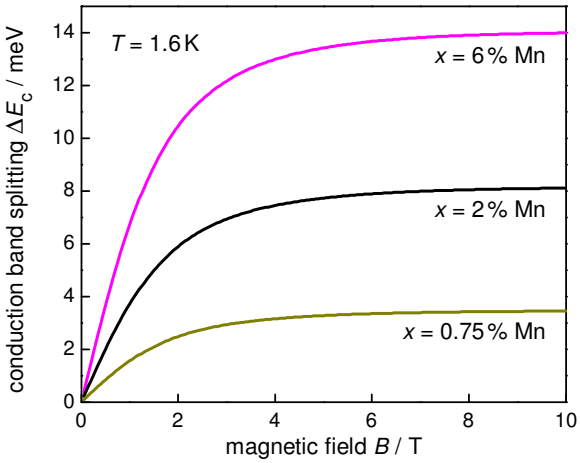

Figure 2.5: The conduction band splitting increases for a given temperature (1.6 K) with increasing manganese content according to equation (2.4) where the effective manganese content is considered.

The energy splitting is symmetric. The energy shift of each spin state relative to the energy in zero field E_0 therefore is $\Delta E_c/2$. The splitting affects not only the extended conduction band states but also the energy of the donor states, as every of these is a superposition of conduction band states, cf. chapter 3. The magnetic field induced lifting of the degeneracy of spin-up and spin-down states can be described as the shifts of two corresponding spin sub-densities of states. Also these facts are schematically illustrated in figure 2.6.

Going beyond this ideal model there are a number of additional aspects which have to be considered. A random distribution of manganese atoms in space throughout the crystalline layer is assumed in concordance with theoretical simulations.[16] Statistics tells us that in this case within specified volumes a certain degree of disorder arises. There will be regions in the layer where the manganese amount will be higher or lower than average. This local manganese distribution $x_{\mathrm{eff}}(\mathbf{r})$ has not only consequences for the local magnetization and conduction band splitting but also for the band gap and thus for the energetic position of the conduction band edge. A detailed analysis of these consequences will be described in chapter 6.

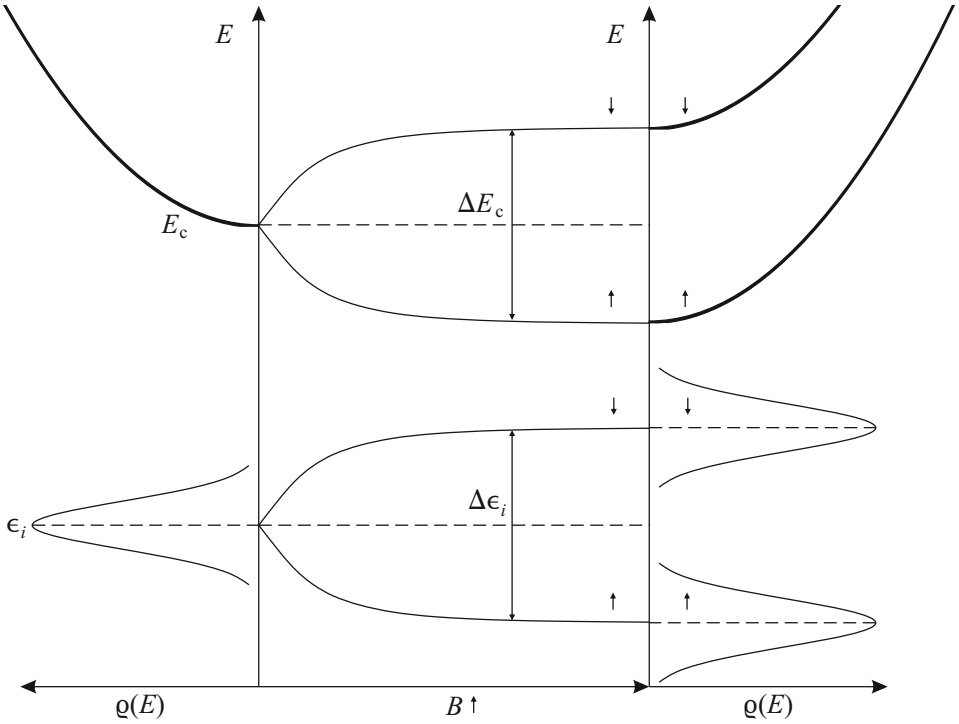

Figure 2.6: The giant Zeeman splitting leads in absolute energies to the depicted schematic situation. The preferential spin orientation shifts to lower energies, while the opposite spin direction shifts to higher energies. This holds for the conduction band states as well as for the donor states. The difference between spin-up and spin-down states is the conduction band splitting ΔE_c. That the density of impurity states does not change its shape, as shown here, does not hold for zinc manganese selenide as will be presented in figure 6.3.

2.1.3 Model devices for spintronics

2.1.3.1 Spin-aligner and spin-injector

A strength of zinc manganese selenide is its suitability to provide spin-polarized charge carriers and to inject them electrically, i.e. voltage driven, into III-V optoelectronic devices at low temperatures. The alternative is to induce spin polarization by optical means. This is of course also quite easy but an additional optical pump device like a laser is needed. Thus polarized light is produced via the optical selection rules for interband transitions yielding a spin asymmetry of the electrons excited into the conduction band. Therefore the direct way of electrically providing polarized electrons has a higher energy efficiency and eliminates the necessity of optical devices. A different commonly used approach is to make use of a ferromagnetic metal contact and then inject spin polarized electrons into a semiconductor. Unfortunately this yields only a poor spin polarization, which is attributed to spin flipping processes at the interface. Because of the reasons given below dilute magnetic semiconductors are best suited for this purpose.

Zinc manganese selenide on gallium arsenide is a good material combination for various reasons. First, due to the conduction band offset between ZnSe and GaAs of less than 100 meV, electrons may be injected close to the bottom of the conduction band of gallium arsenide. Also it is possible to grow these two materials lattice matched on top of one another with a small amount of beryllium on cation site of zinc selenide.[17] However, spin-injection also works if there is a small lattice mismatch, i.e the growth is pseudomorphic.[31] So it seems more important that both materials are semiconductors and that they posses a suitable band alignment. If this requirement is fulfilled, there seems to occur no measurable spin flipping at the interface. In addition the spin-dephasing time for electrons in gallium arsenide is long, so that the preferential spin will have a long diffusion length, accordingly. For these reasons light-emitting diodes (LEDs) or transistors can be provided with spin polarized carriers.

Speaking of the charge carriers, one should mention that the use of electrons for spintronic application based on zincblende semiconductors is preferable to that of holes as the effects of spin-orbit coupling are negligible and thus only two spin bands are present instead of four. In literature heavily doped n-type zinc manganese selenide layers as well as lightly n-type doped ones have been used successfully as spin-injectors, both providing spin-polarized charge carriers.

Material combinations as described above may achieve spin injection efficiencies above 90 % and near unity. This is evident in circular polarized electroluminescense of spin-LEDs, where carriers are spin polarized by zinc manganese selenide and injected into the optical active gallium arsenide.

The spin alignment itself is achieved in the dilute magnetic semiconductor by the giant Zeeman splitting of the conduction band and impurity states and the redistribution of electrons into the energetically favorable lower Zeeman level. This redistribution happens on a picosecond time scale and thus only a thin layer of spin-aligner is needed. The polarization shows the temperature and magnetic field dependence of the spin splitting according to the Brillouin function. Unfortunately the saturation of the splitting at easy accessible fields and a low

thermal disorder is only sufficient at very low temperatures. These circumstances reduce the practical applicability. Nevertheless such devices are ideal model systems for studying spin phenomena in semiconductors and provide essential knowledge for future applications.

Until an ideal system of a ferromagnetic semiconductor that is able to inject electrons into electronics and can operate at room temperature is found, spin electronics remains mainly an interesting research field with niche applications. Good overviews are given by Oestreich [46] and by Heimbrodt and Klar [22].

2.1.3.2 Spin-LED

Asshoff *et al.* gave an example of a spin-LED in their work.[6] Löffler *et al.* alternatively used quantum dots to achieve near unity polarization.[38] Oh *et al.* [47] as well as Kim *et al.* [33] also reported near unity spin polarization for cadmium selenide (CdSe) quantum dots in a zinc manganese selenide matrix.

2.1.3.3 Spin superlattice

Dai *et al.* showed that it is possible to create spin superlattices of ordered of spin-up and spin-down states in a desirable design containing zinc manganese selenide.[8]

2.1.3.4 Spin filter

It is proposed that zinc manganese selenide can act as a spin filter. Therefore a layer structure of ZnSe/ZnMnSe/ZnSe is suitable. In this system the ZnMnSe would be a barrier for one spin orientation while it would be a well for the other orientation. Thus almost only the desired spin would pass this structure and one can switch between the certain spin directions. This concept was suggested and theoretically analyzed by Egues.[15] The experimental proof of principle of this concept was given by Papp *et al.* [48] and by Guo *et al.* [20].

2.1.3.5 Spin-Transistor

A spin-transistor shows the same characteristics as a normal one, but the kind of binary information is changed from the two states voltage and no-voltage to spin-up and spin-down. So it would be controlled by the electron spin and is an essential spintronic device that can be intergrated in spin quantum computers, cf. the work of Imamoglu *et al.* [27].

2.1.3.6 Quantum cryptography

A way to encode information in a transmitting processes is to use quantum cryptography. By this pirated information would be useless, because only sender and the intended receiver will have the original information. To produce such spin- or polarization-encoded information spintronic devices are needed. A corresponding patent is to be found in the work of Jonker *et al.* [31].

2.1.3.7 Novel evolution

Recently with the works of Thurn *et al.* the focus has changed to the spin dynamic in such systems, cf. [64], and the difference between averaging and randomly distributed system, cf. [63], are of interest.

Also spin dependent transport in the variable range hopping regime is of interest.[55]

Chapter 3

Electronic Impurities

3.1 Shallow donor

In the zinc manganese selenide samples studied chlorine was used as n-type dopant, which substitutes selenium in the host lattice. Only four of its five outer electrons are needed for the bonding to the surrounding atoms in the crystal and thus it provides an additional electron. This spare electron is just loosely bound to the donor atom. The density of chlorine atoms also denoted as chlorine, donor or doping concentration will be indicated by N_{Cl}, while also N_{d} or N_0 are used in the literature. The donor has an ionization or binding energy E_{d}, also E_{Cl} or E_0, in ZnSe of about 26 meV.[1] This value is not the absolute energetic position but the energetic distance to the conduction band edge. The absolute energy level is always situated below the conduction band edge in the otherwise forbidden band gap. Therefore it is also referred to as donor depth. As in zinc manganese selenide this energy is very small compared to the band gap energy E_{g}, the wavefunction of a donor electron spreads out over many cubic lattice constants. Thus the host lattice acts as an average background medium only determined by its relative permittivity ε_{r} compared to vacuum. The situation can be described by an effective medium approximation, where an electron is bound to a single positive charge. As this situation is comparable to a hydrogen atom, such a shallow donor is referred to as hydrogen-like. So the description of the hydrogen atom and the results of the calculations are also applicable here with small variations. The static vacuum permittivity ε_0 is replaced by the absolute permittivity of the crystal $\varepsilon = \varepsilon_{\mathrm{r}}\,\varepsilon_0$, and the free electron mass m_{e} is replaced by the conduction band effective mass m^*. Consistently the Bohr radius a_0 is replaced by the effective Bohr radius a_{B}. In semiconductors the Bohr radius is also referred to as localization length, depending on the theoretical model used. Thus the absolute energy of the ground state is $E_{\mathrm{c}} + E_{n=1}$, where $E_{n=1}$ is given by

$$E_{n=1} = -E_{\mathrm{d}} = -\mathrm{Ry}\,\frac{m^*}{\varepsilon_{\mathrm{r}}^2\, m_{\mathrm{e}}}\left(= -\mathrm{Ry}\,\frac{a_0}{\varepsilon_{\mathrm{r}}\, a_{\mathrm{B}}}\right)\,, \tag{3.1}$$

where $\mathrm{Ry} \approx 13.6\,\mathrm{eV}$ is the Rydberg unit of energy, $a_0 \approx 53\,\mathrm{pm}$ is the Bohr radius and a_{B} is the effective Bohr radius given by

$$a_{\mathrm{B}} = \frac{\varepsilon_{\mathrm{r}}\, m_{\mathrm{e}}}{m^*}\, a_0\,. \tag{3.2}$$

In contrast to the ionization energy E_d relative to the conduction band edge the absolute energy position of the donor i is referred to as ϵ_i. The envelop function of the ground state is given by

$$\phi(r) \propto \frac{1}{\sqrt{\pi\, a_\mathrm{B}^3}} \exp\left(-\frac{r}{a_\mathrm{B}}\right), \tag{3.3}$$

where r is the radial distance to the specific donor.

3.2 Transport mechanisms

The electrons provided by donors can contribute in different ways to the electric transport depending on the temperature range and the doping concentration, which yields different transport mechanisms in an n-type material discussed in this section. One has to keep in mind, that the transport mechanisms applicable in a certain temperature range are present at all temperatures, but that a measurement is dominated by the one that yields the best conductivity in this range. So to speak, these mechanisms correspond to a parallel connection in an equivalent circuit diagram. In this context the temperature dependence of the electrical resistivity ρ is given by

$$\frac{1}{\rho(T)} = \frac{1}{\rho_1(T)} + \frac{1}{\rho_2(T)} + \frac{1}{\rho_3(T)} \tag{3.4}$$

$$\Leftrightarrow \rho^{-1}(T) = \rho_1^{-1} \exp\left(-\frac{\varepsilon_1}{k_\mathrm{B}\,T}\right) + \rho_2^{-1} \exp\left(-\frac{\varepsilon_2}{k_\mathrm{B}\,T}\right) + \rho_3^{-1} \exp\left(-\frac{\varepsilon_3}{k_\mathrm{B}\,T}\right), \tag{3.5}$$

where k_B is the Boltzmann constant, T is the absolute temperature, ρ_i are constants and ε_i are activation energies. The first summand with ρ_1 and ε_1 belongs to the band transport

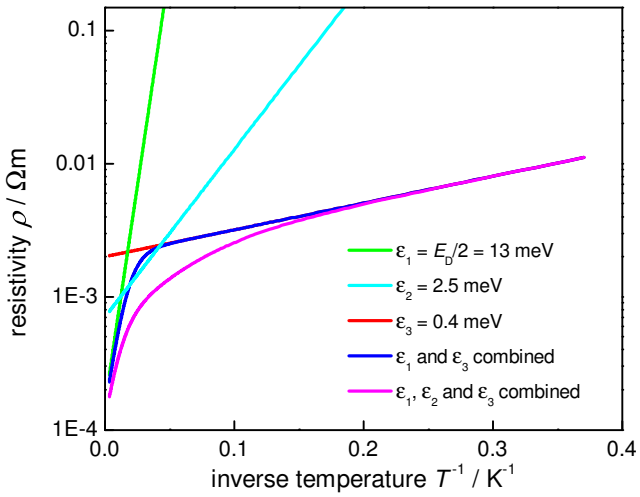

Figure 3.1: Simulation of an Arrhenius plot with 3 different activation energies ε_i and ρ_i. The nature of this being a parallel connection in an equivalent circuit leads to the two resulting curves with and without ε_2. Typically one conduction mechanism dominates in a certain temperature-interval, to be seen by its characteristic slope being proportional to ε_i. Kinks indicate roughly the transition from one to the other.

described in the section below, the second summand with ρ_2 and ε_2 belongs to transport via double occupation in section 3.2.2 and the third summand with ρ_3 and ε_3 belongs to the hopping transport in section 3.2.3. Typical situations are illustrated in figure 3.1.

As doping of a semiconductor is a statistical process it yields a random distribution of donor atoms in the host lattice. This will be of importance later.

In the following the transport mechanisms will be explained in order of decreasing temperature and thus from wider known basics to more specialized cases. The figures shown as well as the mechanisms themselves will sometimes anticipate knowledge that is presented in detail not before the following chapters. So some aspects will be better understandable after reading the whole transport mechanism chapter.

3.2.1 Band transport

Thermally activated transport in the conduction band, also referred to as phonon-assisted band transport, describes the situation where at high temperatures the dominant transport mechanism takes place in the conduction band of the n-type semiconductor.

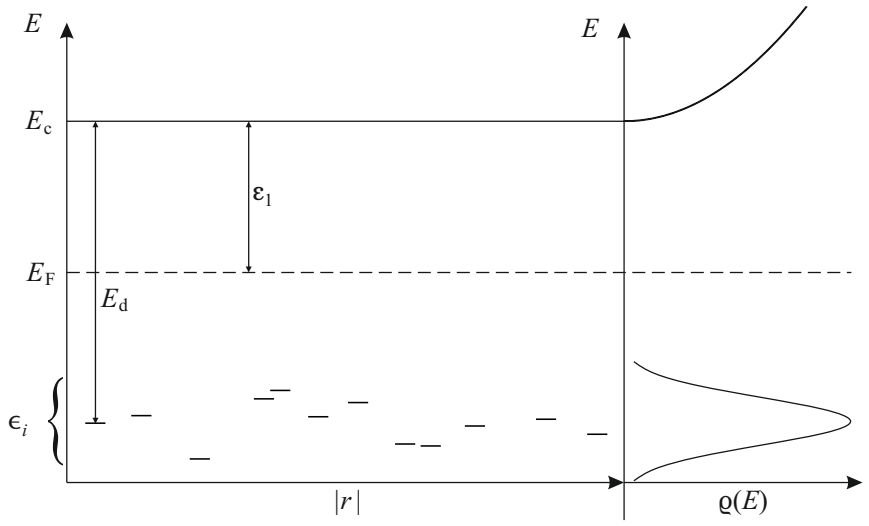

Figure 3.2: Depicted is the energy of the conduction band edge and of the donor states as a function of the location along a percolation path (left). This is compared with the density of states of the conduction band and of the donor states as a function of energy, which is rotated for that reason (right). No schematic bandstructure is shown. Electrons are thermally activated into the conduction band, where they may provide a good electrical conductivity. The Fermi level lies roughly in the middle between the energy of the conduction band edge E_c and the average donor energy $\langle \epsilon_i \rangle$, reflecting a situation with low compensation and a high enough thermal energy. Thus the activation energy ε_1 posses roughly half the value of the ionization energy E_d, i.e. the donor depth. The presented band transport needs high enough temperature, i.e. the thermal energy has to be comparable to the donor depth. As the conductivity is determined by the activated electrons relative to the bound ones, this temperature range is called freeze-out region.

In this case high temperature means that the thermal energy $k_\mathrm{B}\,T$ is comparable to the activation energy ε_i and thus to the ionization energy of the donor E_d, so that a sufficient number of donors are ionized, i.e. that their electrons are no longer bound to a chlorine atom but act as delocalized charge carriers throughout the crystal. Only these carriers contribute to this branch of conductivity as they move through the crystal and are scattered on their paths. This situation is called diffusive transport and a schematic illustration is given in figure 3.2. This circumstance gives rise to the measurable resistivity ρ, which can be analyzed in terms of the free carrier concentration n and total carrier mobility $\mu = \mu_\mathrm{tot}$. The basic dependence, cf. equation (4.1), is given by

$$\frac{1}{\rho} = \sigma = e\,n\,\mu\,, \tag{3.6}$$

In the following n will be called carrier concentration in accordance with the majority of the literature, but one has to keep in mind that it indicates the 3D density of the free charge-carriers. For a n-type semiconductor that are the electrons activated into the conduction band. Other common notations for this quantity are n_e or n_0. For the mobility there is to say that each effect like phonon scattering, scattering by ionized impurities, scattering by isovalent impurities etc. gives its own temperature-dependent mobility limitation, together they yield the total mobility of the charge carriers according to Matthiessen's rule

$$\frac{1}{\mu_\mathrm{tot}(T)} = \sum_i \frac{1}{\mu_i(T)}\,, \tag{3.7}$$

where i indicates the different possible scattering mechanisms mentioned above.

Using Maxwell-Boltzmann statistics and thus ignoring the Pauli exclusion, the temperature dependence of the carrier concentration at low doping concentrations is mainly determined by the following Boltzmann factor

$$n(T) \propto \exp\left(\frac{E_\mathrm{F} - E_\mathrm{c}}{k_\mathrm{B}\,T}\right), \tag{3.8}$$

where E_c is the energy of the conduction band edge and E_F is the Fermi level. The difference of these two energies is referred to as activation energy $\varepsilon_1 = E_\mathrm{c} - E_\mathrm{F}$. In the case of n-type extrinsic band transport the Fermi level E_F lies practically between the energetic position of the donor level E_d and that of the conduction band edge E_c. The activation energy ε_1 therefore resembles half the the ionization energy of the donor ($\varepsilon_1 \approx E_\mathrm{d}/2$). Using the antiproportionality of resistivity and carrier concentration cf. section 4.3, while neglecting the weaker temperature dependence of the mobility, the resistivity contribution

$$\rho_1(T) = \rho_1\,\exp\left(\frac{\varepsilon_1}{k_\mathrm{B}\,T}\right) \tag{3.9}$$

follows. This equation provides the first summand in the equations (3.4) and (3.5) resulting from the above mentioned simplifications.

There is a rapid increase in resistivity with decreasing temperature due to the recapturing of the carriers by the donor atoms according to equation (3.8). This is the reason why this temperature range is also referred to as freeze-out region. The conduction in the impurity band, which takes place at low temperatures can be very poor. In this case the sample shows a high resistance and due to measuring device limitations no second and third summand in the equations (3.4) and (3.5) is observable. This is equivalent to figure 3.1 consisting only of the green ε_1-curve.

3.2.2 Double occupation

Conductivity via double occupation is an effect which may take place. If this is the case, it takes place between the temperature ranges of dominating conduction band (ε_1) transport and dominating hopping transport (ε_3). This fact explains the nomenclature of this as ε_2-conductivity. The main idea is that like in a hydrogen atom even two electrons can be bound to one donor atom in the 1s ground state. Of course, this situation is not the energetic ground state. Energy is needed to create such a double occupied and negatively charged donor. The nature of the transport is a thermally activated tunneling of electrons from donor to donor, a hopping transport process.

The amount of energy to put another electron to an already occupied donor is called Hubbard energy U. This energy is provided by thermal activation and like before the activation energy ε_2 has approximately half its value $\varepsilon_2 \approx U/2$. If an electron has gained the energy U and occupies such a state, the conductivity through the sample is very high compared to classical hopping transport. This is a result of the energy level being higher in energy than the ground state which is accompanied by a larger overlap of the donor wavefunctions in the almost empty Hubbard band. This band also posseses a larger impurity band-width of these exited states due to the larger spatial overlap of the corresponding states. The distinct appearance of this mechanism strongly depends on the Hubbard energy in comparison to the donor ionization energy. If these two energies are to close, meaning that the difference between the absolute levels is comparable to the donor depth, this behavior is not observed. According to Agrinskaya *et al.* [4] the connected argument is formulated, ε_2-conductivity is

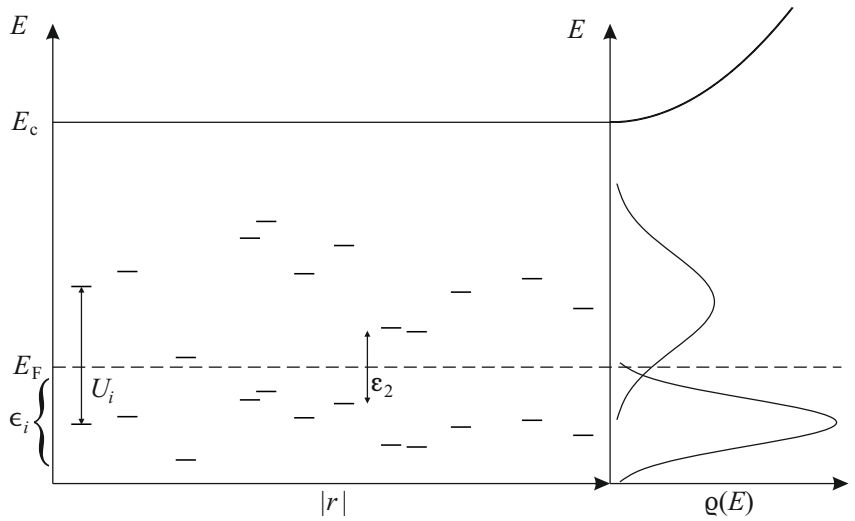

Figure 3.3: In the presence of a Hubbard band the situation depicted in figure 3.2 is extended by the density of states of double occupied donor sites. If the Hubbard energy U is small compared to the donor depth and if the thermal energy is comparable to the activation energy ε_2, this mechanism may yield a contribution to the electron transport. The Fermi level then lies between the distributions of single and double occupied states. The electron transport is due to hopping from a single or double occupied donor site to an empty or single occupied one.

important when U is close to ε_3, which is the case near the metal–insulator transition. And like in the case of variable range hopping, cf. section 3.2.3.2, double occupation may not be the origin of minor effects in the temperature dependence.

Double occupation has some consequences. For example a spin flip may be needed to fulfill the Pauli principle. This is relevant at low temperatures as the conduction electrons in zinc manganese selenide show a large spin polarization even at low external magnetic fields.

3.2.3 Hopping transport

As already mentioned this transport in the impurity band must not significantly contribute to the electrical conductivity. The criterion for this to occur is the concentration of donor atoms, in our case N_{Cl}, to be above a certain magnitude. Below it the wave functions of different donor atoms would be very far apart and thus be isolated, i.e. they have no significant overlap and cannot secure carrier propagation throughout the crystal.

Only above this concentration of donor atoms, also depending on the measurement equipment, hopping transport can be observed.[1] This means electrons move through the crystal by a multitude of hopping events each from one donor site to the next possible donor site. So the macroscopic conduction effect is only recognizable, if percolation paths extend through the entire sample. An example is given in figure 3.4. As this form of transport is different from the classical picture of a free electron gas, also the interpretation of the Hall-measurements in terms of deducing quantities n and μ fails. This is in contrast to the cases of band and metallic-like transport, where this interpretation of measurements in terms of n and μ is applicable.

[1] Only samples, which show conduction inside the impurity band, are presented in this work.

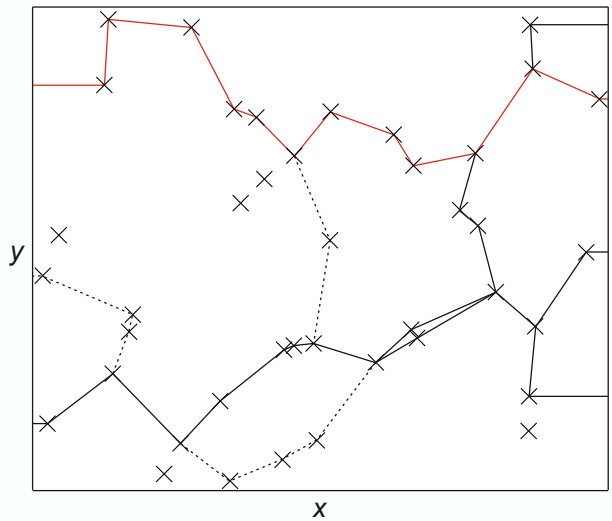

Figure 3.4: In hopping transport charge carriers move along so called percolation paths. To ilustrate this, a simulated 2D random pattern of donor sites with some resulting percolation paths though it is shown. One can see that there are not only isolated paths from the left edge to the right one, but that there are connections between paths, parallel segments as well as dead ends.

The impurity band, where hopping transport takes place, is not an actual band, like the conduction or valence band that are the consequence of a periodically ordered crystal. But it denotes the density of states (DOS) of all impurity levels $\{\epsilon_i\}$, which consists of the energetic position of randomly distributed interacting donor atoms. The energy spread of the impurity band due to level repulsion of the donor energies is very small at low concentrations as every level does not interact with its neighbors and thus is supposed to have the same donor depth. The impurity band becomes wider the more donor atoms are present. This is due to level repulsion as the donor wave functions begin to overlap although we do not have exactly the same situation as for band-formation out of atomic states in a periodic crystal. Furthermore in ternary systems there is also an initial width of the impurity band $\{\epsilon_i, 0\}$ resulting from slightly different energetic positions of the conduction band edge due to chemical shifts, i.e. local variations in the stoichiometry, cf. section 6.1.

Hopping itself is a combined process of thermal activation to gain energy and a tunnel-probability to travel a distance through a barrier. Thermal activation means to absorb a phonon of the amount of energy that is needed to fulfill energy conservation. Miller and Abrahams described the hopping rate exhibiting both contributions for a single hopping event from one site to another by [5, 41]

$$\Gamma_{i,i'} = \nu_0 \exp\left(-2\,\frac{r_{i,i'}}{a_\mathrm{B}}\right) \begin{cases} \exp\left(-\frac{\Delta\epsilon_{i,i'}}{k_\mathrm{B}\,T}\right) & \text{when } \Delta\epsilon_{i,i'} > 0 \\ 1 & \text{when } \Delta\epsilon_{i,i'} \leq 0 \end{cases}, \tag{3.10}$$

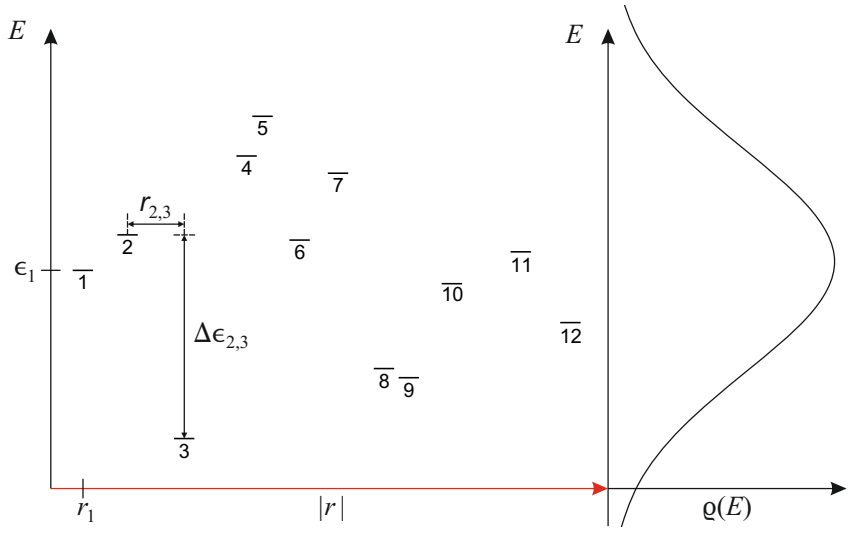

Figure 3.5: The complexity and interconnection of percolation paths, cf. figure 3.4, has to be abandoned to illustrate the following point. Along a simplified 1D percolation path every donor can be described by the distance to its neighbors and its energy. Not only the sites are randomly located, which leads to random distances $r_{i,i'}$, but also every donor energy ϵ_i has a random value inside the density of states $\varrho(E)$ (right) leading to random energy distances $\Delta\epsilon_{i,i'}$. Hopping transport occurs only alongside a multitude of such paths where for the time being an electron can only hop to its direct neighbors. So the conductivity is mainly determined by the limiting steps, the highest $\Delta\epsilon_{i,i'}$ and largest $r_{i,i'}$.

where ν_0 is the attempt-to-escape frequency. The hopping rate $\Gamma_{i,i'}$ from a site i to a site i' depends exponentially on the distance $r_{i,i'} = |\mathbf{r}_{i'} - \mathbf{r}_i|$ between them and on the difference of their energies $\Delta\epsilon_{i,i'}$, which is given by

$$\Delta\epsilon_{i,i'} = \epsilon_{i'} - \epsilon_i - e\,\mathbf{E}\cdot(\mathbf{r}_{i'} - \mathbf{r}_i)\;, \tag{3.11}$$

where $\mathbf{E}$ denotes the external electric field and $\mathbf{r}_i$ and ϵ_i are the position and energy of donor site i, respectively. The hopping rates apply for every individual hopping event contributing to the electric current. This scenario is depicted in figure 3.5.

A few implications of equation (3.10) should be pointed out. The exponential dependence on the distance between two sites results from the exponential term in the envelop function in equation (3.3) and the corresponding dependence of the overlap between two donor wavefunctions. For hopping to occur there have to be vacant donor sites as well as occupied ones. Otherwise with all the states occupied an electron would be unable to move to another site and thus to move at all. To provide empty sites partial compensation is needed. The degree of compensation is denoted by K. As the resistivity ρ is determined by the hopping rates $\Gamma_{i,i'}$ both depend on ν_0, a_B, N_Cl (and consequently also on the position of every single donor atom $\mathbf{r}_i$), K, the donor density of states $\{\epsilon_i(B,T)\}$ and T. All of the parameters are constant for a given sample, except for the last two as we will see in the following.

Correlation between hopping sites may also affect hopping transport. In this context correlation means that two neighboring hopping sites share a certain part of their environment. In our case the characterizing element will be the manganese atoms in the direct vicinity. So every pair of donor atoms shares the manganese atoms between them. So the number of manganese atoms near each single donor is not totally random, but somewhat correlated. In

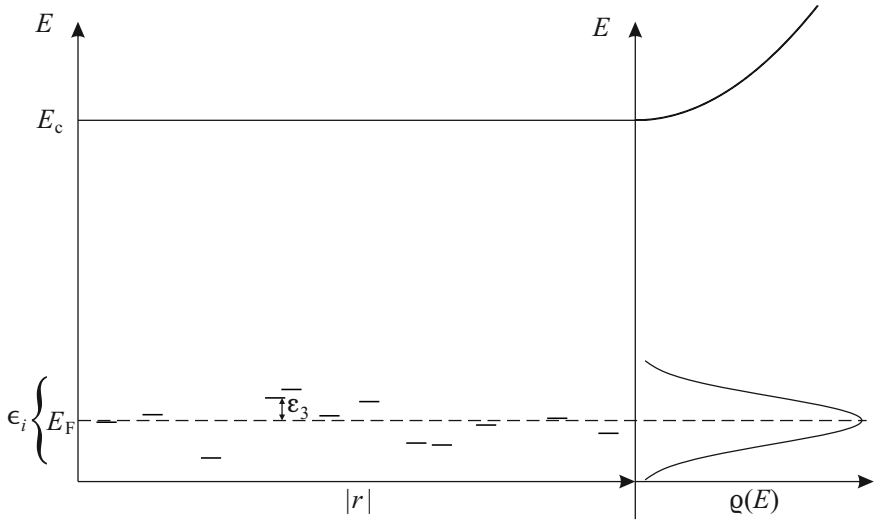

Figure 3.6: Hopping transport takes place only inside the impurity band along percolation paths, cf. figures 3.4 and 3.5. The density of states of the impurity band results from the random donor energies. In the case of a half filled impurity band, i.e. a degree of compensation of 0.5, the Fermi level lies in the middle of its density of states. The thermal energy has to be comparable to ε_3 and thus to the limiting steps. The width of the impurity band relative to the donor depth is depicted larger than it usually is for presentation reasons.

our case the result is that the absolute donor energy levels are no longer entirely statistical distributed but depend on one another. This correlation is of course strongest, if the two donors are close in space in terms of the Bohr radius, and the correlation decreases with increasing distance between donors. As in hopping transport the limiting steps are those between rather distant distinct donors that still contribute to a percolation path, their correlation will be small.

3.2.3.1 Nearest neighbor hopping (NNH)

The following describes the case of the so called nearest neighbor hopping. Meaning that the temperature is high enough to activate an electron from its donor to the nearest donor, which therefore has to be empty. The probability for this activation is not limited by the energy position of the empty donor. Thus the majority of the hopping events occurs, as the name says, between donors closest to one another. Like for the former mechanisms hopping transport is depicted schematically in figure 3.6

Like in the band transport regime, a Boltzmann factor is prominent in the formula for hopping transport, meaning that we have thermally activated transport again.

$$\rho_3(T) = \rho_3 \exp\left(\frac{\varepsilon_3}{k_\mathrm{B}\,T}\right), \tag{3.12}$$

where the activation energy ε_3 is comparable to the limiting $\Delta\epsilon_{i,i'}$.

The Fermi-Dirac distribution on the left of figure 3.7 holds for the occupation of these states. The Fermi level E_F lies inside the impurity band itself between the occupied and

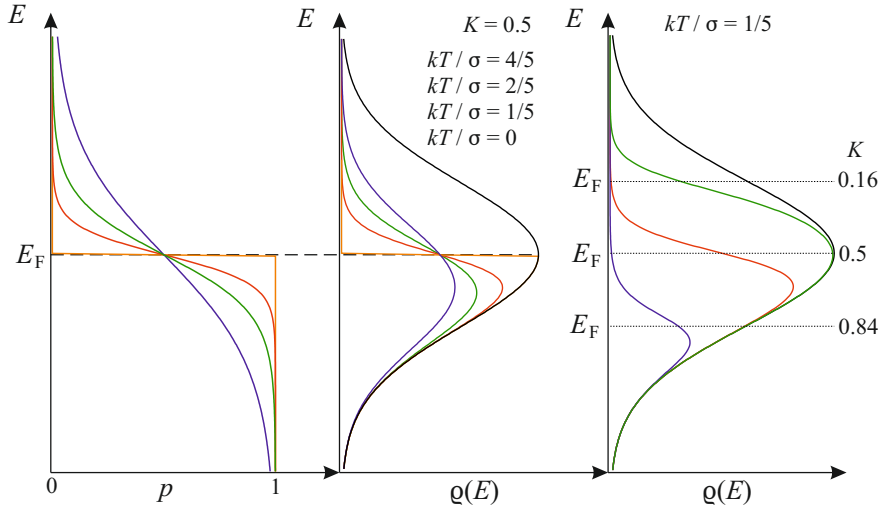

Figure 3.7: left: The Fermi-Dirac distribution for different temperatures gives the probability p to find a Fermion, e.g. an electron, at a certain energy E. The distribution is symmetric around the Fermi level E_F. Applying this on a density of impurity states with $K = 0.5$ yields the thermal occupation inside the impurity band. For low temperatures, i.e. low thermal energy $kT = k_\mathrm{B}\,T$, the Fermi edge becomes clearer. For lower or higher degrees of compensation K the Fermi level changes inside the impurity band.

the unoccupied impurity states. The occupation itself is determined by the density of states $\varrho(E)$, the Fermi-Dirac distribution, the compensation and the temperature as illustrated in figure 3.7.

3.2.3.2 Variable range hopping

At very low temperatures the character of the hopping mechanism may change from nearest neighbor hopping to variable range hopping. In this case the thermal energy needs to be considerably smaller than the impurity band-width. Basis is that the hopping rates are high for a 4-dimensional closeness of the donor sites involved, i.e. close in energy $\epsilon_i \approx \epsilon_{i'}$ and close in space $x_i \approx x_{i'}$, $y_i \approx y_{i'}$ and $z_i \approx z_{i'}$. This closeness can be reduced to a 2-dimensional one by reducing the 3 spacial coordinates to 1, the distance $r_{i,i'} = |\mathbf{r}_{i'} - \mathbf{r}_i|$. The other dimension left stays just like it is, the energy difference $\Delta\epsilon_{i,i'}$. So for hopping to be likely a closeness in space and energy is needed. If the temperature and thus the thermal energy for a phonon assisted hop is very low, not all the donor energies are accessible. In this situation the nearest neighbor donor may have a energy which is to high and in total the next nearest neighbor is preferred due to its closeness in energy despite the longer distance. In other words, the next nearest neighbor is closer in the above mentioned 4-dimensions. Because of this fact the name variable range hopping has been established.

The temperature dependence of the resistivity is theoretically predicted to follow

$$\rho(T) = \rho_0 \exp\left[\left(\frac{T_0}{T}\right)^a\right], \tag{3.13}$$

where in three dimensions $a = 1/4$ for the Mott type and $a = 1/2$ for the Efros-Shklovskii type. They differ in the assumption about the density of states near the Fermi level. Mott assumed the density of states to be constant and $T_0 \propto 1/\varrho(E)$. In the Efros-Shklovskii type on the other hand it is assumed that the density of states vanishes at the Fermi level which equals a soft Coulomb gap. Also intermediate cases are proposed. The Coulomb gap classically results from electron-electron interaction, i.e. level repulsion, but also a polaron shift may be its origin.

According to Michel *et al.* a broad distribution as well as a band tail would yield to a non-Arrhenius temperature dependence of the resistivity.[40] This could easily be misinterpreted as variable range hopping. A similar result for a different situation was presented by Shchamkhalova and Tkach who calculated a non-Arrhenius temperature dependence in the case of low compensations.[53] Before judging the type of hopping conduction one should consider the ratio of thermal energy to impurity band-width.

3.2.4 Metallic transport

Like in the case of hopping transport the donor concentration plays a critical role for entering the regime of so called metal-like transport in the impurity band. This threshold was first described by Mott and is called metal–insulator transition (MIT). The Mott criterion is given by [12, 59]

$$N_{\text{crit.}}^{1/3}\, a_{\text{B}} \approx 0.25\,, \tag{3.14}$$

where N_c is the critical donor concentration or Mott concentration.

At this critical donor concentration N_c a transition occurs which distinguishes the two transport mechanisms. With increasing donor concentration N_d transport turns at N_c from a thermally activated one to a degenerate one. The overlap of the donor wave functions becomes so large that they not only undergo a level repulsion and the impurity band broadens, they also form a degenerate band which may even overlap with the extended conduction band states. Thus carriers are no longer bound to specific donor atoms but are delocalized over a large number of donors. The Fermi level lies inside the impurity band. These two facts bring up the similarity to the electrical conduction in metals, which is why it is called metal-like transport regime. Section 3.2 still holds for this transport regime. As the delocalization is represented in form of the activation energy ε_3, it becomes equal to zero in this case. The vanishing of ε_3 can be observed experimentally at the metal–insulator transition. Therefore equation (3.12) becomes temperature independent and the third summand in section 3.2 is reduced to a constant. Due to the local disorder of donor atoms, i.e. the randomness of donor sites, the metal–insulator transition is a percolation threshold. This means, that it is the limit between non-existence and existence of paths throughout the sample fulfilling the condition of overlapping donor sites each contributing to delocalization.

Still the conduction of this band itself is poor compared to the conduction band, but as the latter freezes out which the metal-like does not, it dominates at low temperatures.

3.3 Experimental transport mechanisms

The temperature dependence of the magnetoresistance of all samples, cf. table A.1, is depicted in form of Arrhenius plots in figure 3.8. The ordering of the hopping samples is done according to their increasing manganese content x (samples a, b and c). The ordering of the high manganese content samples (numbers 1–6 with $x \approx 6\,\%$) is done according to their increasing carrier concentration at room temperature and thereby roughly by their resistivity. As one can see all curves can be divided into two general groups. The origin of this difference and separation is the metal–insulator transition and the samples 3–6 exhibit metallic transport.

Both groups exhibit activated band transport in the high temperature regime. The influence of this mechanism on the overall conduction decreases with increasing carrier concentration as the competing impurity band transport becomes more and more dominant.

The samples with high carrier concentrations have constant resistivities below a certain threshold temperature. These samples show metallic conduction which is explained in detail in section 3.2.4. At low enough temperatures this conduction mechanism is dominant. The impurity band is degenerate meaning that the electrons are not bound to their donor atoms but delocalized over a large number of donors. Thus they do not need to be activated by temperature in any form to contribute to the electric transport. This point is important because this behavior is accompanied by the fact that the contribution of these electrons to the transport is no longer sensitive to the shape of the impurity band.

For the samples with low carrier concentration a thermal activation clearly can be seen at low

temperatures, which is one possible evidence for hopping transport according to section 3.2.3. Thereby the impurity band and more precisely its actual shape has a significant influence on the transport behavior of these samples. This is the reason why only samples which show hopping transport exhibit such a strong magnetic field dependence in this temperature range. Throughout this work the nearest neighbor hopping (NNH or also called Miller-Abrahams hopping) yielded the best description of the data, though for very low temperatures the different types of variable range hopping (VRH) cannot be excluded entirely, as temperatures below 1.5 K could not be accessed with the present setup. In the temperature range between activated band transport and hopping transport there sometimes seems to exist another mechanism. This could be either the ε_2-conductivity or a non-Arrhenius behavior due to its impurity band shape according to Michel *et al.* [40].

Another observation worth mentioning is the fact that the slope, which corresponds to the activation energy ε_3, is increasing with increasing manganese content. Again this indicates the dependence of the resistivity not only on the presence of manganese but also on its actual content x.

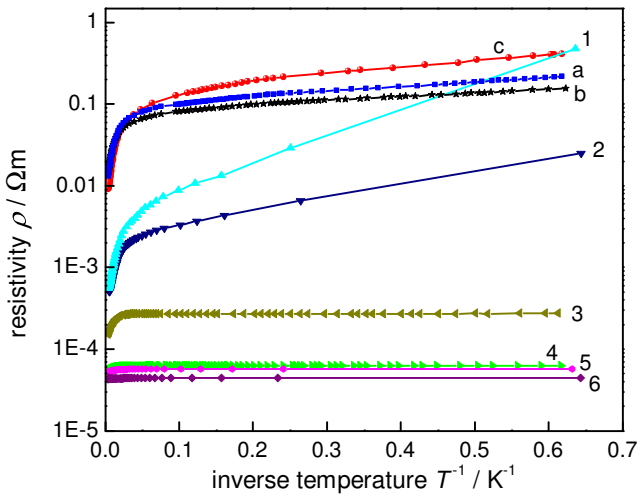

Figure 3.8: Temperature dependence of the resistivity for all samples in form of an Arrhenius plot. The separation into two groups can clearly be seen, the samples which show hopping transport and those showing metallic conduction, respectively. The threshold between these two conduction mechanisms is the metal–insulator transition, which occurs around $n \approx 1 \times 10^{18}\,\mathrm{cm}^{-3}$. At high temperatures the activated conduction band transport is apparent. For some hopping samples an ε_2-conductivity seems possible at an intermediate temperature range. For increasing manganese contents the activation energy ε_3 tends to increase.

Chapter 4

Experimental Setup

4.1 Sample growth and sample parameters

The chlorine-doped zinc manganese selenide samples in this work were bulk-like epitaxial layers. They were grown by molecular beam epitaxy (MBE) on semi-insulating (001) gallium arsenide (GaAs) substrates by the group of M. Hetterich at the Karlsruhe Institute of Technology (KIT). Elemental zinc, selenium and manganese were used as sources for the growth of the zinc manganese selenide. A zinc dichloride ($ZnCl_2$) compound was used as a precursor for the n-type doping of the samples. All these sources were provided by thermal effusion cells.

Before growth the substrates were cleaned in two steps. First they were treated by a wet chemical etching process and then transferred to the growth chamber. There their surfaces were deoxidated at a temperature of 580 °C for 4.5 minutes.

During the growth under selenium rich conditions the substrate temperature was fixed at 280 °C. Optimized growth parameters for doped zinc selenide were adapted for the zinc manganese selenide. The beam equivalent pressures of manganese and chlorine sources were varied to adjust the desired concentrations while the partial pressures of zinc and selenium were kept constant. For example the temperature of the zinc chloride compound source was varied between 180 °C and 240 °C, which led to low or high doping concentrations, respectively.

The thickness d of the layers varies between 880 and 1050 nm, which was determined optically. The accurate determination of the manganese content x in each sample was done by two independent methods: energy dispersive x-ray analysis (EDX) and x-ray diffraction (XRD). The results from these methods were in good agreement and define the uncertainty of every value for the manganese content x, which is about 1 %. Besides the above mentioned quantities, the growers determined the free carrier concentration n and mobility μ, for each sample by room temperature Hall and conductivity measurements in van der Pauw configuration in a magnetic field of 0.9 T. Cloverleaf shaped structures were fabricated out of the epitaxial films by lithographic microstructuring and etching. Indium dots on the edges of the cloverleaf structures were exposed to an annealing process at a temperature of about 190 °C for 4.5 minutes and afterwards contacted using gold wires. For even more detailed information and further reading concerning the growth and the parameter determination see the work

of Daniel *et al.* [9]. The corresponding parameters of the samples studied can be found in table A.1 of appendix A.

4.2 Preparation, geometry, setup and measurements

The measurements of the samples were performed in van der Pauw geometry. This method requires four contacts which have to be placed at the edge of an arbitrarily shaped sample. The layer thickness has to be constant and the material has to be homogeneous in terms of a locally constant resistivity. Furthermore the layer must be one area without any openings. In order to achieve low uncertainties the contacts should be small compared to the length scale of the sample and the distances between the contacts.

The measured samples were rectangular pieces cleaved out of wafers. Typical sizes were $5 \times 5\,\mathrm{mm}^2$. For incorporation into the pressure cell the samples had to be even smaller, about $3 \times 3\,\mathrm{mm}^2$. Indium dots were put on the 4 corners of a sample. For metallization every sample was tempered afterwards at 190 °C under a constant flow of argon gas as a protective atmosphere. The tempering was performed for a period of 40 minutes, followed by a certain time still under argon flow until the temperature was reduced to about 60 °C. Fine copper wires were contacted to the indium dots using a soldering iron.

The measurements were performed in an automated mode by a computer program. The software program was written in LabVIEW by a former member of staff. There are two basic modes of measurement, one at constant magnetic field and a stepwise changing of temperature and the other at a constant temperature where the magnetic field was varied. To control the magnetic field and the temperature the program uses a magnet power supply MPS120 and temperature control unit ITC4 both from Oxford Instruments. The cryostat itself is a system from Oxford Instruments, a super-isolated vacuum shielded dewar with a superconducting magnet coil able to generate magnetic field strengths up to 10 T. The coil is cooled by liquid helium to be in a superconducting state. The liquid helium is also used for cooling the sample which is in direct contact with the cold gas. The gas flow is provided by a vacuum pump and regulated by the admittance through a needle valve. In this setup sample temperatures as low as 1.6 K may be achieved. For higher temperatures, the temperature control provides heat by warming the helium gas to a desired value. As the regulation of the temperature occurs directly at the inlet of the helium gas and the sample temperature may be slightly different especially when adjusting a new setpoint, an additional sensor is used to monitor the accurate sample temperature. Also the sensitivity of this sensor is much higher.

Van der Pauw measurements allow one to obtain the resistivity and the Hall-resistance (in case of diffusive transport the carrier concentration and the carrier mobility) by using only four contacts. In order to switch between the different contact configurations for current and voltage measurements required to extract resistivity and Hall-resistance a switch card is employed, in this setup a Keithley Switch System 7001. The two electrical devices needed for a measurement are a Keithley programmable current source 220 and a Keithley nanovoltmeter 2182. To gain even higher accuracy especially for low conducting samples the current is measured separately using a Keithley picoammeter 6485. To rule out thermal voltage effects

which can lead to errors in the measurement and to provide a higher accuracy both current directions are used as well as positive and negative magnetic field orientations. For each data point the measurement was performed several times and an average value was calculated.

The van der Pauw method defines how the resistivity is calculated from the basic current and voltage measurements for given contact configurations. The only additional parameter needed is the thickness of the layer. In the other van der Pauw contact configurations making use of the Hall effect the Hall-resistance is determined. In case of diffusive transport the Hall-resistance allows a determination of the carrier concentration and the knowledge of both quantities leads to the carrier mobility.

4.3 Physical quantities

The physical quantities that we determine are the electrical resistivity ρ, i.e. the inverse value the electrical conductivity $\sigma = \sigma_\mathrm{e}$. This is possible because our samples can be described as classical 3D-volume crystals with high impurity densities so that they obey Ohm's law. In the more specific case of an electron gas, it is possible to assign the conductivity to the two quantities carrier concentration n and mobility μ in the following form:

$$\sigma_\mathrm{e} = 1/\rho = e\, n\, \mu \; . \tag{4.1}$$

We are interested in their dependence on temperature T, magnetic field B and pressure p. The temperature dependence of the resistivity for instance yields the activation energies. Its magnetic field dependence results in the so called magnetoresistivity $\rho(B)$. Often just the relative value compared to zero field one is considered, which is called relative magnetoresistance often abbreviated as MR or $\mathcal{R}$ and given by

$$\mathcal{R} = \frac{\rho(B) - \rho(0)}{\rho(0)} = \frac{\Delta\rho}{\rho(0)} = \frac{\rho(B)}{\rho(0)} - 1 = \frac{R(B)}{R(0)} - 1 \; . \tag{4.2}$$

Due to the linearity between resistance R and resistivity ρ the relative magnetoresistance is the same for both quantities.

Chapter 5

Magnetotransport

5.1 Magnetoresistance mechanisms

Only magnetoresistance mechanisms that occur in homogeneous materials in the regime of hopping transport are presented in this chapter. Other effects that are apparent at interfaces or in the regime of metal like impurity band or conduction band transport are not specified.

5.1.1 Wave function shrinkage

A well known magnetoresistance effect is based on the magnetic-field induced wave function shrinkage. The shrinkage was first described by Yafet *et al.* [67]. According to their theoretical description the magnetic field leads to a spatial distortion of the electron wave function of a hydrogen-like shallow donor. To be precise the wave function shrinks in all directions but by a different amount, i.e. less shrinkage along the magnetic field direction and more perpendicular to it. The wave function changes from the normal spherical shape to an elliptical one.[1] Suprapto and Butcher used this effect to explain the magnetoresistance behavior in the variable range hopping regime.[60] They also observed that this leads to a magnetic field dependence of the thermal activation energy, $\varepsilon_3(B)$. The theoretical calculations for this and for nearest neighbor hopping can be found in the book by Shklovskii and Efros.[54] In high fields these yield a linear dependence of T_0 on external fields or a exponential magnetic field dependence of ρ, respectively. As this effect is by the above description anisotropic this also holds for the magnetoresistance in terms of perpendicular and parallel magnetoresistance values. In detail this is hard to predict for a given sample as the current paths are random due to the percolation nature of the hopping conductivity. Thus also the parallel magnetoresistance may posses some perpendicular path sections and vice versa. But the general observation is that the perpendicular magnetoresistance is always larger than the parallel one, just the ratio may be different.

According to Kurobe also a negative magnetoresistance is possible in this picture due to the inverse effect of wave function enlargement.[34] The author studied the Anderson localized

[1] The wave-function shrinkage is accompanied by a larger ionization energy of the donor.

regime with variable range hopping and stated that an increase of the localization length yields a negative magnetoresistance. This effect of positive and negative magnetoresistance due to changes of the wave function is also reported by Finlayson *et al.* [18]. According to Raikh *et al.* the low field magnetoresistance has a quadratic dependence on the magnetic field.[51]

Related to the wave-function shrinkage it is possible to undergo a metal–insulator transition, cf. to the work of Wojtowicz *et al.* [66]. This could occur when the carrier concentration at zero ambient magnetic field is slightly larger than the Mott critical concentration. With increasing external magnetic field the Mott critical density will increase as the Bohr radius is reduced. This may result in a change of the conduction mechanism from metallic to thermally activated and thus result in a huge positive magnetoresistance effect.

5.1.2 Impurity band related effects

Concerning the magnetoresistance there are two impurity band correlated effects known: First, the direct influence of the impurity band-width on the magnetoresistance and, second, the relative change of the Fermi level position inside the impurity band.

For the first one there is a very good description given by Raikh *et al.* [51]. The starting point is the already known effect of magnetic field induced wave function shrinkage, cf. section 5.1.1. Simultaneously with the shrinkage a reduction of the overlap of the donor wave functions occurs. In binary semiconductor materials the impurity band-width results only from the Coulomb level repulsion. If now the overlap decreases so does the Coulomb interaction. Thus the donor levels approach each other yielding a reduced impurity band-width. The decreasing impurity band-width is often connected with the fact that the density of states increases. This band narrowing is also accompanied by an absolute shift of the Fermi level. At this stage it is important to understand that the Fermi level shifts only in terms of its absolute position, but that its relative position in the impurity band stays constant. For nearest neighbor hopping the decreasing impurity band-width is important, because it means that the average activation energy is reduced. This leads to a decreasing resistivity, i.e. a negative magnetoresistance contribution. It is obvious that this effect is in direct opposition to the wave function shrinkage, which yields a positive magnetoresistance. The authors showed that at certain magnetic field ranges either one or the other of these two mechanisms is dominant. The negative magnetoresistance determines the low field region while the positive one determines the high field region. As the origin of this effect, i.e. the wave function shrinkage, is anisotropic this also holds for these magnetoresistance mechanisms.

The second effect correlated with the impurity band is the relative change of the Fermi level with respect to the density of states, which is theoretically described by Shchamkhalova and Tkach.[53] The driving force of this mechanism is the normal Zeeman splitting of the donor ground state, more precisely the splitting of the density of states for the two spin directions. As one sees at this point only basic semiconductor materials are considered. Due to the spitting a redistribution of the donor-bound electrons occurs. The analysis is done for low levels of compensation. In this case the Fermi level is located in the high energy tail of the donor density of states. If a magnetic field is applied Zeeman splitting occurs and

the electrons will redistribute until the thermal equilibrium is reached. This yields a higher number of electrons in the energetically favored spin-down states than in the spin-up states. This difference from the former equal occupation has the consequence of the Fermi level being localized at a higher energy relative to the spin density of states for the energetically preferred states and lower relative to the not preferred states. Furthermore the authors assume that spin flips are not relevant. In this framework the hopping transport has two contributions due to the two spin directions. The lower distribution of them having a lower conductivity and the higher distribution a higher conductivity. They performed calculations that show a large negative magnetoresistance resulting from these assumptions. As the Zeeman effect is the origin of this mechanism and it is isotropic, this fact also results in an isotropic magnetoresistance contribution. The presented argumentation contradicts our understanding of hopping transport as the occupation of a donor state with an electron is relevant not its spin.

5.1.3 Hopping of bound magnetic polarons

A bound magnetic polaron (BMP) describes the situation where an donor-bound electron couples to the manganese atoms in its surrounding. The random spin of such an electron leads via exchange interaction to a certain degree of magnetization of the manganese atoms in its vicinity. The coupling of each electron-manganese spin-pair is such that they tend to align. Due to the interaction of the many manganese and the one electron spin orientation at some point one spin direction, however it is randomly orientated, is preferred after the partial aligning of magnetic moments. Thus the formation of a bound magnetic polaron lifts the degeneracy of the donor ground state and leads to a lowering energy of this preferred spin state. The energy difference to the degenerate state is called polaron shift.

The bound magnetic polaron occurs even when no external magnetic field is present. So each hopping event has to bring up the energy difference of the donor states plus the polaron shift. If one applies a magnetic field all the manganese spins will start to align along the field direction.[2] Thus the polaron shift will be decreasing and will become zero when all the free manganese spins are aligned. The polaron shift and its decreasing and vanishing in a magnetic field is directly observable in the magnetic field dependence of the Stokes shift of the photoluminescence.[11] The observed spectra differ from the theoretical conduction band splitting according to the Brillouin function in the low field region, e.g. at zero field the energy is not zero as predicted but has the value twice of the polaron shift.

The main transport characteristic of the bound magnetic polaron hopping is a negative magnetoresistance. Which saturates as the magnetization saturates due to the vanishing of the polaron shift, which acted as a reduction of the total activation energy. However, as Dietl *et al.* demonstrated, there may also occur a positive magnetoresistance in the low field region. The reason for this is the decrease of thermodynamical fluctuations of magnetization at small fields and a corresponding increase of resonant donor sites.[13] One should mention that hopping of bound magnetic polarons gives an isotropic magnetoresistance contribution.

[2] This only holds for the isolated manganese spins and the exception are the antiferromagnetically aligned nearest neighbor manganese pairs, which do not contribute because their total magnetic moment is zero.

Like our proposed model of the positive magnetoresistance in a dilute magnetic semiconductor the main idea is to correlate the magnetization with the resistivity change in the region of hopping transport. But the bound magnetic polaron model alone is not sufficient to explain the positive magnetoresistance behavior in zinc manganese selenide.

5.1.4 Double occupation effects

One long known magnetoresistance effect is attributed to double occupation of donor sites. Many authors present the following explanation.[4, 32, 34, 39] A semiconductor where hopping takes place and where the contributing donor states cannot only be singly occupied but also doubly occupied is considered. In this case the situation with no external magnetic field applied can be the following. Hopping takes place in every energy state that is close to the Fermi level irrespective of it being a ground or a doubly occupied state. In other words some states are in resonance with one another. If now an external magnetic field is applied the singly occupied states start to split while the doubly occupied ones stay constant. This changes the situation and the energy states are no longer in resonance. In other words the mechanism of both types of states contributing to conductivity is suppressed. This on the other hand results in a positive magnetoresistance. This effect like the Zeeman splitting shows a isotropic magnetoresistance. The effect of the suppression of double occupation in the hopping process is sometimes referred to as electron-electron interaction. Caution needs to be taken because this term is also used in metallic or conduction band transport.

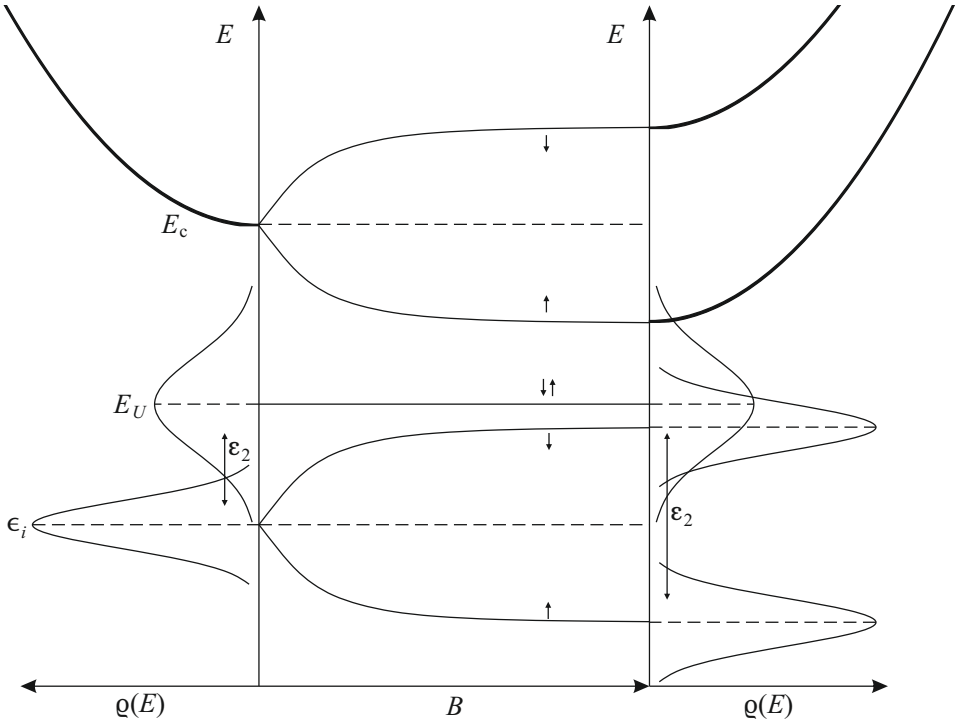

Figure 5.1: Situation for the magnetoresistance due to double occupation is determined by the shifting apart from the single and the double occupied density of states and thus the increase of ε_2.

5.1.5 Interference effects

Another magnetoresistance mechanism is the effect of magnetic field induced interference in hopping transport. For the case of variable range hopping this is given by Sivan *et al.* [56] and a good derivation for nearest neighbor and variable range hopping is given by Raikh *et al.* [51]. In hopping transport there will always be a situation where more than one path from the initial to the final donor will exist. In this case the electron in its nature as a wave reaches the final donor site by not one path but by a mixture of all. The different paths surround an area between the donors involved. If now the magnetic flux through this area changes by applying a magnetic field the interference of the paths changes. More specifically the phase relationship of both paths changes. Also the time reversal invariance is lifted. The combination of both effects leads to a reduced back scattering and thus to a negative magnetoresistance. As the magnetic flux perpendicular to the area is decisive the effect yields an anisotropic magnetoresistance contribution.

5.1.6 Evaluation of possible explanations

The situation we observe in the magnetoresistance measurements in zinc manganese selenide with low manganese content is hard to explain in the light of the existing explanations. The effect of wave-function shrinkage explains the positive magnetoresistance but the observed saturation of the magnetoresistance is not consistent with it. The interference argumentation is limited to a small magnetoresistance effect only. Such a weak effect is then supposed to result in a negative magnetoresistance. As we focus on low manganese contents where only small negative contributions are seen, this mechanism cannot be relevant. The hopping of bound magnetic polarons takes into account the semi-magnetic nature of the material. For the magnetoresistance it predicts a possible positive contribution before the main negative characteristic dominates at high magnetic fields. As this mechanism takes place in our material and has the same origin, the spin alignment, one can only conclude, that both take place at the same time. As the positive effect dominates, the bound magnetic polaron influence must be weaker compared to the strong positive one. Double occupation is hard to prove even as the transport mechanism itself. The evidence we have contradicts this process in the low temperature region where only nearest neighbor hopping is apparent. Nonetheless it is hard to totally rule out this mechanism as it would show the same dependence on the magnetization. And as it is likely that this effect would lead to a positive magnetoresistance, it is still possible. The strongest argument against it, is the very low thermal energy compared to the suggested much larger Hubbard energy U.

5.2 Measurements in literature

We are not the only ones who have observed a large positive magnetoresistance in a dilute magnetic semiconductor. So at this point these observation made by other groups will be presented as an additional motivation for our research.

Shapira [52] examined $Cd_{1-x}Mn_xTe$ with different manganese contents x and different carrier

concentrations n. Some of the samples exhibited hopping conductivity at low temperatures. The most important graph for our purposes is one where a sample with the lowest manganese content ($x = 0.01$) was examined. The sample was low doped and thus exhibited hopping conduction. The magnetoresistance showed a Brillouin-like behavior just like our samples of zinc manganese selenide for low manganese contents. The relative magnetoresistance had its maximal value at about 2.5, while it was in saturation. For the samples with higher manganese contents ($x = 0.05$ and $x = 0.1$) an intermixed behavior of positive and negative magnetoresistance was observed. However, the magnetoresistance always had positive values. One sample with $x = 0.05$ and rather close to the metal–insulator transition showed the same temperature and magnetic field dependence as our sample with $x = 0.06$. First a positive then a negative contribution. The magnetic field value of the peak decreases as a function of decreasing temperature, while the peak itself increases. The authors connected this behavior with the magnetization and the Brillouin function. The discussion was not detailed enough on the magnetoresistance processes in hopping transport and so no sufficient explanation for this behavior was given.

Leighton [36] examined persistent photo-conductivity (ppc) in $Cd_{0.83}Mn_{0.17}Te$. The presented temperature dependence proved the mechanism of nearest neighbor hopping conduction in the sample at every density of free carriers. The range of the magnetic field used for the magnetoresistance measurements was only between $-0.75\,\mathrm{T}$ and $+0.75\,\mathrm{T}$. Still at $3.9\,\mathrm{K}$ a clear positive relative magnetoresistance was observed with values up to 0.5. The authors also observed a decrease of this value with increasing temperature. And the graphs were analyzed in a scaling manner, details in chapter 7. However the origin of this behavior was unclear to the authors as they discussed possible well-established magnetoresistance mechanisms, consistent with our evaluation in section 5.1.6.

Smorchkova [57] examined a 2-dimensional electron gas (2DEG) of a quantum well (QW) consisting of a paramagnetic digital alloy of $(Zn_{0.8}Cd_{0.2}Se)_{m-f}(MnSe)_f$. The system is also a persistent photoconductor (ppc). The transport mechansims could be identified as variable range hopping, which is typical in the studied temperature range between 300 mK and 1.6 K. A positive giant magnetoresistance (GMR) was observed. The dependence is somewhat familiar in terms of an increasing resistivity at low magnetic fields, a peak and followed by a decrease. Despite this positive and negative contribution the values of the relative magnetoresistance are positive in the entire range of the magnetic fields. The maximal value of the peak was 700 %, which was determined at the lowest temperature. The peak position again shifts to lower magnetic field values as the temperature decreases. The authors reduced the number of measurement to a single one using a variable range hopping scaling approach, cf. [39] and chapter 7. By referring to this publication they also followed the argumentation that the conductance was provided by double occupation. In this framework the connection between the magnetoresistance and the magnetization, the Brillouin function and the conduction band splitting was made.

In the above mentioned articles similar magnetoresistance effects were discovered like the ones in this work. In one paper a lot of mechanisms are presented, but none of them can be motivated, in another the lack of an explanation is formulated and a third one provides an explanation which contradicts the different energy scales of variable range hopping and double

occupation. Our proposed magnetoresistance mechanism provides a consistent explanation for all these works. The fact that these measurements were done in different material systems, e.g. CdMnTe and ZnCdMnSe, supports the statement that this mechanism might be also of importance in other dilute magnetic semiconductor than zinc manganese selenide.

5.3 Magnetoresistance results

This work is dedicated to the explanation of the magnetoresistance curves seen in figure 5.2. In the following I would like to point out the similarities to the Brillouin function as well as to discuss the influence of carrier concentration and manganese content on the magnetoresistance curves.

For a dilute magnetic semiconductor the magnetic field dependence of the magnetization and of the conduction band splitting according to the Brillouin function are well known, cf. section 2.1.2. At this point one recognizes the similarities between the shape of the magnetoresistance curves and that of the Brillouin function for example, cf. figure 2.4. The reason for this similarity of magnetic field dependence of the magnetization, the splitting of electron states and the resistivity is not obvious. Every donor site can only be occupied by one electron, without changing the entire energetic situation due to double occupation. In a magnetic field one spin direction will be energetically preferred, which results in spin polarization. But still there is only one electron contributing to the transport and no significant conductance change is expected. None of the state-of-the-art magnetoresistance explanations

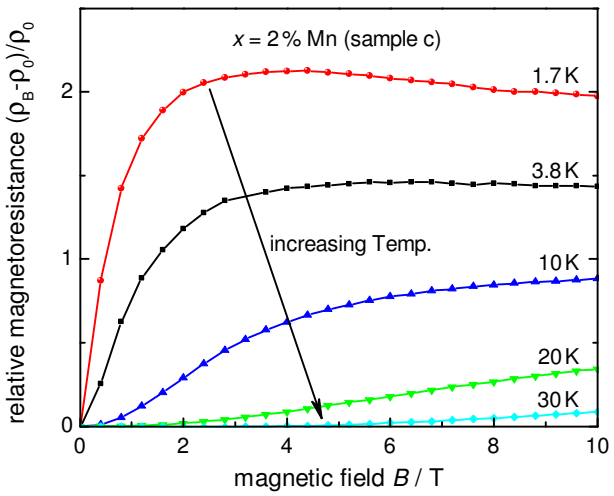

Figure 5.2: Typical measurements of the relative magnetoresistance for a zinc manganese selenide samples with a low manganese content, in this case $x = 2\,\%$ for sample c, at different temperatures is shown. (Sample b is similar, cf. figure 5.9.) One recognizes the characteristic large positive magnetoresistance effect. The effect is largest at the lowest temperature, but the values are always positive. The shape of the curves itself as well as their temperature behavior resemble a lot the Brillouin function and their connected magnetization and conduction band splitting, cf. figure 2.4. This work is dedicated to present the connection of the magnetoresistance and the Brillouin function.

described in section 5.1 may fully explain the behavior observed. So the question arises: How does the Brillouin function influence the resistivity? Before we can answer this question some other aspects need to be considered.

Figure 5.3 illustrates that the magnetoresistance in binary zinc selenide without manganese (sample a) is very different from that of the dilute magnetic semiconductor samples, which evidences that the positive magnetoresistance considered in the current report is due to the presence of manganese, as suggested in our work.[43] Moreover, in the range of manganese contents x studied, the positive magnetoresistance effects increase with increasing x for comparable donor concentrations.

Looking at the two figures 5.2 and 5.4 one observes that the magnetoresistance is higher for sample 1 with a higher manganese content than for sample c with the lower manganese content. This observation is a general one. The value of the maximal magnetoresistance as a function of manganese content is depicted in figure 5.5, i.e. for different samples. This graph shows that with increasing manganese content also the maximal relative magnetoresistance increases. So not only the presence of manganese atoms has an effect on the resistance but it also scales with its actual content. This is another strong indication that manganese is somehow responsible for this effect and its origin.

The magnitude of the magnetoresistance effect as well as the shape of the curve seen in figures 5.4 and 5.6 are very different for the same manganese content. At doping concentrations above the metal–insulator transition (cf. figure 3.8) as well as for the pure host material in

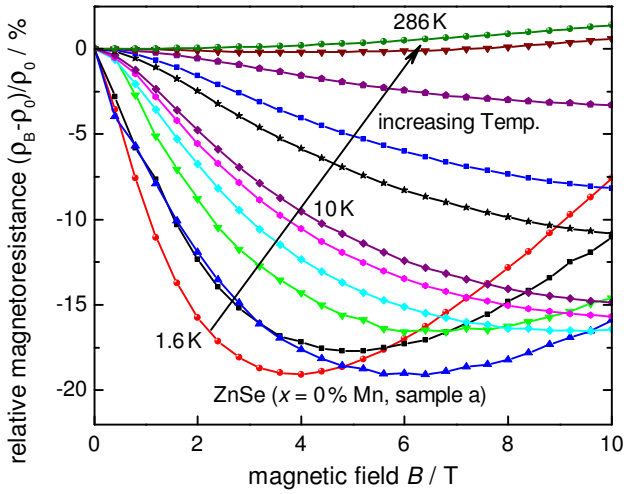

Figure 5.3: Measurements of the relative magnetoresistance for the zinc selenide reference, sample a, without manganese at different temperatures. Both samples a and c show hopping transport and are therefore somewhat comparable. The difference to the zinc manganese selenide sample is that the amplitude of the relative magnetoresistance effect is one order of magnitude smaller and that the sign is different, i.e. we are dealing with a negative magnetoresistance effect except for the highest temperatures. What sample a and c have in common is the fact that both effects are more pronounced at lower temperatures. For low temperatures even a positive contribution at high magnetic fields is observed.

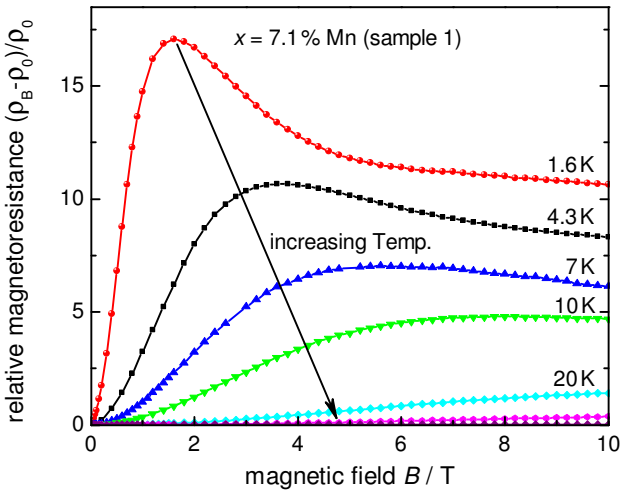

Figure 5.4: A typical measurement of the relative magnetoresistance for a zinc manganese selenide samples with a high manganese content, in this case $x = 7.1\,\%$ for sample 1, at different temperatures is shown. (Sample 2 is similar.) In contrast to the samples with low manganese content an additional negative contribution is visible. This is most likely due to the more complex behavior of the conduction band edge as a function of x, cf. chapter 9.

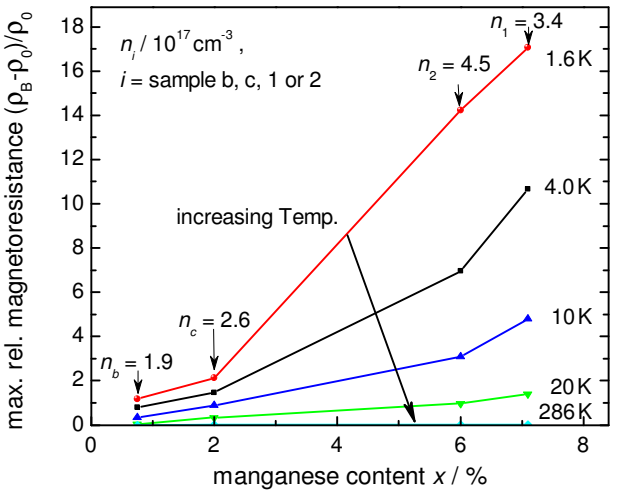

Figure 5.5: The dependence of the maximal relative magnetoresistance is shown as a function of the manganese content, i.e. for the different hopping samples, at different temperatures. As the samples have slightly different carrier concentrations at room temperature these are also indicated. For all temperatures increasing values are to be seen for increasing manganese content. The increase is uniformly continuous and more than linear, but one has to be careful because only four samples are presented and because the carrier concentration has also an influence, which will be shown in the following. However, the shown behavior is an indicator for the direct influence of the magnetic ions on the carrier transport. Later a theoretical prediction will be given, to compare this experimental result with our model, cf. figure 8.4.

figure 5.3 the effect vanishes. So again it is clear that the presence of manganese atoms somehow leads to this behavior only in the regime of hopping transport. Again a simple comparison of all samples can be done. The maximal magnetoresistance as a function of carrier concentration is depicted in figure 5.7. At high carrier concentration there is only a very small magnetoresistance effect to be seen in order of a few percent. But below a certain threshold of about $1 \times 10^{18}\,\mathrm{cm}^{-3}$ the values are much higher. Section 3.2 tells us that the metal–insulator transition is this threshold. As the effect, which is to be investigated, is again clearly below the metal–insulator transition this gives reason for a detailed look at the mechanisms happening in the regime of hopping transport.

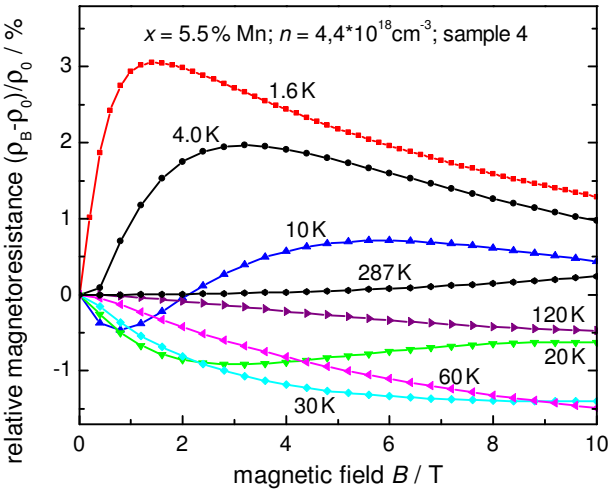

Figure 5.6: A typical measurement of the relative magnetoresistance in zinc manganese selenide samples with a high carrier concentration, in this case $n = 7.1 \times 10^{18}\,\mathrm{cm}^{-3}$ for sample 4, at roughly the same manganese content $x \approx (6.4 \pm 1)\,\%$ and at different temperatures is shown. (Samples 5 and 6 have a similar appearance.) Positive and negative contributions are to be seen. However, most important is the fact that the presented effects for metallic conduction are almost three orders of magnitude smaller compared to the samples which show hopping transport.

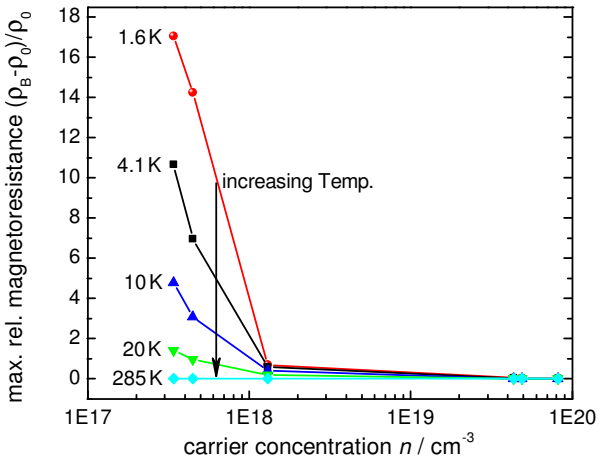

Figure 5.7: The dependence of the maximal relative magnetoresistance as a function of the room-temperature carrier concentration, i.e. for the samples with roughly the same manganese content x on both sides of the metal–insulator transition, at different temperatures. While the hopping samples show a large magnetoresistance effect, the metallic ones only posses values of about a few percent. Sample 3 shows intermediate values and may be closest to the metal–insulator transition. As the manganese content itself has also an influence on the values, the correlation of n and x has to be taken into account.

5.4 Empirical description

The solid lines in the figure 5.8 and 5.9 show the resistivity as a function of the magnetic field for the two samples b and c with manganese contents $x = 2\,\%$ and $x = 0.75\,\%$, respectively. Both samples[3] show somewhat similar magnetoresistance curves. The curves are dominated by a pronounced positive magnetoresistance contribution, which increases rapidly at low magnetic fields and then saturates at high magnetic fields. Additionally a smaller negative contribution sets in at high fields, which will be ignored for the time being and possible explanations will be presented in chapter 9. For sample c with $x = 2\,\%$ the relative magnetoresistance is about $200\,\%$ at saturation, for the sample b with $x = 0.75\,\%$ slightly lower. The saturation field increases with increasing temperature.

One first recognizes the similarities between the magnetoresistivity curves and curves of the Brillouin function (figure 2.4) and thus with the linked magnetization. This is not only true for the initial increase and the saturation but also holds for the temperature dependence. As the resistivity can be described by a ε_3-hopping conductivity, the explanation of the magnetoresistance effect must originate from a hopping effect. From literature there are three basic magnetic field dependent mechanisms in this regime known, the change of the activation energy, the wave-function shrinkage and the bound magnetic polaron effect. All of them were presented in the sections 5.1.1 to 5.1.3, respectively. For the reasons given in

[3] We chose these two samples of low manganese content because in contrast to high manganese contents no additional negative contribution to the magnetoresistance occurs. The latter is explained in more detail in chapter 9.

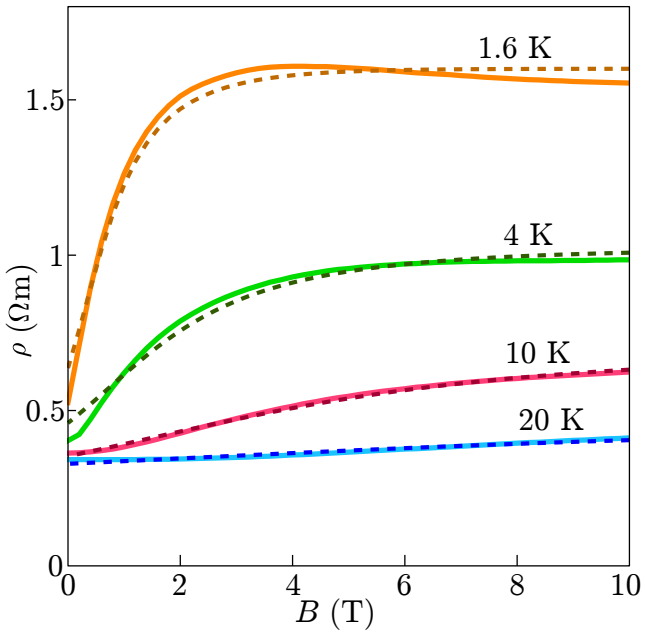

Figure 5.8: Applying the fitting function from equation (5.1) on the resistivity measurements of sample c one obtains good results. This supports our main idea of the resistivity having an exponential dependence on the magnetization. Also this function provides an easy approach to fit resistivity curves of the same form in other dilute magnetic semiconductors.

the corresponding chapters the magnetic field dependence of the activation energy seems most likely to dominate the magnetoresistance behavior. The exponential dependence of the ε_3 hopping conductivity make it tempting to fit the resistivity with an exponential expression. This works rather well if one assumes a linear dependence of the activation energy on the magnetization. This leads to a fitting function of the form

$$\rho(B,T) = \rho_0 \exp\left[b\, M(B,T)\right] . \tag{5.1}$$

Only taking the magnetic field dependence at fixed temperatures this function gives a good fit to the individual magnetoresistivity curves as shown by the dashed lines in the two figures 5.8 and 5.9. The fitting parameters ρ_0 and b were treated independently for each temperature.

This resemblance and the agreement of the fit support our magnetoresistance mechanism due to a variation of the disorder-induced impurity band-width and consequently the widening of the energetic donor distribution.

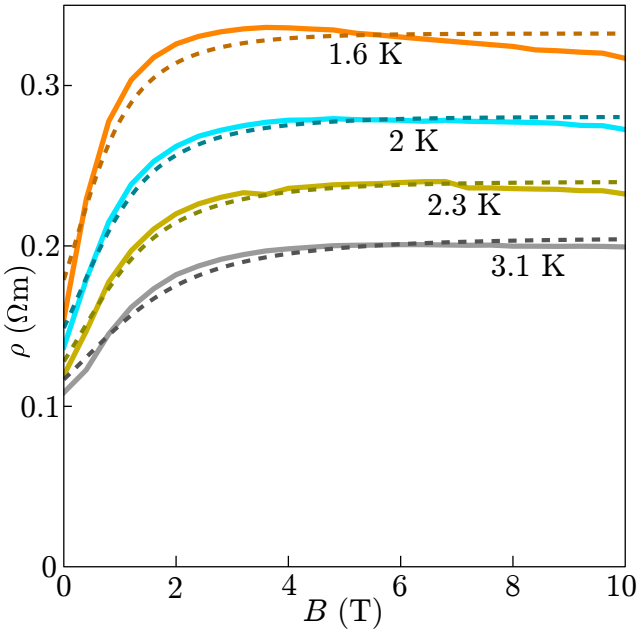

Figure 5.9: Applying the fitting function from equation (5.1) on the resistivity measurements of sample b (with $x = 0.75\,\%$ and $4.3{\times}10^{17}\,\mathrm{cm}^{-3}$) one also obtains good results. The temperatures of the measurements are lower and closer together, but still the fit works well.

Chapter 6

Disordered Crystal

The starting point of our explanation of the magnetoresistance effect in zinc manganese selenide is compositional disorder. By this there is meant the random replacement of the zinc cations by manganese cations. Averaging over this random distribution in space yields the manganese content x. However, if one looks on the microscopic scale there is of course a different number of manganese atoms at different places, i.e. in different characteristic mesoscopic volumes. So not only the mean value of the manganese content x is of interest but also its statistic deviation Δx. For us such a mesoscopic volume is characterized as the local environment of a donor atom and its length scale is the effective Bohr radius a_{B}. Important for the further considerations is that each donor possesses its own local manganese environment. The choice of the effective Bohr radius as the decisive length scale is clear as every electron bound to a certain donor undergoes an exchange interaction with the manganese atoms inside its envelope wave function. When this number differs for different donors so will the strength of the exchange interaction and thus, for example, the conduction band splitting or the donor state splitting. Also the chemical shift of its initial energy at zero field, i.e. the conduction band edge, will be affected. The details of these two effects will be discussed in section 6.2 and section 6.1, respectively.

6.1 Chemical shift

To determine the formula of the chemical shift of the energetic position of a single donor, we have to know the x-dependence of the band gap or better conduction band edge, and of the donor energy.

The compositional variation of the band gap $\mathrm{d}E_{\mathrm{g}}/\mathrm{d}x$ for zinc manganese selenide is well established in literature.[7, 19, 26, 58, 61] The most recent and by this best publication for our purposes might be the one by Hwang *et al.* which is depicted in figure 6.1 [26]. However, all of them clearly show a bowing of the band gap at low manganese contents. This means that due to compositional variation the band gap decreases at low x, before it starts to rise linearly as predicted by virtual-crystal approximation (VCA) at higher x-values.

From the band gap dependence it is possible to make conclusions about the conduction band

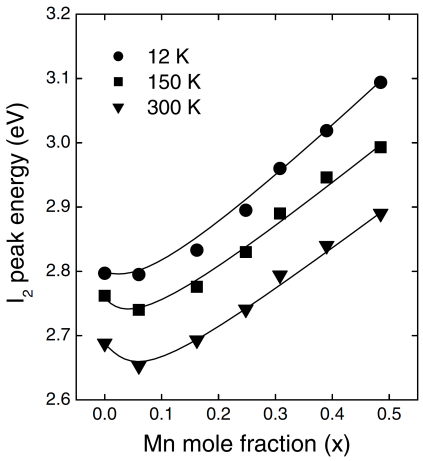

Figure 6.1: The strongest emission peak (I_2) as a function of manganese content x from the work of Hwang *et al.* [26]. This peak was observed in a photoluminescence setup and according to the authors it is attributed to a donor-bound exciton. Important is that it represents the absolute energy change of the donor level as a function of x and also the bowing of the conduction band edge.

edge dependence, and thus also about the donor energy dependence. According to Mycielski *et al.* in II-VI compound systems the two are almost equal to one another ($\mathrm{d}E_\mathrm{g}/\mathrm{d}x \approx \mathrm{d}E_\mathrm{c}/\mathrm{d}x$).[42] And as we know from section 3.1 the donor binding energy is at a fixed energy distance E_d from the conduction band edge. Therefore we denote the absolute energetic position of the donor i at zero magnetic field by $\epsilon_{i,0}$ in concordance with section 3.2.3 and we can assume the same dependence on the manganese content ($\mathrm{d}\epsilon_i/\mathrm{d}x = \mathrm{d}E_\mathrm{c}/\mathrm{d}x \approx \mathrm{d}E_\mathrm{g}/\mathrm{d}x$).

The decreasing of the absolute donor energy with increasing manganese content can be approximated by a linear function $\epsilon(x) \propto -x$. This is justified as the values for the local manganese content x_i due to statistic fluctuations in the vicinity of the donor i will be close to the average x.

To evaluate the zero-field value of the energetic position $\epsilon_{i,0}$ of the i-th donor due to the chemical shift we have to sum over all manganese atoms m. Every position $\mathbf{r}_m$ is weighted by the envelope function ϕ_i of the specific donor bound electron, cf. equation (3.3). The value is given by

$$\epsilon_{i,0} = y \sum_m |\phi_i(r_m)|^2 \ , \tag{6.1}$$

where y is a coefficient fulfilling the proportionality. It is clear that due to the weighting the manganese atoms in the direct vicinity are most relevant although the sum contains every manganese atom. The formula shows explicitly that the donor energy depends on the manganese content: $\epsilon_{i,0}(x_i)$. The possibility of antiferromagnetic coupling is not considered in our theoretical descriptions, as we are dealing with very low manganese contents. In the scaling theory this simplification is only overcome by the use of the effective manganese content x_eff. To extend this in the simulation approach in future one would have to imply a step after the simulation of the lattice, in which every neighboring pair of manganese atoms will not be considered for the effective content of paramagnetic manganese ions.

This situation is schematically illustrated in figure 6.2. The manganese fluctuation and its

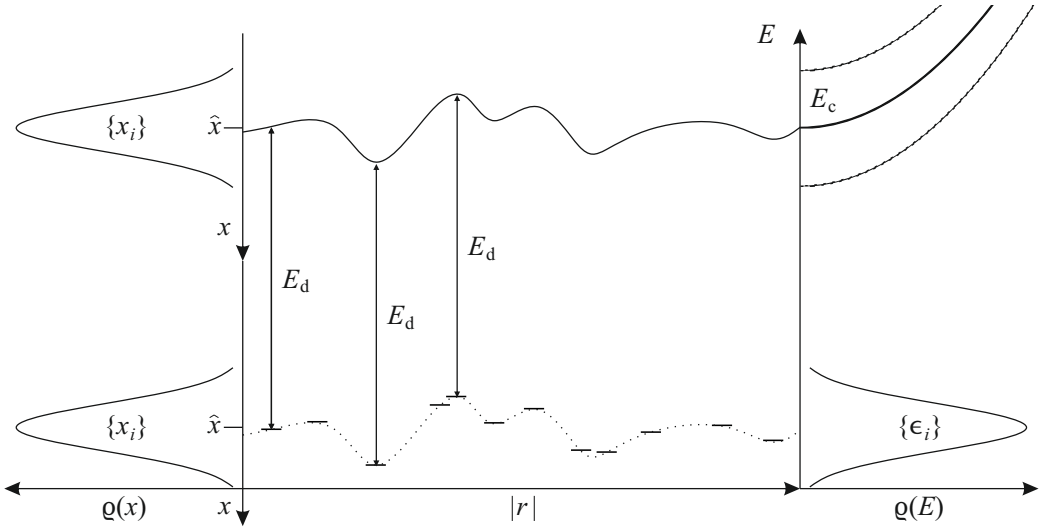

Figure 6.2: Schematic diagram of the origin of the impurity band-width in zinc manganese selenide. Our model attributes to every donor i its own manganese environment x_i, represented by its interaction strength. The distribution $\{x_i\}$ is located around the average value $\hat{x}$. According to the bowing, cf. figure 6.1, every x_i has its own value of the conduction band edge. So the spatial fluctuations of x_i result in fluctuations of E_c and thus in the fluctuations of the donor energy positions $\{\epsilon_i\}$. So in consequence the apparent impurity band-width results from the random placement of manganese atoms in the crystal. It is to mention that a donor with rather low local manganese content has a high position inside the impurity band and vice versa.

effect on the energy position of every donor ϵ_i is shown. This energy fluctuation results in the density of states $\varrho(E)$ of donor levels, which resembles that of the manganese distribution.

6.2 Splitting of a single donor level

To determine the splitting of a single donor level due to exchange interaction we start from the standard s-d spin Hamiltonian. In other words we have to consider the exchange interaction $\hat{V}_{\mathrm{ex}}$ between the spin $\mathbf{s}_i$ ($s_{z,i} = s_z = \pm 1/2$) of the s-like electron on the i-th donor and the total angular momentum $\mathbf{J}_m$ of the d-shell of the m-th manganese atom:

$$\hat{V}_{\mathrm{ex}} = \alpha \left|\phi_i(r_m)\right|^2 \, \mathbf{s}_i \cdot \mathbf{J}_m \ , \tag{6.2}$$

where α is the material-dependent exchange constant. Summation over all manganese atoms m results in a spin-dependent correction $\epsilon_{i,\mathrm{ex}}$ to every donor energy level, which is given by

$$\epsilon_{i,\mathrm{ex}} = s_z \sum_m \alpha \left|\phi_i(r_m)\right|^2 \, J_m \ . \tag{6.3}$$

Averaging over all orientations of the angular momenta yields to

$$\epsilon_{i,\mathrm{ex}}(x_i,\, s_z,\, B,\, T) = \alpha \, s_z \, \langle J_z \rangle \sum_m \left|\phi_i(r_m)\right|^2 \ , \tag{6.4}$$

where $\langle J_z \rangle = J \, \mathrm{B}_J(B,\, T)$, where B_J is the Brillouin function given by equation (2.2). In this step the sum over every single angular momentum of an individual manganese atom was replaced by the average value of all of them. This step of a mean-field approximation is a simplification that requires some justification. For the sample parameters in this work, there is always a sufficiently large number of manganese atoms inside the envelop function of each donor according to basic statistical considerations. Therefore such an approximation is reasonable. With this step we eliminate thermal fluctuations of the manganese spins from our further considerations.

One should mention that the exchange contribution to the donor energy is zero when no external magnetic field is applied: $\epsilon_{i,\mathrm{ex}}(B = 0) = 0$. But the most important part of this equation is that it provides us with the magnetic-field dependence of the donor energy and thus with that of the distribution or density of states of the donor energies.

In section 2.1.2 we considered the conduction band splitting ΔE_{c}, cf. equation (2.4), in the mean field approach. The mesoscopic conduction band splitting in a magnetic field and hence the energy-splitting of a single donor state is given by

$$\begin{aligned} \Delta\epsilon_i =& \epsilon_{i,\mathrm{ex}}(s_z = +1/2) - \epsilon_{i,\mathrm{ex}}(s_z = -1/2) && (6.5) \\ =& \alpha \, \langle J_z \rangle \sum_m \left|\phi_i(r_m)\right|^2 \ . && (6.6) \end{aligned}$$

6.3 Impurity band formation

The different donor energies $\tilde{\epsilon}_{i,0}$ in a binary material, in our case that would be our host material zinc selenide, occur due to level repulsion of the donor energy states. As this effect is also present in the ternary system, we have to consider it too.

In sum the three contributions due to level repulsion, chemical shift and exchange splitting yield a realistic energy ϵ_i of the donor i on the absolute energy scale and its magnetic field

dependence. Some of them are magnetic field dependent, and thereby spin degenerate in zero-field, and some are not (indicated by the digit 0). In total the energy of a donor is given by

$$\epsilon_i = \tilde{\epsilon}_{i,0} + \epsilon_{i,0}(x_i) + \epsilon_{i,\mathrm{ex}}(x_i,\, s_z,\, B,\, T,\,) \;. \tag{6.7}$$

The splitting of the energy is still given by equation (6.5) as the other two contributions are independent on the magnetic field.

The density of impurity states $\{\epsilon_i\}$ also called the impurity band arises from all the donor energies combined. Here we see that some mechanisms contribute to the impurity band-width (IBW) of zinc manganese selenide and that some of them show a dependence on manganese content, on spin orientation, on magnetic field and on temperature.

Already at this stage it is clear that the lower spin-impurity band broadens with increasing magnetic field. This is a consequence of the $\epsilon_{i,0}$ being lower for a higher local manganese content x_i and these ϵ_i exhibit a larger splitting. This situation is illustrated in figure 6.3.

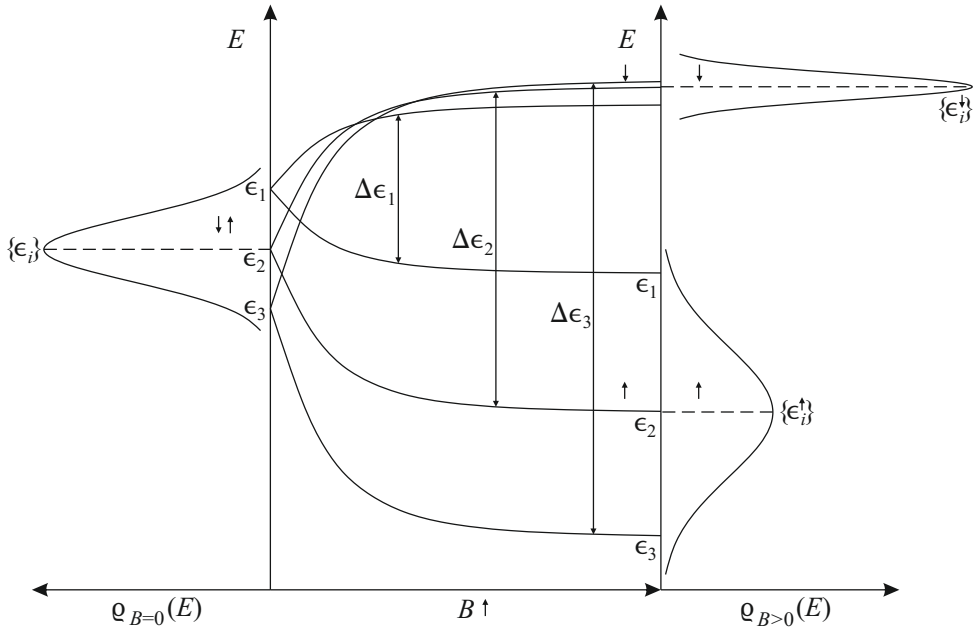

Figure 6.3: The zero-field impurity band, resulting from figure 6.2 and equation (6.1), splits into the spin-up and the spin-down impurity band. Three representative energies ϵ_1–ϵ_3 are given. The highest energy ϵ_1 having the lowest manganese content in its vicinity splits therefore only by a small amount, for the lowest energy ϵ_3 it is the other way round, cf. equation (6.4). Due to this the lower spin-band broadens while the upper one narrows. As electrons prefer the lower spin state only the increase of this impurity band-width is of importance.

Chapter 7

Scaling Approach

Scaling is well known from literature. Here are some examples for the use on electronic transport. The basic step of reducing the temperature and the magnetic field dependence in a Zeeman situation to just one variable holds for all the following authors. Ivanova *et al.* [28] used this method to point out the dependence on the ratio $H/(T+\Theta)$. The use was to reduce the temperature and magnetic field dependent magnetoresistance to a single curve. Matveev [39] used this scaling argument in the case of variable range hopping. But both authors were interested in the description of non-magnetic semiconductor, where normal Zeeman splitting takes place. The description of variable range hopping alters the ratio of $x = B/T$ to a more complex expression. Additionally the authors introduce the function F(x) in their theory to explain the magnetic field dependence. This step is similar to the one we use in the second step of the scaling approach. Terry also describes variable range hopping. First only the temperature dependence is scaled [62], but later he also uses the ratio B/T. His argumentation is based on the dependence of the relative permittivity and of the magnetoresistance on this new variable. But the important facts are that this argumentation was used to describe a dilute magnetic semiconductor and that the use of this new variable was related to the susceptibility χ. The working group around Leighton has done some studies on a permanent photo current (ppc) dilute magnetic semiconductor.[35, 36] In the second publication they used the dependence of the magnetoresistance on the ratio $B/(T+\Theta)$ in the hopping regime to reduce all curves to a single one, just like we do.

Before the actual discussion of the scaling approach, some additional considerations are required:

i) The normal Zeeman splitting may be neglected, as its energy $s_z\, g\, \mu_\mathrm{B}\, B$ is about an order of magnitude smaller than the Giant Zeeman splitting in these sample and at the magnetic field and temperature values of the measurements ($T < 10\,\mathrm{K}$ and $B < 10\,\mathrm{T}$), cf. section 2.1.2.

ii) Transport is only modeled in the lowest of the two impurity spin-bands $\{\epsilon_i(s_z = -1/2)\}$. The justifying arguments are the following. Every electron bound to a donor has two possible spin configuration. Even at low magnetic fields one of them is energetically preferred. We extend this argument to zero field, as we consider no other spin-related

effects, such as special mechanisms or energies for a spin flip, to occur. Essential is that a donor site is empty so that an electron may hop there and may do this preferentially to the spin state lower in energy. The only relevant reason for this is the assumption that an electron preferentially is to be found in or hops to the lower energy level, independent of the fact that it has to flip its spin or not. The supporting argument for this point of view is that the time scale of our measurements is orders of magnitude larger than the spin-flip dephasing time, so that in equilibrium always the state at every site with the lowest energy is occupied. So we start our calculations with spin-polarized electrons even at zero field.

iii) Of course there are limits to this approach. As long as the thermal energy is comparable to the conduction band splitting there will be no near unity spin-polarization of electrons. But on the one hand, at 10 K and $x = 2\,\%$ the magnetic field for $\Delta E_\mathrm{c} > k_\mathrm{B}\,T$ is approximately 0.8 T. For even lower temperatures this critical field strength is even further decreased. So at least our approach is justified above this threshold of B and x. However there are no other spin requirements established in literature, that contradict our assumption that only the energy levels and not the spins themselves are relevant. Therefore without other relevant spin-flip mechanisms or energies our description for spin-polarized electrons equals that of unpolarized ones. So there should be no difference in hopping rates and thus in resistivity.

Because of these reasons we state that only the energy of the lowest of the two impurity spin bands $\{\epsilon_i(s_z = -1/2)\}$ contributes to the hopping transport and that not spin flips are not decisive, but only the energy levels of the donor states.

iv) For applicability of the scaling approach it is necessary to assume: $\Theta = 0$ in order to simplify the expression for ξ given in equation (2.3) to

$$\xi = \frac{g\,\mu_\mathrm{B}\,J\,B}{k_\mathrm{B}\,T} \propto \frac{B}{T}\,. \tag{7.1}$$

This assumption is based on the demand that the manganese content is low, so that also the antiferromagnetic interaction is weak. This step is needed to simplify the dependence of the Brillouin function only on the ratio of B/T.

v) We do not consider hopping of bound magnetic polarons as at low manganese contents no significant negative contribution to the magnetoresistance arises which could be originated due to this effect. Therefore, it will not be the dominating magnetoresistance mechanism. The qualitative analysis of this simplification and its limits will be presented in the corresponding next chapters.

vi) Another assumption is that the effective Bohr radius is unaffected by the magnetic field, as the energy position of the conduction band edge and that of the donor shift at the same rate, i.e. that the donor depth remains constant. From the experimental point of view the temperature dependence should give reason for a change of the activation energy or that of the Bohr radius.

vii) A change of the Fermi level inside the impurity band is also neglected, because for this to happen there has to be a magnetic-field induced change of compensation. As no such process is known, we excluded this possible effect.

7.1 Gaussian distribution

Inserting equation (6.1) and equation (6.4) into equation (6.7) the energy of a spin-down state of a donor bound electron is given by

$$\begin{aligned}\epsilon_i(s_z = -1/2) &= \tilde{\epsilon}_{i,0} + \epsilon_{i,0} + \epsilon_{i,\mathrm{ex}} \\ &= \tilde{\epsilon}_{i,0} + \left(y - \frac{1}{2}\,\alpha\,\langle J_z\rangle\right) \sum_m |\phi_i(r_m)|^2 \qquad (7.2) \\ &= \tilde{\epsilon}_{i,0} + \left(y - \frac{1}{2}\,\alpha\,J\,\mathrm{B}_J\right) \sum_m |\phi_i(r_m)|^2 \ . \qquad (7.3)\end{aligned}$$

An important and characteristic simplification for the scaling approach is now to assume that all the distributions due to level repulsion $\{\tilde{\epsilon}_{i,0}\}$, due to chemical shift $\{\epsilon_{i,0}\}$ and due to the exchange interaction $\{\epsilon_{i,\mathrm{ex}}\}$ are described by Gaussian distributions and the first and the later two are not correlated. From this assumption follows that the distribution of the sum also will be Gaussian. The variance σ^2 of this combined spin sub-band impurity distribution $\{\epsilon_i\}$ is given by

$$\sigma^2 = \mathrm{Var}(\tilde{\epsilon}_{i,0}) + \left(y - \frac{1}{2}\,\alpha\,J\,\mathrm{B}_J\right)^2 \mathrm{Var}(\Sigma)\ , \text{with} \qquad (7.4)$$

$$\Sigma = \sum_m |\phi_i(r_m)|^2 \ . \qquad (7.5)$$

This means that the variance has a quadratic dependence on the Brillouin function $\mathrm{B}_J(B/T)$. Hence also the standard deviation is dependent on the ratio of magnetic field to temperature: $\sigma(B/T)$. For our purposes the relative value, i.e. the ratio of the B/T-dependent width to the zero-field value, is relevant. The calculation given in appendix A.2 leads to

$$\frac{\sigma(B/T)}{\sigma_0} = \sqrt{1 - \gamma_1^2 + \left[\gamma_1 + \gamma_2\,\mathrm{B}_J(B/T)\right]^2}\ , \qquad (7.6)$$

where γ_1 and γ_2 are dimensionless parameters defined as

$$\gamma_1 = -y\sqrt{\frac{\mathrm{Var}(\Sigma)}{\mathrm{Var}(\tilde{\epsilon}_{i,0}) + y^2\,\mathrm{Var}(\Sigma)}} \qquad (7.7)$$

$$\gamma_2 = \frac{1}{2}\,\alpha\,J\sqrt{\frac{\mathrm{Var}(\Sigma)}{\mathrm{Var}(\tilde{\epsilon}_{i,0}) + y^2\,\mathrm{Var}(\Sigma)}} \qquad (7.8)$$

In the assumption of Gaussian distributions the width σ of the donor level distribution $\{\epsilon_i\}$ in the presence of manganese atoms depends only on the ratio of magnetic field to temperature: $\sigma(B/T)$. Our estimations show further that the donor level distribution broadens in a magnetic field, due to the field dependence of the magnetization of the manganese spins and due to the bowing of the conduction band edge. This situation is illustrated in figure 7.1.

7.2 Resistivity scaling

The resistivity ρ depends on the attempt-to-escape frequency ν_0, on the Bohr radius a_B, on the concentrations of donors N_Cl, on the compensation K, on the width σ of the distribution of donor energies and on the temperature T. All these parameters, except σ and T, are constant

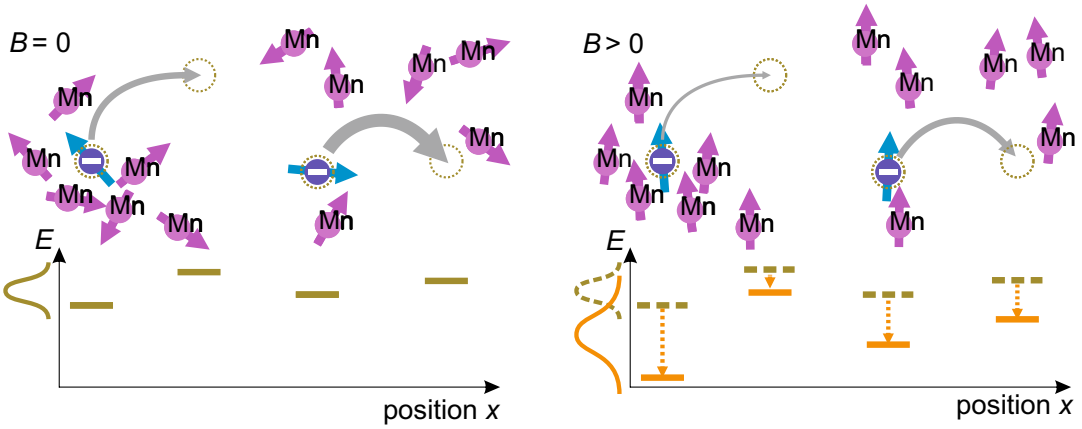

Figure 7.1: Schematic of the basic idea: The donors with a low local manganese content posses high energies in the impurity band and vice versa. These high energy states split less, because of their low x_i. The low energy states split more than everage, because of their high x_i. In consequence an external magnetic field yields due to the alignment of manganese spins an increasing Gaussian impurity band-width σ for the preferred spin band and thus to decreasing hopping rates (indicated by the arrows) and a higher resistivity. The origin of this effect is the local disorder of manganese atoms.

for a given sample. Therefore, the magnetoresistance at a given temperature is dominated by the magnetic-field induced change of the width σ: $\rho = \rho(\sigma, T)$. As described in the previous section the cause of changing σ in magnetic field is due to the exchange interaction between the electrons bound to donors and magnetic impurities. The magnetization of the manganese atoms is controlled by the external magnetic field.

To determine the resistivity we first have to take a look at the hopping rate. The expression for hopping rates in equation (3.10) itself possesses a remarkable feature: when the energies $\epsilon_{i'}$ and ϵ_i, the temperature T and the electric field $\mathbf{E}$ are scaled by some factor λ, the rate remains unchanged:

$$\Gamma_{i,i'}(\lambda\epsilon_i, \lambda T, \lambda\mathbf{E}) = \Gamma_{i,i'}(\epsilon_i, T, \mathbf{E}) \; . \tag{7.9}$$

If we now go from the hopping rate between two sites to the percolation current paths throughout the entire sample one aspects some changes. We have to correlate the energy difference of two sites with the width σ of the impurity band. Concomitantly the current density $\mathbf{j}$ remains unchanged:

$$\mathbf{j}(\lambda\sigma, \lambda T, \lambda\mathbf{E}) = \mathbf{j}(\sigma, T, \mathbf{E}) \; . \tag{7.10}$$

Expressing the current density $\mathbf{j}$ via the resistivity ρ,

$$\mathbf{j}(\sigma, T, E) = \mathbf{E}/\rho(\sigma, T) \; , \tag{7.11}$$

According to Ambegaokar *et al.* another aspect is essential in this context, namely that the ratio ρ/T is a function of one variable only, the ratio σ/T.[5] Let us denote this function as $\tilde{f}$:

$$\frac{\rho(\sigma, T)}{T} = \tilde{f}\left(\frac{\sigma}{T}\right) \; . \tag{7.12}$$

Implicit that means that ρ/T remains unchanged when σ and T are scaled simultaneously:

$$\frac{\rho}{T}(\lambda\sigma, \lambda T) = \frac{\rho}{T}(\sigma, T) \; . \tag{7.13}$$

For studying the magnetoresistance, it is convenient to define a new function f as

$$f\left(\frac{\sigma}{\sigma_0 T}\right) = \tilde{f}\left(\frac{\sigma}{T}\right) \; , \tag{7.14}$$

where σ_0 is the width of the energy-level distribution at zero magnetic field. A combination of the equations (7.12) and (7.14) yields

$$\frac{\rho}{T} = f\left(\frac{\sigma}{\sigma_0 T}\right) . \tag{7.15}$$

Equation (7.15) is the key relation of our scaling approach. It will be used below to extract the magnetic-field dependence of the width σ from the experimental data. This will be done in two steps: (i) extracting the function f, and (ii) determining the ratio σ/σ_0 as a function of magnetic field B and temperature T.

The function f can be derived from the temperature dependence of the resistivity. Since $\sigma = \sigma_0$ at $B = 0$, one obtains from equation (7.15)

$$\frac{\rho}{T} = f\left(\frac{1}{T}\right) \text{ at } B = 0 \; . \tag{7.16}$$

Plotting ρ/T versus $1/T$, one obtains the function f (see inset on the left side of figure 7.2a).[1] With known f and using equation (7.15), we can restore the ratio $\sigma(B,T)/\sigma_0$ from experimental data for $\rho(B,T)$,

$$\frac{\sigma(B,T)}{\sigma_0} = T\, f^{-1}\left(\frac{\rho(B,T)}{T}\right) . \tag{7.17}$$

7.3 Experimental data

First we determined the function f in equation (7.16) from the temperature dependence of the zero field resistivity. The result is depicted in the inset on the left side of figure 7.2.

Then we used the inverse function f^{-1} the extract the relative impurity band-width from the magnetic field and temperature dependent resistivity according to equation (7.17). The result is given on the left side of figure 7.2.

The most remarkable feature of σ/σ_0 is the similarity of the magnetic field-dependence at different T values. In order to make this more evident, on the right side of figure 7.2 we plot the same data as functions of the ratio B/T. One can see that the dependences $\sigma(B/T)$ for all temperatures are almost identical. One can see that the resemblance for values below 0.6 is very good, but that for higher ratios a discrepancy between theory and experiment occurs. The real impurity band-width saturates faster than the model predicts. There may be a negative contribution to σ, that we do not consider and which increases with increasing x,

[1] The extrapolation of the function f in the region $0.6\,\mathrm{K}^{-1} < 1/T < 1.5\,\mathrm{K}^{-1}$ in the inset on the left side of figure 7.2 is used for processing the magnetoresistance data at $T = 1.6\,\mathrm{K}$ only.

cf. chapter 9. However, the concept itself works as can be seen by the almost ideal reduction of the experimental to one scaling function.

Using the comparison of theoretical and experimental curves in figure 7.2(b) one can recalculate theoretical predictions for the magnetoresistance curves and compare them with the

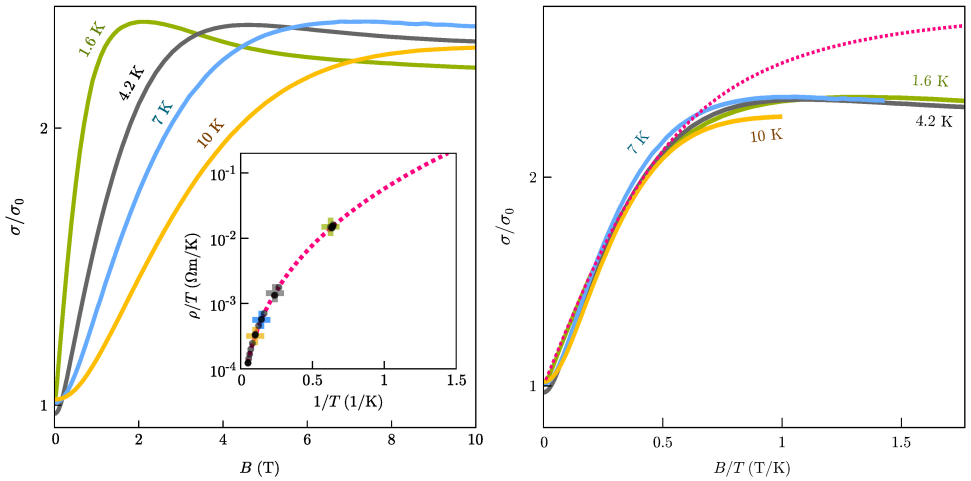

Figure 7.2: a) Using the temperature-dependence (inset) one is able to extract from the magnetoresistance curves the relative impurity band-width change. b) This ratio can be reduced to a single general curve by introducing the parameter B/T. This curve can now be compared to the curve resulting from our ideal theoretical model.

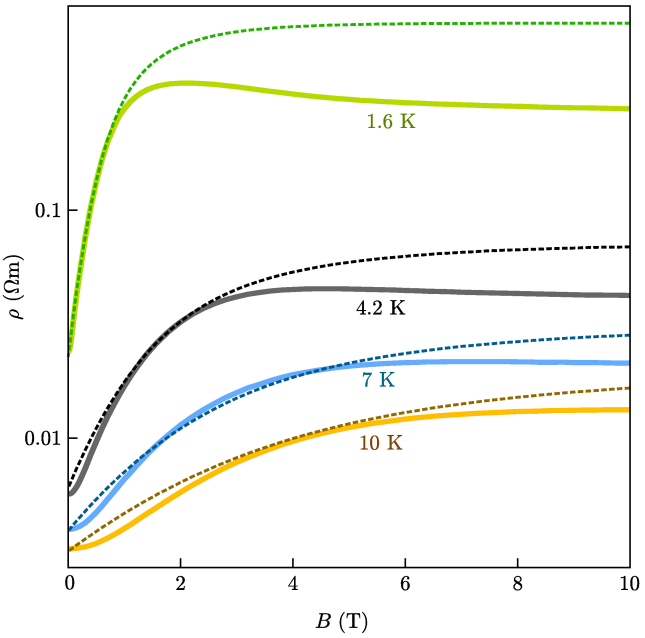

Figure 7.3: With the given results above one is able to reconstruct the ideal magnetoresistance measurements in dashed lines. Comparing these with the experimental results, solid lines, one sees a good agreement. But one also observes the discrepancy at higher magnetic fields mentioned before. And also for higher temperatures there seams to be a little overestimation of the theoretical curves, which is not apparent at 1.6 K.

corresponding experimental data. This is done in figure 7.3. In general they are in good agreement, but a certain discrepancy can be seen originating from the one on the right side of figure 7.2.

Chapter 8

Simulation

In the simulation approach we will not be using the simplification of the former scaling chapter. The manganese correlated energy distributions, which contribute to the total donor energy distribution, are no longer regarded as Gaussian. Instead they will be determined by numerical calculations. Thus the accuracy and the resembling of theory and the real lattice will be much higher. Afterwards it is possible to compare the two approaches and estimate possible errors.

In the following step the hopping conductivity will be numerically simulated in a random network of donors. Each of them is related to a local environment of manganese atoms and thus for every donor the energetic position and its magnetic field and temperature dependence are known. Again this yields a even better representation of the real physical transport properties than a simplified view in terms of general statements for an assumed Gaussian distribution.

To achieve this we will avoid the averaging steps yielding to the commonly known results of mean-value and deviation only in which all random disorder is considered. Starting with the exchange energy contribution according to equation (6.4)

$$\epsilon_{i,\mathrm{ex}} = \alpha\, s_z\, \langle J_z \rangle \sum_m |\phi_i(r_m)|^2 \ ,$$

and replacing $\phi_i(r_m)$ by the strength of the envelop function of the i-th donor on the site of the m-th manganese atom according to equation (3.3)

$$\phi_i(r_{i,m}) \propto \frac{1}{\sqrt{\pi\, a_\mathrm{B}^3}}\, \exp\left(-\frac{r_{i,m}}{a_\mathrm{B}}\right) ,$$

leads to

$$\epsilon_{i,\mathrm{ex}} = \alpha\, s_z\, \langle J_z \rangle \frac{1}{\pi\, a_\mathrm{B}^3} \sum_m \exp\left(-2\,\frac{r_{i,m}}{a_\mathrm{B}}\right) . \tag{8.1}$$

Handling the chemical shift from equation (6.1) in the same fashion yields:

$$\epsilon_{i,0} = \frac{y}{\pi\, a_\mathrm{B}^3} \sum_m \exp\left(-2\,\frac{r_{i,m}}{a_\mathrm{B}}\right) . \tag{8.2}$$

The absolute site energy of the spin-down state evolves from equation (7.3) to

$$\epsilon_i(s_z = -1/2) = \tilde{\epsilon}_{i,0} + \left(y - \frac{1}{2}\,\alpha\, J\, \mathrm{B}_J\right) \frac{1}{\pi\, a_\mathrm{B}^3} \sum_m \exp\left(-2\,\frac{r_{i,m}}{a_\mathrm{B}}\right) . \tag{8.3}$$

In order to determine the distribution of exchange energies $\{\epsilon_{i,\mathrm{ex}}\}$ and the energies of the chemical shift $\{\epsilon_{i,0}\}$, the distribution of the value of the sums in equations (8.1) to (8.3)

$$w = \sum_m \exp\left(-2\,\frac{r_{i,m}}{a_\mathrm{B}}\right), \tag{8.4}$$

must be evaluated. Every sum is a measure of the individual s-d interaction strength of the donor i with all the manganese atoms m in its vicinity. Thus the density of this interaction strength of all donors $g(w)$ represents the density of impurity states by performing the transitions $w \to -\epsilon$ and $g(w) \to \varrho(E)$, cf. equation (8.2). To calculate the sum is the first step in the simulation process. The distributions were obtained numerically, by evaluating equation (8.4) for randomly created systems. Each of these systems contained one chlorine donor surrounded by zinc atoms on a face-centered cubic lattice, where each zinc atom was replaced by manganese with a probability x.

The results of the simulation processes are given as histograms shown in figure 8.1. As one can see there is a certain degree of fluctuation around the mean value for the interaction of randomly distributed donors with randomly distributed manganese atoms. First there is to mention, that the calculated distribution is fairly close to a Gaussian one of the same variance derived, for the manganese contents and Bohr radii of the samples. However, there are small

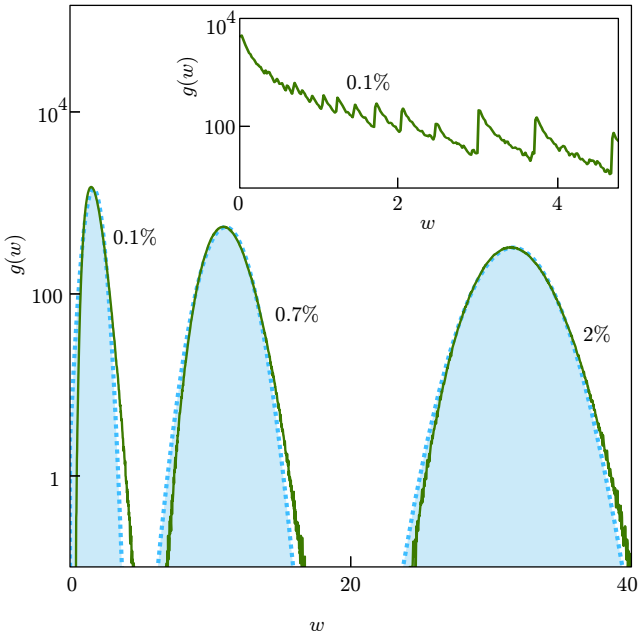

Figure 8.1: Results of the simulation are presented in form of the density of this interaction strength of all donors $g(w)$ as a function of the individual s-d interaction strength w. This is done for different manganese contents. The sum w is a measure of the individual s-d interaction strength of the donor i with all the manganese atoms m in its vicinity. In particular $g(w)$ represents the density of impurity states. This is compared to a Gaussian distribution (doted line). These two approaches are similar but differences between them are to be seen at both edges of the impurity band. For very small manganese contents and a small Bohr radius the appearance changes drastically and the discrete nature of the lattice is recognizable (inset).

deviations between the two that might be important. Always the calculated histograms are asymmetric, steeper at smaller values of w and more extended at larger ones. This asymmetry becomes less important with increasing manganese content and thus the approximation by the Gaussian distribution approaches the precise calculations at higher x. But even though a Gaussian distribution might be a good approximation of the actual interaction strength, the results may be very different for these two approaches. This depends on the position of the Fermi level inside the impurity band. If it is close to one of the edges, i.e. for very high or very low compensation, this will have a major impact, as the donor energy levels close to the Fermi level contribute most to the hopping transport. At very low manganese contents and at small Bohr radii, i.e. comparable to the lattice constant, a Gaussian distribution is no longer justified. This can be seen in the inset of figure 8.1 where the origin of the shape with multiple peaks is the discrete nature of the crystal lattice.

As $g(w)$ represents the density of impurity states, figure 6.3 has to be modified accordingly as we now have a better knowledge of the density of states $\varrho(E)$. The non-Gaussian shape of $\varrho(E)$ is preserved under magnetic field influence, cf. figure 8.2.

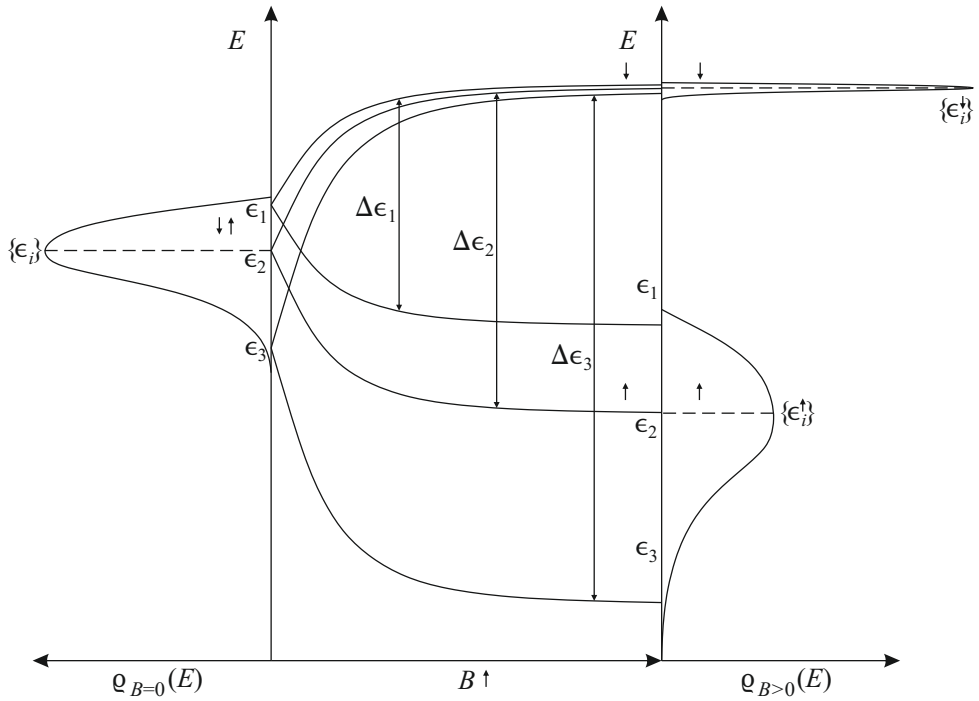

Figure 8.2: Schematic of the simulated density of impurity states at zero-field and its splitting according to equations (8.1) and (8.2), respectively. Thus the lower and the higher spin-band arise, with electrons preferentially occupying the lower one. This lower spin-band broadens while keeping the same shape. The dashed line at the center can be interpreted as the Fermi level of a roughly half filled impurity band at 0 K.

8.1 Hopping transport simulation

In the following hopping transport is simulated in a system where the site energy of each donor is determined according to equation (8.3), with $\tilde{\epsilon}_{i,0}$ chosen from a Gaussian distribution. Again the hopping only takes place in the spin-down sub-distribution of donor states, which are never doubly occupied.

The simulated system contains 25^3 randomly placed donors. The corresponding sum of the individual interaction w is derived for randomly placed manganese atoms in the system by equation (8.4). For the hopping rates between the donors, Miller-Abrahams rates $\Gamma_{i,i'}$ according to equation (3.10) are used. From the site energies and hopping rates in the system, the steady-state occupation probabilities p_i for all donors $\{i\}$ are determined by solving a set of non-linear balance equations.[29, 30, 49, 69] In the steady state, the electron flow into each site equals the electron flow out:

$$\sum_{i' \neq i} p_i \, \Gamma_{i,i'} \, (1 - p_{i'}) = \sum_{i' \neq i} p_{i'} \, \Gamma_{i',i} \, (1 - p_i) \; . \tag{8.5}$$

This set of equations, one for each site i, is solved using Newton's method. From the occupation probabilities the current density in the system is determined,

$$j = \frac{e}{V} \sum_{i,i' \neq i} p_i \, \Gamma_{i,i'} \, (1 - p_{i'}) \, \frac{\mathbf{E}}{|\mathbf{E}|} \cdot (\mathbf{r}_{i'} - \mathbf{r}_i) \; , \tag{8.6}$$

where e is the electron charge, V is the volume of the simulated system, $\mathbf{E}$ is the external electric field, and $\mathbf{r}_i$ is the position of hopping site i. Periodic boundary conditions are applied in all directions.

It is worth mentioning that the simulation approach presented here takes correlation effects of neighboring donors implicitly into account. So no model conceptions are needed and no assumption have to be made to include these effects.

Results of the simulated resistivity for zinc manganese selenide with $x = 0.75\,\%$ as a function of magnetic field B for different temperatures are presented as dashed lines in figure 8.3 together with their measured counterparts as solid lines (which were already plotted in figure 5.8). The calculated curves show a good agreement with experimental data. Both the shape and the values of magnetoresistivity match well. The small deviations will be discussed later on the basis of the parameter choice and fitting procedure described below.

Values for the model parameters used in the simulation of the magnetoresistivity are the following. All these values for natural reasons were fixed before the start of the actual simulation. The density of cationic sites N_0 in zinc selenide and the s-d exchange integral $N_0\,\alpha$, which are known from literature, are set to $N_0 = 2.19 \times 10^{22}\,\mathrm{cm}^{-3}$ and $N_0\,\alpha = 260\,\mathrm{meV}$.[23] From the growth and measurements the manganese content x is known and because of the small value it is directly used as the approximate value $x = 0.75\,\%$ without considering its effective one. For the chlorine (donor) concentration N_{Cl} the situation is harder. As we cannot be certain about the degree of compensation, from section 2.1 we know that K increases with increasing manganese content, but no reliable data of the precise value is at hand. So at this stage we simply use the carrier concentration at room temperature, $n = 1.86 \times 10^{17}\,\mathrm{cm}^{-3}$, knowing that this can be a lower limit only.

The following values were determined during the simulation process. The relative importance of the two disorder terms $\{\epsilon_{i,0}\}$ and $\{\tilde{\epsilon}_{i,0}\}$ is not clear a priori. We find, that in order to obtain a good fit to the low-magnetic-field part of the magnetoresistance curves, the $\{\epsilon_{i,0}\}$ term is decisive. This is obvious as the influence of the zero-field width of the impurity band is strongest in this field range. Nonetheless one has to keep in mind that affecting its width cannot be done without changing the exchange part too. The simulation values for the intrinsic impurity band-width of $\{\tilde{\epsilon}_{i,0}\}$ were always close to zero. Therefore and to reduce the number of fitting parameters, for simplicity $\{\tilde{\epsilon}_{i,0}\}$ is set to 0, meaning that all energetic disorder is related to the presence of manganese atoms. This is consistent with the findings in chapter 7 and our work.[43]

The values of the other model parameters were adjusted so as to mimic the experimental magnetoresistivity best: the attempt-to-escape frequency in the Miller-Abrahams hopping rates takes $\nu_0 = 1.94 \times 10^{13}\,\mathrm{s}^{-1}$, 20 % of the donors are compensated (i.e. empty), the Bohr radius of the donor sites takes $a_\mathrm{B} = 4.0\,\mathrm{nm}$ and the interaction integral $N_0\,\gamma$ is set to $-650\,\mathrm{meV}$.

The fitting value of $N_0\,\gamma = -650\,\mathrm{meV}$ corresponds to the slope of the conduction band edge $\mathrm{d}E_\mathrm{c}/\mathrm{d}x$ at low manganese contents ($x < 5\,\%$). A negative value is reasonable as the variation of the band gap E_g with x shows bowing for $x < 10\,\%$ with a minimum near $x = 5\,\%$, cf. figure 6.1.[7, 23, 26] The fitting value of the effective Bohr radius of donor states, $a_\mathrm{B} = 4.0\,\mathrm{nm}$, appears larger than the bare Bohr radius $a_\mathrm{B0} = 2.84\,\mathrm{nm}$.[59] This larger magnitude of the Bohr radius might be due to interdependence of the following values. As mentioned above

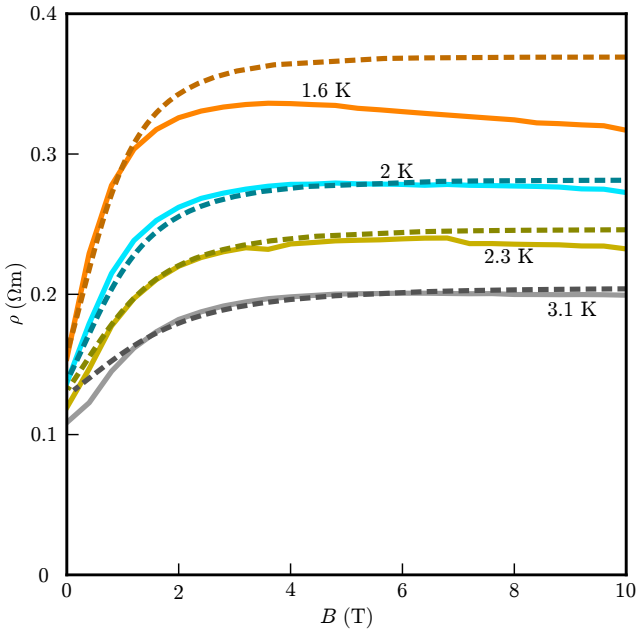

Figure 8.3: Simulating the hopping transport with a given set of parameters inside the calculated density of impurity states yields the dashed curves. Experimental results for the same temperatures are shown for comparison. The resemblance is good, but there are still some minor differences. For the lowest temperature the high-field part shows a differences. Also the temperature dependence at zero magnetic field seems not to satisfy the experimental data.

the used value for the chlorine density is only a lower limit. So it is obvious that by choosing a larger value the fit would give a smaller Bohr radius. But the chlorine density cannot be much larger as the transport measurement confirms that the sample is still far from the metal–insulator transition. If on the other hand the real compensation might be higher this would also lead to a smaller Bohr radius. There might even be a correlated explanation combining the two statements. As the simulation converges at this values it is most likely that effects, that are not included in this simplified calculation like the hopping of bound magnetic polarons or the coexistence of both spin bands at low fields, are the reason for the large Bohr radius derived.

As already mentioned above, the fitting parameters are not entirely uncorrelated. In addition different combinations of parameters are also fairly close to the best fit presented in figure 8.3. In other words reproducing the measured curves by our simulation scheme is possible not only with that given set of parameter values. The number of free parameters is fairly large and their effects on the magnetoresistivity are not entirely uncorrelated. Finite values of $\tilde{\sigma}_0$, for instance, do also allow for a good agreement between experiment and computer simulation when $N_0\,\gamma$ and ν_0 are adjusted accordingly. On the contrary, finite values of the manganese induced alloy shifts $\{\epsilon_{i,0}\}$, which do spatially correlate with the manganese spin induced exchange energies $\{\epsilon_{i,\mathrm{ex}}\}$, turn out to be essential in order to fit all of the magnetoresistivity curves at different temperatures but with the same set of parameters. Due to the large number of unknown parameters in the model, we are not able to precisely determine the parameter values of the experimental system in terms of one absolute parameter set. However, the values of parameters obtained by fitting are reasonable when compared to known values, showing that our simple model is able to explain the experimental observations. In particular, the model reproduces the magnitudes and the shapes of the $\rho(B,T)$ curves as a function of both temperature and magnetic field in the range studied.

The reason for the discrepancy between the theoretical and experimental results at $T = 1.6\,\mathrm{K}$ might be the following one. At a such low temperature a transition to Efros-Shklovskii variable range hopping might occur. The occurance of variable range hopping itself is no problem for the simulation as all correlated effects are implicitly accounted for in the model. However, the special version that was proposed by Efros and Shklovskii has some special features our model does not consider. These are long-range Coulomb interactions. As pointed out in Ref. [43], where the temperature dependence of the resistivity has been studied. There it was shown that the Efros-Shklovskii regime based on the effect of Coulomb correlations might take place at $T = 1.6\,\mathrm{K}$ and temperatures below. Therefore our approach is justified at $T > 1.6$ K, i.e. for the three curves in figure 8.3 corresponding to $T = 2\,\mathrm{K}$, $2.3\,\mathrm{K}$ and $3.1\,\mathrm{K}$. With respect to the data at $T = 1.6\,\mathrm{K}$, the validity of our theoretical approach is not certain. So the question might arise, whether our theoretical approach with neglecting the effect of long-range Coulomb interactions on the density of states is justified or not.

At low magnetic fields there is a small deviation to be seen. As mentioned before our simulation approach does not account for the hopping of bound magnetic polarons and also neglects the upper spin band. Both simplifications are decisive at low fields and vanish before saturation. Therefor we attribute the deviation to these two phenomena, which are not included. The deviations at low magnetic fields might also arise from a non-perfect fit.

8.1.1 Comparison of Gaussian and simulated impurity bands

Finally, we show in figure 8.4 the effect of the shape of the exchange energy distribution on the relative magnetoresistance at saturation magnetization, $\mathcal{R} = [\rho(B_{\rm sat}) - \rho(0)]/\rho(0)$, as a function of the manganese content x. For this purpose, we have performed the simulation, on the one hand, using the numerical approach described above, i.e. deriving the alloy shift and exchange energy distributions according to equations (8.1) and (8.2), and, on the other hand, applying a Gaussian distribution approximation for the alloy shifts and exchange energies $\{\epsilon_{i,0} + \epsilon_{i,\rm ex}(s_z = -1/2)\}$ with the variance given by[42]

$$\sigma_{0+\rm ex}^2 = \left(N_0\,\gamma - s_z\,\langle J_z\rangle\,N_0\,\alpha\right)^2 \frac{1}{8\,\pi\,a_{\rm B}^3\,N_0}\,x\,(1-x)\,. \tag{8.7}$$

As we have no particular sample in mind but instead are interested in general trends the choice of parameters in this calculation partially deviates from the values given above. Here, the width of the Gaussian background energy fluctuations due to the host material $\tilde{\sigma}_0$ is 0.3 meV, the perturbation constant $N_0\,\gamma$ is zero, the Bohr radius of donor states a_B is 2.8 nm, and the compensation level is 10 %.

Let us denote the two saturation magnetoresistances with $\mathcal{R}_{\rm Sim.}$ for the numerical approach with a random distribution of manganese atoms, and $\mathcal{R}_{\rm Gauss}$ for the Gaussian approximation. As can be seen in figure 8.4, the two calculated magnetoresistances, $\mathcal{R}_{\rm Sim.}$ and $\mathcal{R}_{\rm Gauss}$, show both a general dependence on x but deviate from each other, cf. figure 8.4. Spatial correlations between the energies of nearby donors, which are incorporated in the numerical approach for $\{\epsilon_{i,0} + \epsilon_{i,\rm ex}\}$, and which are known to be important for hopping transport in principle,[14, 29, 45] can be ruled out as the origin for the observed difference here because the average spacing between donors, $R_{\rm Cl} = N_{\rm Cl}^{-1/3}$, is much larger than their Bohr radius. In fact, it is the difference in the slopes of both distributions of energies $\{\epsilon_{i,0} + \epsilon_{i,\rm ex}\} \propto w_i$ shown in figure 8.1 which causes the deviations between $\mathcal{R}_{\rm Sim.}$ and $\mathcal{R}_{\rm Gauss}$. Moreover, it is worth noting that the increasing difference $|\mathcal{R}_{\rm Sim.} - \mathcal{R}_{\rm Gauss}|$ with increasing x does not automatically contradict the previous statement that the Gaussian approximation of $\{\epsilon_{i,0} + \epsilon_{i,\rm ex}\}$ improves with higher manganese contents x. The reason is that $\mathcal{R}(x)$ vanishes for $x \to 0$ for any reasonable distribution $\{\epsilon_{i,0} + \epsilon_{i,\rm ex}\}$ in our model, where the magnetic field couples only to the manganese spins, so that, in turn, the difference in $\mathcal{R}(x)$ between any two distributions $\{\epsilon_{i,0} + \epsilon_{i,\rm ex}\}$ must increase with increasing x at least for small values of x. Indeed, the relative difference, $[\mathcal{R}_{\rm Gauss} - \mathcal{R}_{\rm Sim.}]\,/\,\mathcal{R}_{\rm Sim.}$, decreases with increasing x as expected for two converging energy distributions.

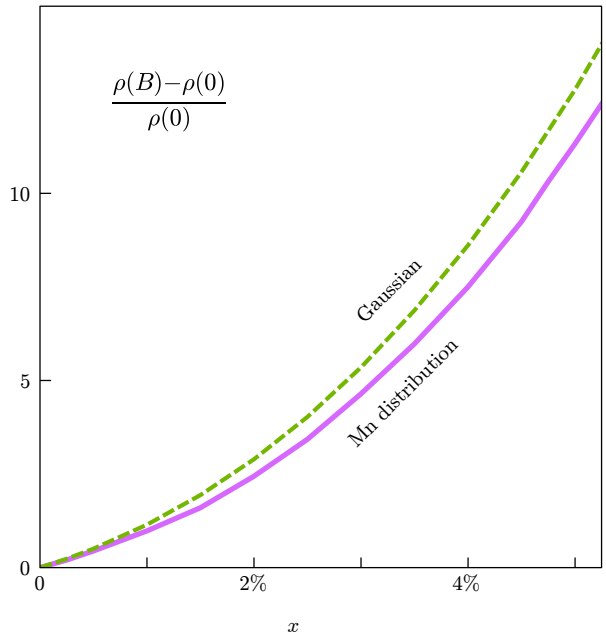

Figure 8.4: Simulations of maximal magnetoresistance for the calculated manganese influence are compared with the results from a Gaussian distribution as a function of x. Both show the same trend and differ only slightly in terms of absolute values. However, both represent the experimentally observed super-linear increase of the maximal relative magnetoresistance in figure 5.5. In this point our model provides also a good agreement with the experiments.

Chapter 9

High Manganese Content

The subject of this chapter is sample 1 with $x = 7.1\,\%$ and $n = 3.2 \times 10^{17}\,\mathrm{cm}^{-3}$. The measurements of the relative magnetoresistance are presented in figure 9.1. A special feature can be seen, i.e. a strong negative contribution to the magnetoresistance at high magnetic fields. The overall magnetoresistance is still positive but the negative contribution cannot be ignored. In the following we will present a qualitative explanation consistent with our proposed model. Basically we want to show that the dependence of the resistivity on the impurity band-width still holds although a simple correlation between the Brillouin function and the impurity band-width no longer exists.

For the measurement of the temperature dependence a slightly different procedure than the usual one for the measurement of the magnetic field dependence was used. The magnetic field was held constant while the temperature was changed. As no significant difference occurs

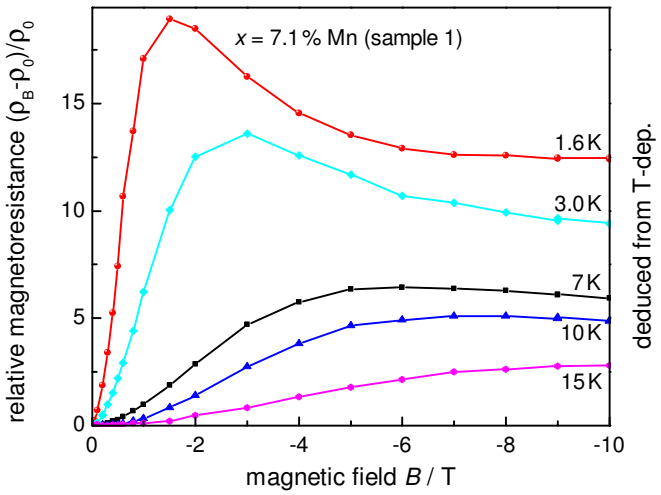

Figure 9.1: The relative magnetoresistance of sample 1 calculated from the temperature dependence done at several magnetic field values. The deduced curves resemble very well the ones obtained the normal magnetic field measurement at different temperatures, cf. figure 5.4. Therefore one can be sure that no errors between the two experimental approaches occur, although only one direction of the magnetic field is used.

when the magnetoresistance is measured for one field direction only instead of averaging the values obtained for both field directions, switching of the field direction was omitted in the temperature dependent resistivity measurements at constant field value.

Detailed temperature dependence were obtained at various magnetic fields. The curves are presented in figure 9.2. In figure 9.2 one observes that for an increasing magnetic field the temperature dependence changes giving rise to the magnetoresistance in figure 9.1. At temperatures above about 50 K the curves merge and the differences become negligible. The assumptions made in the model, in particular that the giant Zeeman splitting dominates, hold for temperature up to 30 K.

From the temperature dependence in figure 9.2 the values for the hopping activation energy ε_3 in figure 9.3 and the maximal conductivity of the conduction channel ρ_3 in figure 9.4 were determined. The names ε_3 and ρ_3 were used although the phenomenon at 12.5–22 K could be due to double occupation (ε_2 and ρ_2). Even from the temperature dependence it is obvious, that no single fit is able to describe the behavior. Dividing the low temperature region into four intervals allows one to apply a numerical linear fit. The observed behavior contradicts our simple model used for low manganese contents where we assume only one interval where only the activation energy changes and the maximal conductivity remains constant. On the basis of the experimental observations, this is no longer justified at higher manganese content. What we observe is four regimes instead of one and a change in almost all four activation energies ε_3 as well as maximal conductivities ρ_3. The dependence of the quantities are given in figures 9.3 and 9.4, respectively. All activation energies show the characteristic feature of a curve that increases at low fields then passes a maximum and in the following decreases

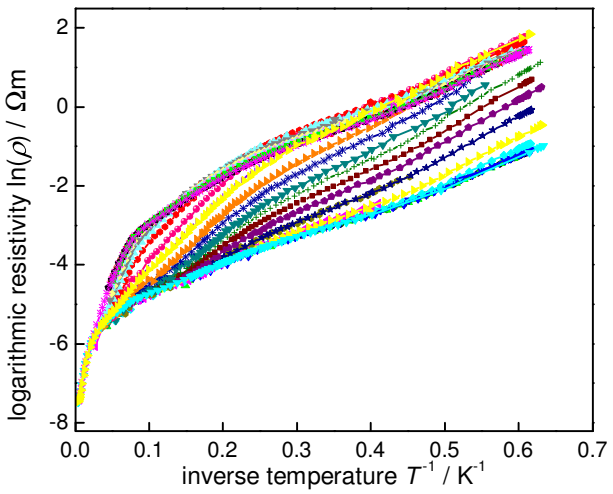

Figure 9.2: The temperature dependence of sample 1 in form of an Arrhenius plot for different magnetic fields. New information may be gathered by this method. Important for us is the change of the activation energy as a function of the magnetic field. To get this information linear fits of the temperature dependence have been done. To be accurate the low temp region has to be divided into four separate temperature regimes, in which linear fits are appropriate. This will be discussed further in the text. If one uses this fitting values to recalculate the relative magnetoresistance, i.e. a vertical line through the measurement, one ends with the presented curves in figure 9.1.

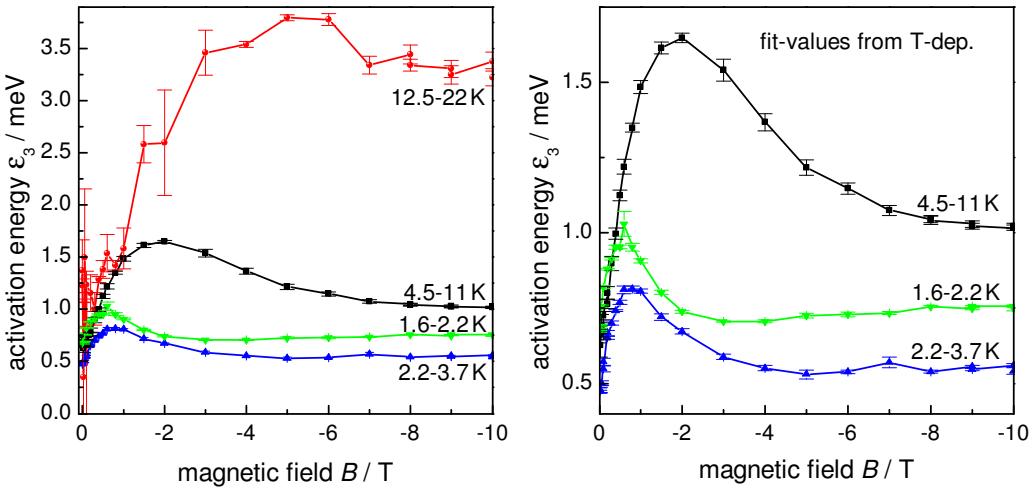

Figure 9.3: The activation energies for the four temperature regions as a function of the external magnetic field are shown here, on the right hand side a zoom of the three lowest temperatures is given. All of them show an increasing, then a maximum and afterward a decrease ending in saturation. This is one reason for the appearance of the magnetoresistance curves, which follows exactly our model idea. But these dependence is too low to explain the magnitude of the magnetoresistance effect. The discussion of the four activation energies can be found in the text.

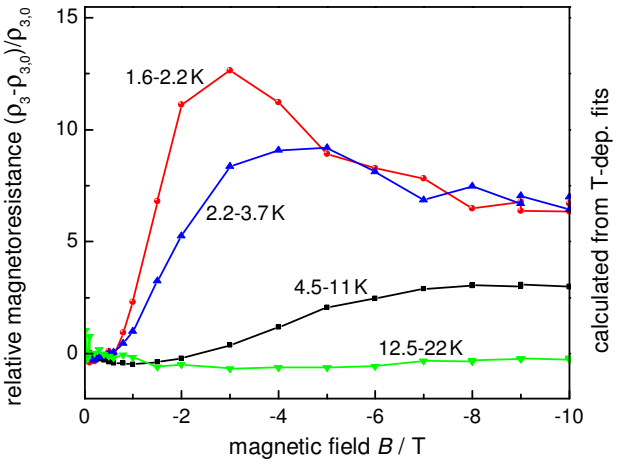

Figure 9.4: The relative change of fitting values ρ_3 as a function of the magnetic field show a behavior very similar to the magnetoresistance itself. The changes are larger and the field values of the maximum are lower at lower temperatures, all curves saturate at high fields. In contrast to the temperature dependence of the resistivity the zero-field values are not uniformly continuous. According to our model these values should stay constant, so for high x the conductivity of the channel itself plays a role in transport.

and ends in saturation. This is somewhat comparable with the magnetoresistance itself. The lower the temperature of the regime is the lower are the field values of the maximum. This behavior resembles the faster saturation of the Brillouin function for lower temperatures.

Analyzing the maximum conductivity $\rho_{3,i}$ of every channel one observes a similar behavior.

The lower the temperature the lower the field value of the maximum. And again the trend is comparable with the magnetoresistance itself. But this only holds if the relative changes are depicted. In the absolute values no consistent similarity is apparent. This result is the dependence of the maximal channel conductivity on the magnetic field. Until now there is no validated explanation for this behavior at hand. This may be a sign for the suppression of bound magnetic polaron hopping.

A negative magnetoresistance effect should occur for very high x-values above the minimum of the conduction band bowing, for example for $x > 15\,\%$. In this case the energies on the high energy tail of the impurity band correspond to high local x and those in the low energy tail to low local x. Thus, the preferential spin states of the former will exhibit a larger shift to lower energies than the latter leading overall to a narrowing of the transport-carrying impurity band and, thus, to a negative magnetoresistance. Therefor it is clear that for x-values near the minimum of the conduction band bowing a transition of the magnetoresistance behavior must occur. According to our understanding this may be the origin of the observed positive and negative contribution to the magnetoresistance observed for sample 1 in in figure 9.1. For such intermediate x the impurity band-width σ shows a rather complicated behavior as depicted in figure 9.5. It does no longer show a continuous increase as for low x or a continuous decrease as for high x, instead it results from both shares. As a consequence the impurity band-width does not vary monotonously anymore and even worse the shape of the impurity band changes. The reason is that the position of the donor energies in zero field is no longer a linear function of x as depicted in figures 6.3 and 8.2.

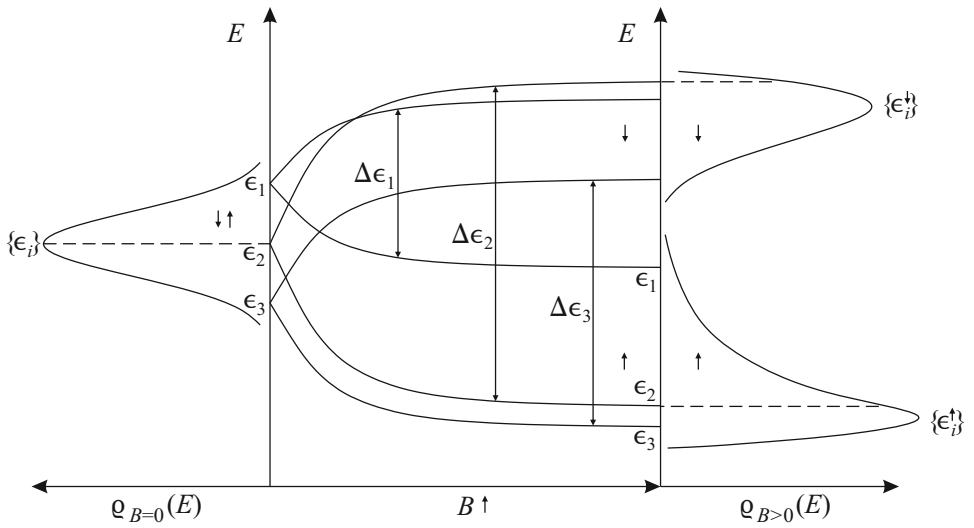

Figure 9.5: Hypothesis how the impurity band changes due to the applied magnetic field for high x-values. This situation is close to the minimum of the conduction band edge. In this region a linear dependence is no longer valid. If this is the case energies in both impurity band tails would exhibit a smaller splitting than an energy in the middle. As depicted this situation would lead to a complex change of the impurity band shape. In this framework both positive and negative contributions to the magnetoresistance are possible, but hard to predict. To be precise even the starting density of states is no longer a Gaussian one, but this was chosen to show the shape changing character.

Chapter 10

Pressure Dependence

10.1 Resistivity changes under hydrostatic pressure

The pressure dependence of the resistivity at different temperatures and at zero magnetic field is shown on the left of figure 10.1. One can observe a super-exponential increase of the resistivity with increasing pressure at every temperature. At lower temperatures the increase is even higher. Both effects must be related to bandstructure changes under hydrostatic pressure. Several effects may possibly play a role here.

At room temperature, where activated transport into the free conduction band states is

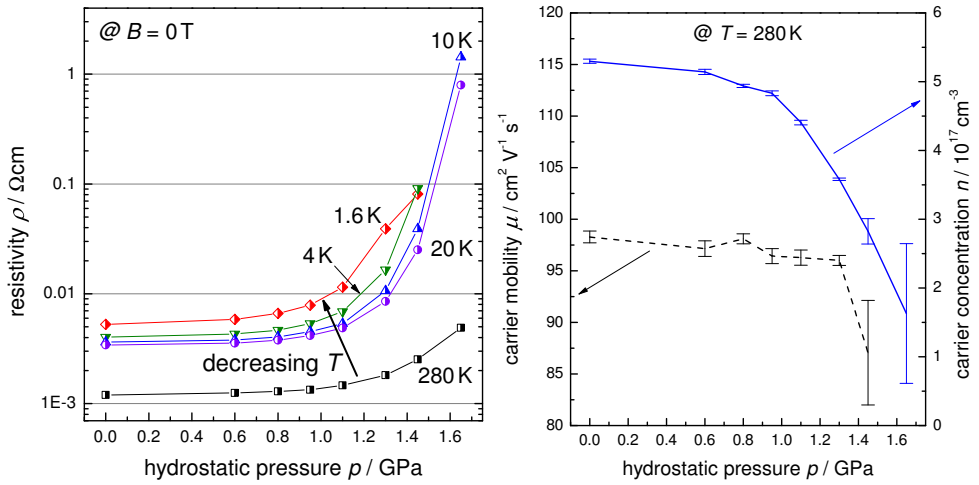

Figure 10.1: left: The resistivity increases as a function of hydrostatic pressure at zero magnetic field and at differenttemperatures. The increase is more than exponentially and larger for lower temperatures. For the curve at 280 K it is possible to analyze the resistivity ϱ in terms of carrier concentration n and mobility μ (left). The increase of ϱ is mainly determined by the decrease of n by more than a factor of two, while μ stays almost constant. The reason for the carrier loss could be due to an increasing carrier trapping. This would also partially explain the behavior at low temperatures. But judging by the magnitude of the effect, there seems to exist another origin.

dominant, the Hall and resistivity data may be analyzed in terms of carrier mobility μ and the carrier concentration n. The two quantities obtained from the measurements performed at 280 K are plotted as a function of hydrostatic pressure on the right of figure 10.1. The carrier concentration shows a decrease, which is mainly responsible for the increase of the resistivity at room temperature (solid line on the right of figure 10.1) whereas the mobility is almost constant and decreases only slightly at higher pressures. It should be noted that the results obtained at the highest pressures have the largest error bars.

The decreasing carrier concentration is qualitatively in accordance with an increasing donor depth. A possible explanation is schematically illustrated on the left of figure 10.2. Firstly, the applied pressure leads to an increase of the band gap E_g or rather an up-shift of the conduction band edge E_c away from the valence band edge. According to $\vec{k} \cdot \vec{p}$ theory this is accompanied by an increase of the electron effective mass m^*. For hydrogen-like shallow donors a higher effective mass implies a higher donor binding energy E_d, cf. equation (3.1). However, quantitatively this effect appears too large, so that other contributions may be relevant.

In section 2.1 already the observation of a too small carrier concentration in the presence of

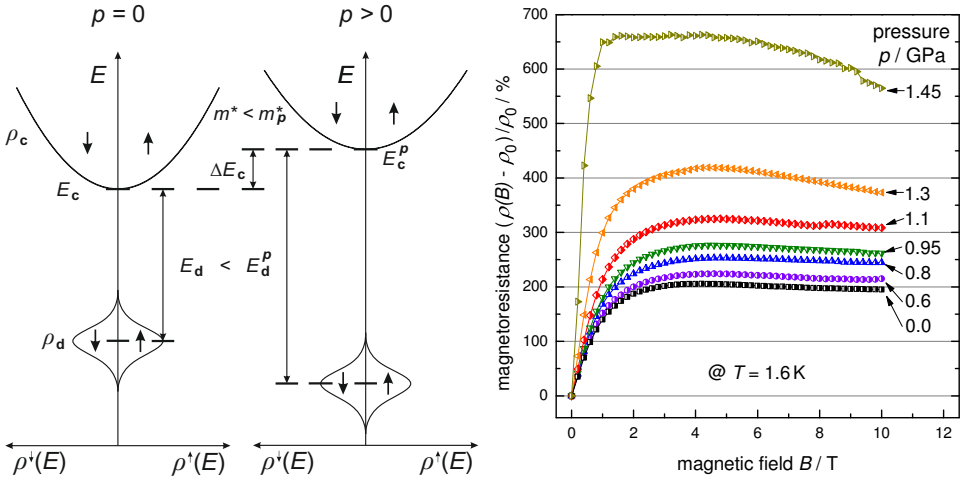

Figure 10.2: The second reason for the increase of ρ is most likely a decreasing Bohr radius. The concept behind this is illustrated on the left hand side. Applying hydrostatic pressure on zinc manganese selenide leads to a increasing of the conduction band edge due to an increasing bandgap E_g. This situation is accompanied by a higher effective mass m^*. As we know a higher effective mass yields a increased donor depth and a smaller Bohr radius. This last effect, not depicted here, would result in a massive increase of resistivity, just like the one we observe at low temperatures. right: Looking at the relative magnetoresistance as a function of magnetic field at different ambient pressures shows an increase of the effect by more of a factor 3. This is of course small compared to the resistivity changes at zero magnetic field. Our model predicts on the first order no such increase, but two explanations are possible. Ether the carrier loss enhances the magnetoresistance effect, like we have seen before in figure 5.7, or the non-Gaussian impurity band tail leads to this deviation.

manganese is mentioned. Also the low chlorine doping efficiency, that corresponds with the poor incorporation of chlorine atoms, indicates a certain degree of compensation. A possible cause may be the manganese-induced formation of trap states in the vicinity of the conduction band edge e.g. manganese pairs or higher manganese clusters. If hydrostatic pressure is applied even more of these manganese states would come into resonance with the donor states and also the total number of states beneath the donor energy levels would increase. Accompanied with this energy shifts an increasing compensation may occur, which in turn would explain the decreasing carrier concentration.

For low temperatures the situation is different, but the same effects could affect the electron transport. The transition from band transport to hopping transport occurs in the temperature range between 15 and 30 K. At low temperatures the transport is not diffusive and mainly takes place via hopping processes in the impurity band, thus, a description by means of a free carrier concentration and a mobility is no longer valid. In general, the hopping probability between two sites is a function of the difference in site energies and of the distance between the sites relative to the Bohr radius, cf. equation (3.10). A reduced effective Bohr radius, cf. to the left of figure 10.2, as well as increasing compensation under pressure are discussed above. Both effects lead to a decrease of the hopping probability, yielding a higher resistivity under pressure.

The former arguments for an increasing donor binding energy E_d accompanied by a smaller a_B may also apply at low temperatures. A decreasing Bohr radius leads to a reduced overlap of the wavefunctions of adjacent donors. As the donor wavefunction drops exponentially with increasing distance from the donor ion, the latter effect has a major impact on the low-temperature hopping transport which solely takes place in the impurity band. Due to this effect and the different types of conduction mechanisms it is expected that this is more significant at low temperatures than at high temperatures in agreement with experiment.

In this low temperature region where hopping takes place compensation could also explain the dependence of the resistivity on hydrostatic pressure. Assuming a situation where the Fermi level is located below the middle of the impurity band distribution due to the mentioned compensation at ambient pressure the following argumentation would apply. According to Davis and Compton [10] and Stutius [59] in this case a further lowering of the Fermi energy inside the impurity band due to a higher compensation yields a higher activation energy for hopping transport. This effect is obvious as less electrons contribute to the transport and as the average energy distance of donor levels is higher closer to the tail of the donor distribution. Both effects lead to an increase of the resistivity under hydrostatic pressure.

At this stage it is very hard to estimate the relative importance of both effects, i.e. pressure induced wave-function shrinkage and the increasing compensation. Therefore we take a look at the magnetoresistance measurements.

10.2 Magnetoresistance under pressure

The magnetoresistance as a function of magnetic field at different pressure values and at a temperature of 1.6 K is shown on the right of figure 10.2. The magnetoresistance effects at

the highest pressure are more than three times larger than at ambient pressure. This effect is not due to the increase of the resistivity with pressure as the relative magnetoresistance is shown. The shape of the curves resembles the Brillouin function at all pressures. The negative magnetoresistance contribution at high magnetic fields is very small but it gets stronger with increasing pressure. As the characteristics of the curves are hardly altered under pressure, it may be anticipated that the effect is still the spreading of the impurity band but that this somehow has a larger effect on the relative magnetoresistance.

However, solely on the basis of equation (2.4) one cannot fully explain this behavior as the effective manganese content as well as the Brillouin function itself are the same at all pressures, and the exchange integral $N_0\alpha$ should only increase slightly, at maximum by 10 %, with increasing pressure [21]. Thus, this effect cannot explain the rise of the magnetoresistance by more than a factor of 3. An alternative explanation is based on the increasing compensation and decreasing a_B state was already proposed in the previous section. Both will also be discussed in the following.

Looking at the right of figure 10.2 a somewhat similar effect occurs like when the carrier concentration is successively reduced in a series of samples, cf. figure 5.7. In case of a lower carrier concentration the relative magnetoresistance is larger. This could mean that in case of this sample applying pressure leads to a shift away from the activated regime rather close to the metal–insulator transition more to the insulating side of the metal–insulator transition. This would be consistent with the decreasing Bohr radius under pressure discussed in section 10.1. However, one has to keep in mind that such a reduction of the Bohr radius is also accompanied by a reduced influence of the manganese spins on the donor energy. So one would also expect the opposing effect of a reduced splitting of the donor states. Then the positive magnetoresistance effect of wave-function shrinkage would be dominant compared to the negative one due to reduced state splitting.

Another argument based on compensation is plausible. In a Gaussian impurity band compensation would basically result in the same relative magnetoresistance due to the fact that the scaling argument is the same for every compensation. But as the detailed simulation has shown the impurity band has an asymmetry and the lower tail is more pronounced compared to that in a Gaussian approximation. If now compensation shifts the Fermi level closer to the end of this tail, one can qualitatively state that the relative magnetoresistance effect would be larger.

Unfortunately the coexistence of both explanation approaches still holds for $\rho(p)$ and for the relative magnetoresistance measurements, so none of them could be ruled out. Or that at least in the presence of both the dominant one could be identified.

In general one can see that our model is applicable to get qualitative results even for this measurements under hydrostatic pressure and that no observations contradict our assumptions.

Chapter 11

Conclusion

In this work a novel explanation for the large positive magnetoresistance effect is presented, which occurs in the dilute magnetic semiconductor zinc manganese selenide in the hopping transport regime. In literature no conclusive explanation for this large positive magnetoresistance effect is known, so we set out to fill this gap. The appearance of hopping transport is a necessary requirement for this effect to occur, as is the presence of magnetic ions in the material. Thus the explanation given here is valid not only for zinc manganese selenide but for all dilute magnetic semiconductor at low temperatures. Another aspect is important for the description, i.e. that the conduction band edge of an n-type material has to decrease with increasing content of the magnetic cation, in our case manganese. This means it has to occur a large bowing of the conduction band edge and by this a large discrepancy from the virtual crystal approximation.

Our explanation includes the statistical distribution of magnetic as well as donor atoms in the crystal, manganese and chlorine respectively. The random distribution of manganese leads to fluctuations of the conduction band edge according to its bowing. The energy position of the donors reproduces these fluctuations. This fluctuating donor levels are represented in the density of donor states. This donor energy distribution is called impurity band and can be described by its width and its shape.

An external magnetic field affects the spins of the manganese atoms and leads to a magnetization proportional to the Brillouin function. This magnetization leads to a splitting of the conduction band and of the donor levels, which is again proportional to the Brillouin function. At this point it is important that the splitting is different for different energetic positions inside the impurity band. This fluctuation of the splitting leads to a change of the width of the impurity band, while its shape remains unaffected. Using only basic hopping rates this increasing impurity band-width results in a increasing resistivity, i.e. a positive magnetoresistance.

In this work all these steps of this novel explanation were motivated and confirmed. This process was accompanied by two theoretical approaches, which allowed us to illuminate the model from different angles. In the scaling approach it was possible to model this magnetoresistance mechanism and to reduce all data to a universal function of an idealized Gaussian

impurity band-width and to explain why this is possible. As this only leads to a relative change of the impurity band-width this may seem to be only a qualitative analysis, but as this process allows one to reconstruct theoretical magnetoresistance curves also a quantitative analysis is given.

To specify this in more detail and to give a quantitative explanation simulations were performed. They offered a detailed view on the shape of the impurity band and were able to reproduce the measurements in all aspects with a reasonable set of parameters. In both theoretical frameworks it was possible to show that the maximal resistivity increases with increasing manganese content. This finding is also in good agreement with the experimental results.

It is possible to give a fitting function for the magnetic field dependence in agreement with our model. With this function an easy and fast fitting of experimental data is provided.

All this is the main part of this work, to provide this new magnetoresistance mechanism to explain the large positive magnetoresistance effect in zinc manganese selenide. But in the end this led to a lot more facets. For instance if hydrostatic pressure is applied the relative magnetoresistance increases. This could be due to carrier trapping and thus due to an increased compensation which affects the occupation of the impurity band tail.

At high manganese contents the presented concept has to be modified to represent the different experimental situation, i.e. the decreasing conduction band edge is no longer certain. In the region of the conduction band minimum an additional negative contribution opposes the positive one. The intermixed magnetoresistance behavior observed in our samples for x-values close to the x-values corresponding to the minimum of the conduction band bowing supports the theoretical explanation first suggested by Mycielski *et al.* [42] and refined here by us in our model. It gives an alternative to attributing the negative magnetoresistance effect to bound magnetic polarons.

It seems that our model not only applies for zinc manganese selenide but also for other materials. A number of measurements support that this effect occurs in all (II,Mn)VI dilute magnetic semiconductor.

11.1 Outlook

There are a few aspects which are interesting for future investigations and one being carried out separately. The work presented here does not explicitly treat the variable range hopping regime. But the model has recently been expanded to this case in a mostly theoretical manner.[44]

The simulation approach is expandable for the effect of bound magnetic polaron hopping. This is a work that could be done simply by adding the polaron shift to every energy difference before performing the transport simulation. However, it is not possible to include bound magnetic polaron hopping into the scaling approach.

Our model could be applied to more dilute magnetic semiconductor materials with a large

bowing to check if this truly is a universal explanation for this material class. In this light also the concept for high manganese contents could be intensified. A model dealing with every conduction band behavior is more complex but could support our suggestion for high x.

Also the behavior under high pressure is not fully understood and needs a more detailed investigation.

Appendix A

Supporting Information

A.1 Sample parameters

name	original name	thickness d/nm	Mn content x/%	$n/10^{17}\,\mathrm{cm}^{-3}$
a	B0-188	1050	0	4.3 ± 0.3
b	B0-182	1000	0.75	4.3 ± 0.3
c	B0-175	1050	2.0	4.3 ± 0.3
1	BD-233	881	7.1	3.2
2	BD-230	1037	6.0	4.2
3	BD-274	895 ± 9	6.2	13
4	BD-275	904	5.5	45
5	BD-231	1022	6.8	49
6	BD-232	948	7.3	84

Table A.1: sample parameters see section 4.1

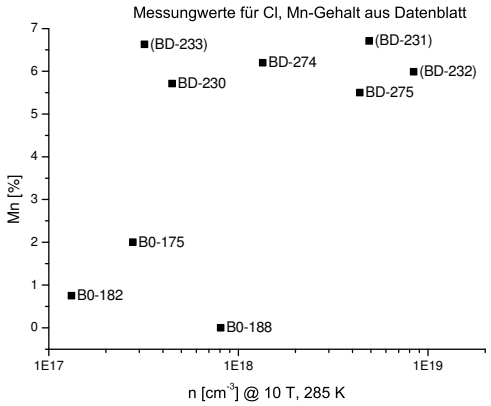

Figure A.1: The

A.2 Term conversion

in section 7.1

$$\sigma^2 = \mathrm{Var}(\tilde{\epsilon}_{i,0}) + \left(y - \frac{1}{2}\,\alpha\,\langle J_z\rangle\right)^2 \mathrm{Var}(\Sigma) \tag{A.1}$$

$$= \mathrm{Var}(\tilde{\epsilon}_{i,0}) + \left(y - \frac{1}{2}\,\alpha\,J\,\mathrm{B}_J\right)^2 \mathrm{Var}(\Sigma) \tag{A.2}$$

$$, \text{with } \Sigma = \sum_m |\phi_i(r_m)|^2 \tag{A.3}$$

$$\sigma^2_{B=0} = \sigma_0^2 = \mathrm{Var}(\tilde{\epsilon}_{i,0}) + y^2\,\mathrm{Var}(\Sigma)\ , \text{as } \mathrm{B}_J(B=0) = 0 \tag{A.4}$$

$$\frac{\sigma^2}{\sigma_0^2} = \frac{\mathrm{Var}(\tilde{\epsilon}_{i,0}) + \left(y - \frac{1}{2}\,\alpha\,J\,\mathrm{B}_J\right)^2 \mathrm{Var}(\Sigma)}{\mathrm{Var}(\tilde{\epsilon}_{i,0}) + y^2\,\mathrm{Var}(\Sigma)} \tag{A.5}$$

$$\left(\frac{\sigma}{\sigma_0}\right)^2 = \frac{\mathrm{Var}(\tilde{\epsilon}_{i,0})}{\mathrm{Var}(\tilde{\epsilon}_{i,0}) + y^2\,\mathrm{Var}(\Sigma)} + \frac{\left(y - \frac{1}{2}\,\alpha\,J\,\mathrm{B}_J\right)^2 \mathrm{Var}(\Sigma)}{\mathrm{Var}(\tilde{\epsilon}_{i,0}) + y^2\,\mathrm{Var}(\Sigma)} \tag{A.6}$$

$$, \text{for shortening we insert } X = \frac{\mathrm{Var}(\Sigma)}{\mathrm{Var}(\tilde{\epsilon}_{i,0}) + y^2\,\mathrm{Var}(\Sigma)} \text{ and extend the first summand} \tag{A.7}$$

$$= \frac{\mathrm{Var}(\tilde{\epsilon}_{i,0}) + y^2\,\mathrm{Var}(\Sigma) - y^2\,\mathrm{Var}(\Sigma)}{\mathrm{Var}(\tilde{\epsilon}_{i,0}) + y^2\,\mathrm{Var}(\Sigma)} + \left(y - \frac{1}{2}\,\alpha\,J\,\mathrm{B}_J\right)^2 X \tag{A.8}$$

$$= 1 - \frac{y^2\,\mathrm{Var}(\Sigma)}{\mathrm{Var}(\tilde{\epsilon}_{i,0}) + y^2\,\mathrm{Var}(\Sigma)} + \left(y - \frac{1}{2}\,\alpha\,J\,\mathrm{B}_J\right)^2 X \tag{A.9}$$

$$= 1 - y^2\,X + X\left(y - \frac{1}{2}\,\alpha\,J\,\mathrm{B}_J\right)^2 \tag{A.10}$$

$$, \text{now we have two independent variables } (y,\ X), \text{but they are not yet dimensionless} \tag{A.11}$$

$$= 1 - \gamma_1^2 + \left[\sqrt{X}\left(-y + \frac{1}{2}\,\alpha\,J\,\mathrm{B}_J\right)\right]^2 \tag{A.12}$$

$$, \text{with } \gamma_1^2 = y^2\,X \Longleftrightarrow \gamma_1 = -y\sqrt{X} = -y\sqrt{\frac{\mathrm{Var}(\Sigma)}{\mathrm{Var}(\tilde{\epsilon}_{i,0}) + y^2\,\mathrm{Var}(\Sigma)}} \tag{A.13}$$

$$= 1 - \gamma_1^2 + \left[-y\sqrt{X} + \frac{1}{2}\,\alpha\,J\,\sqrt{X}\,\mathrm{B}_J\right]^2 \tag{A.14}$$

$$, \text{with } \gamma_2 = \frac{1}{2}\,\alpha\,J\,\sqrt{X} = \frac{1}{2}\,\alpha\,J\sqrt{\frac{\mathrm{Var}(\Sigma)}{\mathrm{Var}(\tilde{\epsilon}_{i,0}) + y^2\,\mathrm{Var}(\Sigma)}} \text{ the term becomes} \tag{A.15}$$

$$\left(\frac{\sigma}{\sigma_0}\right)^2 = 1 - \gamma_1^2 + [\gamma_1 + \gamma_2\,\mathrm{B}_J]^2 \tag{A.16}$$

$$\frac{\sigma}{\sigma_0} = \sqrt{1 - \gamma_1^2 + [\gamma_1 + \gamma_2\,\mathrm{B}_J]^2} \tag{A.17}$$

i could name $\sqrt{X} = Y$?

Bibliography

[1] H. Abad, B. T. Jonker, W. Y. Yu, S. Stoltz, and A. Petrou.
n-type doping of the diluted magnetic semiconductor $Zn_{1-x}Mn_xSe$.
Appl. Phys. Lett., 66(18):2412–2414, 1995.
doi: 10.1063/1.113957.
URL `http://link.aip.org/link/?APL/66/2412/1`.

[2] K. C. Agarwal, B. Daniel, M. Gruen, P. Feinaeugle, C. Klingshirn, and M. Hetterich.
Carrier-density-dependent electron effective mass in $Zn_{1-x}Mn_xSe$ for $0 < x < 0.13$.
Appl. Phys. Lett., 86(18):181907, 2005.
ISSN 00036951.
doi: 10.1063/1.1924867.
URL `http://dx.doi.org/doi/10.1063/1.1924867`.

[3] K. C. Agarwal, B. Daniel, C. Klingshirn, and M. Hetterich.
Phonon and free-charge-carrier properties of $Zn_{1-x}Mn_xSe$ epilayers grown by molecular-beam epitaxy.
Phys. Rev. B, 73:045211, Jan 2006.
doi: 10.1103/PhysRevB.73.045211.
URL `http://link.aps.org/doi/10.1103/PhysRevB.73.045211`.

[4] N. V. Agrinskaya and V. I. Kozub.
Magnetoresistance related to on-site spin correlations in the nearest neighbor hopping conductivity.
Solid State Commun., 108(6):355 – 359, 1998.
ISSN 0038-1098.
doi: 10.1016/S0038-1098(98)00358-5.
URL `http://www.sciencedirect.com/science/article/pii/S0038109898003585`.

[5] Vinay Ambegaokar, B. I. Halperin, and J. S. Langer.
Hopping conductivity in disordered systems.
Phys. Rev. B, 4:2612–2620, Oct 1971.
doi: 10.1103/PhysRevB.4.2612.
URL `http://link.aps.org/doi/10.1103/PhysRevB.4.2612`.

[6] Pablo Asshoff, Andreas Merz, Heinz Kalt, and Michael Hetterich.
A spintronic source of circularly polarized single photons.
Appl. Phys. Lett., 98(11):112106, 2011.
doi: 10.1063/1.3564893.

URL http://link.aip.org/link/?APL/98/112106/1.

[7] R. B. Bylsma, W. M. Becker, J. Kossut, U. Debska, and D. Yoder-Short.
Dependence of energy gap on x and T in $Zn_{1-x}Mn_xSe$: The role of exchange interaction.
Phys. Rev. B, 33:8207–8215, Jun 1986.
doi: 10.1103/PhysRevB.33.8207.
URL http://link.aps.org/doi/10.1103/PhysRevB.33.8207.

[8] N. Dai, H. Luo, F. C. Zhang, N. Samarth, M. Dobrowolska, and J. K. Furdyna.
Spin superlattice formation in $ZnSe/Zn_{1-x}Mn_xSe$ multilayers.
Phys. Rev. Lett., 67:3824–3827, Dec 1991.
doi: 10.1103/PhysRevLett.67.3824.
URL http://link.aps.org/doi/10.1103/PhysRevLett.67.3824.

[9] B. Daniel, K. C. Agarwal, C. Klingshirn, and M. Hetterich.
Electrical and infrared-optical investigations of n-doped (Zn,Mn)Se epilayers.
AIP Conf. Proc., 772(1):171–172, 2005.
doi: 10.1063/1.1994048.
URL http://scitation.aip.org/content/aip/proceeding/aipcp/10.1063/1.1994048.

[10] E. A. Davis and W. Dale Compton.
Compensation dependence of impurity conduction in antimony-doped germanium.
Phys. Rev., 140:A2183–A2194, Dec 1965.
doi: 10.1103/PhysRev.140.A2183.
URL http://link.aps.org/doi/10.1103/PhysRev.140.A2183.

[11] T. Dietl and J. Spałek.
Effect of thermodynamic fluctuations of magnetization on the bound magnetic polaron in dilute magnetic semiconductors.
Phys. Rev. B, 28:1548–1563, Aug 1983.
doi: 10.1103/PhysRevB.28.1548.
URL http://link.aps.org/doi/10.1103/PhysRevB.28.1548.

[12] Tomasz Dietl.
Diluted Magnetic Semiconductors.
World Scientific, 1991.
ISBN 9789810201760.

[13] Tomasz Dietl, Jaroslaw Antoszewski, and Leszek Swierkowski.
Hopping conduction of the bound magnetic polarons in n-CdMnSe.
Physica B+C, 117&118, Part 1(0):491 – 493, 1983.
ISSN 0378-4363.
doi: 10.1016/0378-4363(83)90568-5.
URL http://www.sciencedirect.com/science/article/pii/0378436383905685.

[14] D. H. Dunlap, P. E. Parris, and V. M. Kenkre.
Charge-dipole model for the universal field dependence of mobilities in molecularly doped polymers.

Phys. Rev. Lett., 77(3):542–545, Jul 1996.
doi: 10.1103/PhysRevLett.77.542.

[15] J. Carlos Egues.
Spin-dependent perpendicular magnetotransport through a tunable ZnSe/$Zn_{1-x}Mn_xSe$ heterostructure: A possible spin filter?
Phys. Rev. Lett., 80:4578–4581, May 1998.
doi: 10.1103/PhysRevLett.80.4578.
URL `http://link.aps.org/doi/10.1103/PhysRevLett.80.4578`.

[16] J. M. Fatah, T. Piorek, P. Harrison, T. Stirner, and W. E. Hagston.
Numerical simulation of antiferromagnetic spin-pairing effects in diluted magnetic semiconductors and enhanced paramagnetism at interfaces.
Phys. Rev. B, 49:10341–10344, Apr 1994.
doi: 10.1103/PhysRevB.49.10341.
URL `http://link.aps.org/doi/10.1103/PhysRevB.49.10341`.

[17] R. Fiederling, M. Keim, G. Reuscher, W. Ossau, G. Schmidt, A. Waag, and L. W. Molenkamp.
Injection and detection of a spin-polarized current in a light-emitting diode.
Nature, 402:787 – 790, 1999.
doi: 10.1038/45502.

[18] D. M. Finlayson, J. Irvine, and L. S. Peterkin.
Electrical conduction in CdSe near the metal-insulator transition.
Phil. Mag. B, 39(3):253–266, 1979.
doi: 10.1080/13642817908245361.

[19] J. K. Furdyna.
Diluted magnetic semiconductors.
J. Appl. Phys., 64(4):R29–R64, 1988.
doi: 10.1063/1.341700.
URL `http://link.aip.org/link/?JAP/64/R29/1`.

[20] Yong Guo, Fei-Ruo Shen, and Xin-Yi Chen.
A tunable spin filter in periodic diluted magnetic semiconductor/semiconductor superlattices.
Appl. Phys. Lett., 101(1):012410, 2012.
doi: http://dx.doi.org/10.1063/1.4733668.
URL `http://scitation.aip.org/content/aip/journal/apl/101/1/10.1063/1.4733668`.

[21] F. Hamdani, A. R. Goni, K. Syassen, and R. Triboulet.
Magnetoexcitons in $Zn_{0.98}Mn_{0.02}Te$ under high hydrostatic pressure.
Phys. Status Solidi B, 223(1):171–175, 2001.
ISSN 1521-3951.
doi: 10.1002/1521-3951(200101)223:1⟨171::AID-PSSB171⟩3.0.CO;2-6.
URL `http://dx.doi.org/10.1002/1521-3951(200101)223:1<171::AID-PSSB171>3.0.CO;2-6`.

[22] W. Heimbrodt and P. J. Klar.
Magnetic Nanostructures, volume 10.
ASP, ISBN: 1-58883-001-2, 2002.
Chapter 1.

[23] Wolfram Heimbrodt and Peter J. Klar.
Magnetic semiconductor nanostructures.
Enc. Nanosci. Nanotechnol., 4:835–897, 2004.
URL http://www.ingentaconnect.com/content/asp/enn/2004/00000004/00000001/art00037.

[24] M. Hetterich, B. Daniel, C. Klingshirn, P. Pfundstein, D. Litvinov, D. Gerthsen, K. Eichhorn, and D. Spemann.
Lattice parameter and elastic constants of cubic $Zn_{1-x}Mn_xSe$ epilayers grown by molecular-beam epitaxy.
Phys. Status Solidi C, 1(4):649–652, 2004.
ISSN 1610-1642.
doi: 10.1002/pssc.200304143.
URL http://dx.doi.org/10.1002/pssc.200304143.

[25] T. Hofmann, U. Schade, K. C. Agarwal, B. Daniel, C. Klingshirn, M. Hetterich, C. M. Herzinger, and M. Schubert.
Conduction-band electron effective mass in $Zn_{0.87}Mn_{0.13}Se$ measured by terahertz and far-infrared magnetooptic ellipsometry.
Appl. Phys. Lett., 88(4):042105, 2006.
doi: 10.1063/1.2168258.
URL http://scitation.aip.org/content/aip/journal/apl/88/4/10.1063/1.2168258.

[26] Y. H. Hwang, Y. H. Um, and J. K. Furdyna.
Temperature dependence of the band-edge photoluminescence of $Zn_{1-x}Mn_xSe$ films.
Semicond. Sci. Technol., 19:565–570, 2004.
doi: 10.1088/0268-1242/19/5/002.
URL http://iopscience.iop.org/0268-1242/19/5/002/.

[27] A. Imamoglu, D. D. Awschalom, G. Burkard, D. P. DiVincenzo, D. Loss, M. Sherwin, and A. Small.
Quantum information processing using quantum dot spins and cavity QED.
Phys. Rev. Lett., 83:4204–4207, Nov 1999.
doi: 10.1103/PhysRevLett.83.4204.
URL http://link.aps.org/doi/10.1103/PhysRevLett.83.4204.

[28] G. N. Ivanova, D. D. Nedeoglo, A. V. Simashkevich, and I. N. Timchenko.
Negative magnetoresistance in zinc selenide.
Phys. Status Solidi B, 103(2):643–652, 1981.
ISSN 1521-3951.
doi: 10.1002/pssb.2221030223.
URL http://dx.doi.org/10.1002/pssb.2221030223.

[29] F. Jansson, S. D. Baranovskii, G. Sliaužys, R. Österbacka, and P. Thomas.
Effective temperature for hopping transport in a Gaussian DOS.
Phys. Status Solidi C, 5:722–724, 2008.
doi: 10.1002/pssc.200777567.

[30] Fredrik Jansson.
Charge transport in disordered materials – simulations, theory, and numerical modeling of hopping transport and electron–hole recombination.
PhD thesis, Åbo Akademi University, 2011.

[31] B. T. Jonker, Y. D. Park, B. R. Bennett, H. D. Cheong, G. Kioseoglou, and A. Petrou.
Robust electrical spin injection into a semiconductor heterostructure.
Phys. Rev. B, 62:8180–8183, Sep 2000.
doi: 10.1103/PhysRevB.62.8180.
URL `http://link.aps.org/doi/10.1103/PhysRevB.62.8180`.

[32] Hiroshi Kamimura, Atsushi Kurobe, and Tadashi Takemori.
Magnetoresistance in Anderson-localized systems.
Physica B+C, 117&118, Part 2(0):652 – 654, 1983.
ISSN 0378-4363.
doi: 10.1016/0378-4363(83)90615-0.
URL `http://www.sciencedirect.com/science/article/pii/0378436383906150`.

[33] C.S. Kim, M. Kim, S. Lee, J. Kossut, J. K. Furdyna, and M. Dobrowolska.
CdSe quantum dots in a $Zn_{1-x}Mn_xSe$ matrix: new effects due to the presence of Mn.
J. Cryst. Growth, 214215(0):395 – 399, 2000.
ISSN 0022-0248.
doi: 10.1016/S0022-0248(00)00116-0.
URL `http://www.sciencedirect.com/science/article/pii/S0022024800001160`.

[34] A. Kurobe.
Theory of magnetoresistance in the Anderson-localised regime of semiconductors.
J. Phys. C, 19(13):2201, 1986.
URL `http://stacks.iop.org/0022-3719/19/i=13/a=011`.

[35] C. Leighton, I. Terry, and P. Becla.
Metal-insulator transition in the persistent photoconductor $Cd_{1-x}Mn_xTe$:In.
Europhys. Lett., 42(1):67, 1998.
URL `http://stacks.iop.org/0295-5075/42/i=1/a=067`.

[36] C. Leighton, I. Terry, and P. Becla.
Nearest neighbor hopping in $Cd_{0.83}Mn_{0.17}Te$:In, controlled by persistent photoconductivity.
Solid State Commun., 110(10):531 – 536, 1999.
ISSN 0038-1098.
doi: 10.1016/S0038-1098(99)00131-3.
URL `http://www.sciencedirect.com/science/article/pii/S0038109899001313`.

[37] D. Litvinov, D. Gerthsen, B. Daniel, C. Klingshirn, and M. Hetterich.

Defects and phase distribution in epitaxial ZnMnSe layers analyzed by transmission electron microscopy.
J. Appl. Phys., 100(2):023523, 2006.
doi: 10.1063/1.2218493.
URL http://scitation.aip.org/content/aip/journal/jap/100/2/10.1063/1.2218493.

[38] W. Löffler, M. Hetterich, C. Mauser, S. Li, T. Passow, and H. Kalt.
Parallel preparation of highly spin-polarized electrons in single InAs/GaAs quantum dots.
Appl. Phys. Lett., 90(23):232105, 2007.
doi: 10.1063/1.2746405.
URL http://link.aip.org/link/?APL/90/232105/1.

[39] K. A. Matveev, L. I. Glazman, Penny Clarke, D. Ephron, and M. R. Beasley.
Theory of hopping magnetoresistance induced by Zeeman splitting.
Phys. Rev. B, 52:5289–5297, Aug 1995.
doi: 10.1103/PhysRevB.52.5289.
URL http://link.aps.org/doi/10.1103/PhysRevB.52.5289.

[40] C. Michel, S. D. Baranovskii, P. J. Klar, P. Thomas, and B. Goldlücke.
Strong non-Arrhenius temperature dependence of the resistivity in the regime of traditional band transport.
Appl. Phys. Lett., 89(11):112116, 2006.
doi: 10.1063/1.2348771.
URL http://scitation.aip.org/content/aip/journal/apl/89/11/10.1063/1.2348771.

[41] Allen Miller and Elihu Abrahams.
Impurity conduction at low concentrations.
Phys. Rev., 120:745–755, Nov 1960.
doi: 10.1103/PhysRev.120.745.
URL http://link.aps.org/doi/10.1103/PhysRev.120.745.

[42] J. Mycielski, A. M. Witowski, A. Wittlin, and M. Grynberg.
Energy distribution of donor ground states in mixed crystals.
Phys. Rev. B, 40:8437–8442, Oct 1989.
doi: 10.1103/PhysRevB.40.8437.
URL http://link.aps.org/doi/10.1103/PhysRevB.40.8437.

[43] A. V. Nenashev, F. Jansson, M. Wiemer, S. Petznick, P. J. Klar, M. Hetterich, A. V. Dvurechenskii, F. Gebhard, and S. D. Baranovskii.
Scaling approach to hopping magnetoresistivity in dilute magnetic semiconductors.
Phys. Rev. B, 88(11):115210, 2013.

[44] A. V. Nenashev, F. Jansson, S. Petznick, M. Wiemer, P. J. Klar, A. V. Dvurechenskii, F. Gebhard, and S. D. Baranovskii.
Scaling description of positive magnetoresistivity in doped dilute magnetic semiconductors.

J. Magn. Magn. Mater., 383(0):44 – 49, June 2015.
ISSN 0304-8853.
doi: http://dx.doi.org/10.1016/j.jmmm.2014.11.069.
URL `http://www.sciencedirect.com/science/article/pii/S0304885314011883`.

[45] S. V. Novikov.
Organic glasses: cluster structure of the random energy landscape.
Ann. Phys., 18(12):949–953, 2009.
doi: 10.1002/andp.200910394.
(Berlin).

[46] Michael Oestreich.
Materials science: Injecting spin into electronics.
Nature, 402:735–736, 1999.
doi: 10.1038/45406.
URL `http://dx.doi.org/10.1038/45406`.

[47] Eunsoon Oh, K. J. Yee, S. M. Soh, J. U. Lee, J. C. Woo, H. S. Jeon, D. S. Kim, S. Lee, J. K. Furdyna, H. C. Ri, H. S. Chany, and S. H. Park.
Spin polarization of self-assembled CdSe quantum dots in ZnMnSe.
Appl. Phys. Lett., 83(22):4604–4606, 2003.
doi: 10.1063/1.1630381.
URL `http://scitation.aip.org/content/aip/journal/apl/83/22/10.1063/1.1630381`.

[48] G. Papp, S. Borza, and F. M. Peeters.
Spin transport through a ZnSe-based diluted magnetic semiconductor resonant tunneling structure in the presence of electric and magnetic fields.
Phys. Status Solidi B, 243(8):1956–1962, 2006.
ISSN 1521-3951.
doi: 10.1002/pssb.200541504.
URL `http://dx.doi.org/10.1002/pssb.200541504`.

[49] W. F. Pasveer, J. Cottaar, C. Tanase, R. Coehoorn, P. A. Bobbert, P. W. M. Blom, D. M. de Leeuw, and M. A. J. Michels.
Unified description of charge-carrier mobilities in disordered semiconducting polymers.
Phys. Rev. Lett., 94(20):206601, 2005.
doi: 10.1103/PhysRevLett.94.206601.

[50] A. G. Petukhov and M. Foygel.
Bound magnetic polaron hopping and giant magnetoresistance in magnetic semiconductors and nanostructures.
Phys. Rev. B, 62:520–531, Jul 2000.
doi: 10.1103/PhysRevB.62.520.
URL `http://link.aps.org/doi/10.1103/PhysRevB.62.520`.

[51] M. E. Raikh, J. Czingon, Qiu-yi Ye, F. Koch, W. Schoepe, and K. Ploog.
Mechanisms of magnetoresistance in variable-range-hopping transport for two-dimensional electron systems.

Phys. Rev. B, 45:6015–6022, Mar 1992.
doi: 10.1103/PhysRevB.45.6015.
URL http://link.aps.org/doi/10.1103/PhysRevB.45.6015.

[52] Y. Shapira, N. F. Oliveira, D. H. Ridgley, R. Kershaw, K. Dwight, and A. Wold.
Magnetoresistance and Hall effect near the metal-insulator transition of $Cd_{1-x}Mn_xSe$.
Phys. Rev. B, 34:4187–4198, Sep 1986.
doi: 10.1103/PhysRevB.34.4187.
URL http://link.aps.org/doi/10.1103/PhysRevB.34.4187.

[53] B. S. Shchamkhalova and Yu. Ya. Tkach.
Giant negative magnetoresistivity in weakly compensated semiconductors.
Solid State Commun., 99(4):261 – 264, 1996.
ISSN 0038-1098.
doi: http://dx.doi.org/10.1016/0038-1098(96)00226-8.
URL http://www.sciencedirect.com/science/article/pii/0038109896002268.

[54] B. I. Shklovskii and A. L. Efros.
Electronic Properties of Doped Semiconductors.
Springer-Verlag, 1984.
URL http://www.ftpi.umn.edu/shklovskii/.

[55] A. V. Shumilin and V. I. Kozub.
Interference mechanism of magnetoresistance in variable-range hopping conduction: The effect of paramagnetic electron spins and continuous spectrum of scatterer energies.
Phys. Rev. B, 85:115203, Mar 2012.
doi: 10.1103/PhysRevB.85.115203.
URL http://link.aps.org/doi/10.1103/PhysRevB.85.115203.

[56] U. Sivan, O. Entin-Wohlman, and Y. Imry.
Orbital magnetoconductance in the variable-range-hopping regime.
Phys. Rev. Lett., 60:1566–1569, Apr 1988.
doi: 10.1103/PhysRevLett.60.1566.
URL http://link.aps.org/doi/10.1103/PhysRevLett.60.1566.

[57] I. P. Smorchkova, N. Samarth, J. M. Kikkawa, and D. D. Awschalom.
Giant magnetoresistance and quantum phase transitions in strongly localized magnetic two-dimensional electron gases.
Phys. Rev. B, 58:R4238–R4241, Aug 1998.
doi: 10.1103/PhysRevB.58.R4238.
URL http://link.aps.org/doi/10.1103/PhysRevB.58.R4238.

[58] Jolanta Stankiewicz and Jose R. Fermin.
Electroreflectance and wavelength-modulated reflectivity spectra of $Zn_{1-x}Mn_xSe$ alloys.
J. Appl. Phys., 63(8):3300–3302, 1988.
doi: 10.1063/1.340817.
URL http://scitation.aip.org/content/aip/journal/jap/63/8/10.1063/1.340817.

[59] W. Stutius.
Conduction mechanism in low-resistivity n-type ZnSe prepared by organometallic chemical vapor deposition.
J. Appl. Phys., 53(1):284–291, 1982.
doi: 10.1063/1.329928.
URL `http://link.aip.org/link/?JAP/53/284/1`.

[60] B. B. Suprapto and P. N. Butcher.
DC hopping conduction by magnetically frozen electrons.
J. Phys. C, 8(22):L517, 1975.
URL `http://stacks.iop.org/0022-3719/8/i=22/a=007`.

[61] Masao Takahashi.
Coherent-potential approach to magnetic and chemical disorder in diluted magnetic semiconductors.
Phys. Rev. B, 60:15858–15865, Dec 1999.
doi: 10.1103/PhysRevB.60.15858.
URL `http://link.aps.org/doi/10.1103/PhysRevB.60.15858`.

[62] I. Terry, T. Penney, S. von Molnár, and P. Becla.
Low-temperature transport properties of $Cd_{0.91}Mn_{0.09}Te$:In and evidence for a magnetic hard gap in the density of states.
Phys. Rev. Lett., 69:1800–1803, Sep 1992.
doi: 10.1103/PhysRevLett.69.1800.
URL `http://link.aps.org/doi/10.1103/PhysRevLett.69.1800`.

[63] C. Thurn and V. M. Axt.
Quantum kinetic description of spin transfer in diluted magnetic semiconductors.
Phys. Rev. B, 85:165203, Apr 2012.
doi: 10.1103/PhysRevB.85.165203.
URL `http://link.aps.org/doi/10.1103/PhysRevB.85.165203`.

[64] C. Thurn, M. Cygorek, V. M. Axt, and T. Kuhn.
Non-Markovian spin transfer dynamics in magnetic semiconductors despite short memory times.
Phys. Rev. B, 87:205301, May 2013.
doi: 10.1103/PhysRevB.87.205301.
URL `http://link.aps.org/doi/10.1103/PhysRevB.87.205301`.

[65] A. Twardowski, H. J. M. Swagten, W. J. M. de Jonge, and M. Demianiuk.
Magnetic behavior of the diluted magnetic semiconductor $Zn_{1-x}Mn_xSe$.
Phys. Rev. B, 36:7013–7023, Nov 1987.
doi: 10.1103/PhysRevB.36.7013.
URL `http://link.aps.org/doi/10.1103/PhysRevB.36.7013`.

[66] T. Wojtowicz, M. Sawicki, J. Jaroszynski, T. Dietl, and W. Plesiewicz.
Conductivity in a spin-polarized band near the metal-insulator critical point.
Physica B, 155(13):357 – 361, 1989.

ISSN 0921-4526.
doi: http://dx.doi.org/10.1016/0921-4526(89)90529-2.
URL http://www.sciencedirect.com/science/article/pii/0921452689905292.

[67] Y. Yafet, R. W. Keyes, and E. N. Adams.
Hydrogen atom in a strong magnetic field.
J. Phys. Chem. Solids, 1(3):137 – 142, 1956.
ISSN 0022-3697.
doi: http://dx.doi.org/10.1016/0022-3697(56)90020-8.
URL http://www.sciencedirect.com/science/article/pii/0022369756900208.

[68] D. R. Yoder-Short, U. Debska, and J. K. Furdyna.
Lattice parameters of $Zn_{1-x}Mn_xSe$ and tetrahedral bond lengths in $A^{II}_{1-x}Mn_xB^{VI}$ alloys.
J. Appl. Phys., 58(11):4056–4060, 1985.
ISSN 00218979.
doi: 10.1063/1.335585.
URL http://dx.doi.org/doi/10.1063/1.335585.

[69] Z. G. Yu, D. L. Smith, A. Saxena, R. L. Martin, and A. R. Bishop.
Molecular geometry fluctuation model for the mobility of conjugated polymers.
Phys. Rev. Lett., 84(4):721–724, Jan 2000.
doi: 10.1103/PhysRevLett.84.721.

Danksagung

An dieser Stelle möchte ich all denen danken, die maßgeblich zum Entstehen diese Arbeit beigetragen haben. Ich danke hierfür

- Prof. Dr. Peter J. Klar für die Möglichkeit diese Arbeit in seiner Arbeitsgruppe anfertigen zu können und die Betreuung währenddessen
- Prof. Dr. Bruno K. Meyer† für die Aufnahme im Institut
- dem Zweitkorrektor und den Prüfern Prof. Dr. Detlev M. Hofmann, Prof. Dr. Christian Heiliger und Prof. Dr. Jürgen Janek
- Prof. Dr. Sergei D. Baranovski für die Kooperation und die hilfreichen Gespräche
- Prof. Dr. Jean Geurts für die die hilfreichen Gespräche
- Dr. habil. Michael Hetterich und seiner Arbeitsgruppe für die Herstellung und die zur Verfügung gestellten (Zn,Mn)Se-Proben
- Dr. Fredrik Jansson, Martin Wiemer und den anderen Mitgliedern der Vielteilchen-Gruppe an der Phillipps-Universität in Marburg
- Dr. Gerd Homm für die Einarbeitung an der Messapparatur
- Martin Fischer, Dr. Matthias "Max" Elm den Mitgliedern des Arbeitsbereichs Transport
- Allen Doktoranden, Diplomanden, Master- und Bachelorstudenten sowie allen Angehörigen des I. Physikalischen Instituts für die gute Zusammenarbeit, die abwechslungsreichen Gespräche und den herzlichen Umgang
- Martin Fischer, Julian Benz, Dr. Sabrina Darmawi, Dominique Schüpfer und Daniela Schön für die angenehme Gesellschaft im Büro
- Martin Becker und Dr. Daniel Reppin für die gute Gesellschaft, die Diskussionen und die Hilfestellungen
- Meiner Familie

Erklärung

Ich erkläre: Ich habe die vorgelegte Dissertation selbständig und ohne unerlaubte fremde Hilfe und nur mit den Hilfen angefertigt, die ich in der Dissertation angegeben habe. Alle Textstellen, die wörtlich oder sinngemäß aus veröffentlichten Schriften entnommen sind, und alle Angaben, die auf mündlichen Auskünften beruhen, sind als solche kenntlich gemacht. Bei den von mir durchgeführten und in der Dissertation erwähnten Untersuchungen habe ich die Grundsätze guter wissenschaftlicher Praxis, wie sie in der Satzung der Justus-Liebig-Universität Gießen zur Sicherung guter wissenschaftlicher Praxis niedergelegt sind, eingehalten.

Ort und Datum	Unterschrift